

AD-A099 662

LOCKHEED-GEORGIA CO MARIETTA

F/G 20/4

AERODYNAMIC INVESTIGATION OF C-141 LEADING EDGE MODIFICATIONS F--ETC(U)

APR 81 R A LARGE, W T BLACKERBY

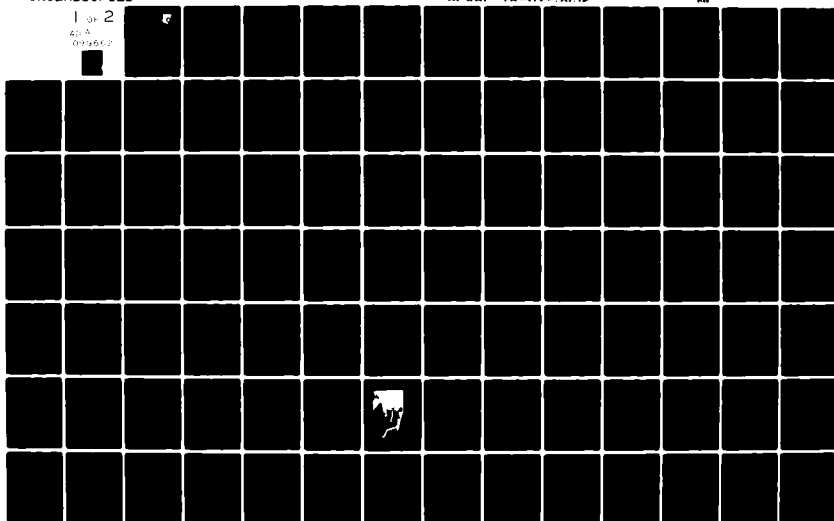
UNCLASSIFIED

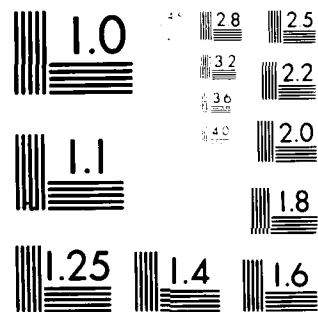
AFWAI -TR-A1-3092

MI

1 of 2

AD-A  
099662





MICROCOPY RESOLUTION TEST CHART  
NATIONAL BUREAU OF STANDARDS-1963-A

AD A099662

LEVEL III

AFWAL-TR-81-3032

A077688

AERODYNAMIC INVESTIGATION OF C-141 LEADING EDGE MODIFICATIONS  
FOR CRUISE DRAG REDUCTION -- TEST 2



Robert A. Large, Captain, USAF  
Aerodynamics & Airframe Branch  
Aeromechanics Division  
Flight Dynamics Laboratory

W.T. Blackerby  
Lockheed-Georgia Company  
86 South Cobb Drive  
Marietta, Georgia 30063

April 1981

DTIC  
ELECTE  
S JUN 3 1981 D  
A

Final Report October 1978 to July 1980

Approved for public release; distribution unlimited.

FLIGHT DYNAMICS LABORATORY  
AIR FORCE WRIGHT AERONAUTICAL LABORATORIES  
AIR FORCE SYSTEMS COMMAND  
WRIGHT-PATTERSON AIR FORCE BASE, OHIO 45433

DTIC FILE COPY

81 6 03 056


NOTICE

When Government drawings, specifications, or other data are used for any purpose other than in connection with a definitely related Government procurement operation, the United States Government thereby incurs no responsibility nor any obligation whatsoever; and the fact that the government may have formulated, furnished, or in any way supplied the said drawings, specifications, or other data, is not to be regarded by implication or otherwise as in any manner licensing the holder or any other person or corporation, or conveying any rights or permission to manufacture use, or sell any patented invention that may in any way be related thereto.

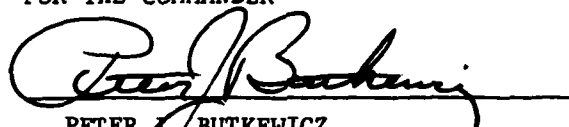
This report has been reviewed by the Office of Public Affairs (ASD/PA) and is releasable to the National Technical Information Service (NTIS). At NTIS, it will be available to the general public, including foreign nations.

This technical report has been reviewed and is approved for publication.

  
ROBERT A. LARGE, Capt, USAF

  
LOWELL C. KEEL, Major, USAF  
Ch, Aerodynamics & Airframe Br  
Aeromechanics Division

FOR THE COMMANDER

  
PETER J. BUTKEWICZ  
Colonel, USAF  
Chief, Aeromechanics Division

"If your address has changed, if you wish to be removed from our mailing list, or if the addressee is no longer employed by your organization please notify AFWAL FIMM, W-PAFB, OH 45433 to help us maintain a current mailing list".

Copies of this report should not be returned unless return is required by security considerations, contractual obligations, or notice on a specific document.

SECURITY CLASSIFICATION OF THIS PAGE (When Data Entered)

19 REPORT DOCUMENTATION PAGE		READ INSTRUCTIONS BEFORE COMPLETING FORM	
1. REPORT NUMBER AFWL - 81-3032 ✓	2. GOVT ACCESSION NO. AD-A099 662	3. RECIPIENT'S CATALOG NUMBER	
4. TITLE (and Subtitle) AERODYNAMIC INVESTIGATION OF C-141 LEADING EDGE MODIFICATIONS FOR CRUISE DRAG REDUCTION — TEST 2.		5. TYPE OF REPORT & PERIOD COVERED Technical - Final Report October 1978 - August 1980	6. PERFORMING ORG. REPORT NUMBER
7. AUTHOR(s) Robert A. Large, Capt, USAF, AFWAL/FIMM W. T. Blackerby, Lockheed-Georgia Company		8. CONTRACT OR GRANT NUMBER(s)	
9. PERFORMING ORGANIZATION NAME AND ADDRESS Lockheed-Georgia Company 86 South Cobb Drive Marietta, Georgia 30063		10. PROGRAM ELEMENT, PROJECT, TASK AREA & WORK UNIT NUMBERS 2404-10-48 17) 2 X	
11. CONTROLLING OFFICE NAME AND ADDRESS Flight Dynamics Laboratory (FIMM) Air Force Wright Aeronautical Laboratories Wright-Patterson AFB, Ohio 45433		12. REPORT DATE April 1981	
14. MONITORING AGENCY NAME & ADDRESS (if different from Controlling Office)		13. NUMBER OF PAGES 145	
		15. SECURITY CLASS. (of this report) Unclassified	
		15a. DECLASSIFICATION DOWNGRADING SCHEDULE	
16. DISTRIBUTION STATEMENT (of this Report) Approved for public release; distribution unlimited.			
17. DISTRIBUTION STATEMENT (of the abstract entered in Block 20, if different from Report)			
18. SUPPLEMENTARY NOTES			
19. KEY WORDS (Continue on reverse side if necessary and identify by block number) C-141, Drag Reduction, Transonic, Wing Design, Wing Modification, Leading Edge Modification, Fuel Savings, Wing Drag Rise, Airfoil Drag Rise, Pressure Distributions			
20. ABSTRACT (Continue on reverse side if necessary and identify by block number) A wing leading edge modification for cruise drag reduction on the C-141 aircraft has been designed and wind tunnel tested. The modification was designed using a CONMIN optimizer linked to a transonic airfoil code. It was tested in the AEDC 16-Foot Transonic Facility, using a 0.044 scale C-141B model, to determine the effects of the modifications on C-141 cruise aerodynamic characteristics and wing chordwise pressure distribu- tions. Measured chordwise pressure distributions were used for correlations with transonic theory. Force data results were analyzed			

DD FORM 1 JAN 73 1473 EDITION OF 1 NOV 65 IS OBSOLETE

SECURITY CLASSIFICATION OF THIS PAGE (When Data Entered)

210063

20. (cont'd)

to determine the effects on C-141 cruise drag, drag rise, and cruise performance. A fuel savings evaluation was made based on measured cruise performance improvements.

The effects of Lockheed designed swept wing tip extensions and trailing edge anti-drag bodies were also investigated in combination with the wing leading edge modification.

Accession For	
NTIS GRA&I	<input checked="" type="checkbox"/>
DTIC TAB	<input type="checkbox"/>
Unannounced	<input type="checkbox"/>
Justification	
By	
Distribution/	
Availability Codes	
Dist	Avail and/or Special

## FOREWORD

This report is a follow-up to an earlier effort documented in AFFDL-TR-79-3059, June 1979. Inaccuracies in model construction for the earlier effort left unanswered questions which are addressed in this report. The new leading edges tested for this report were designed and built by Lockheed-Georgia Company, Marietta, Georgia, under IRAD funding. The Flight Dynamics Laboratory work was performed in-house under work unit 24041048. FDL provided funding for the AEDC wind tunnel test of the leading edge modification while Lockheed-Georgia purchased additional time in conjunction with this test to test their swept wing tips and anti-drag bodies.

At Lockheed-Georgia Mr. J. D. Wallace was the original IRAD Program Manager and Mr. W. T. Blackerby was the Technical Leader. Mr. Blackerby assumed the dual responsibilities of Program Manager/Technical Leader when Mr. Wallace transferred to Lockheed-California. The wing leading edge modification design was accomplished by P. R. Smith and J. K. Johnson. The Advanced Flight Sciences Department at Lockheed-Georgia developed the technology base for this program, in the form of transonic analysis and numerical optimization methods for wings and airfoils.

Technical direction for the FDL in-house program and the AEDC wind tunnel test was provided by Capt R. A. Large of the Air Force Wright Aeronautical Laboratories/FIMM.

The authors wish to thank Mr. R. Boles, Lockheed-Georgia and Mr. S. Brown, AEDC, for their assistance in conducting the wind tunnel test and Mr. J. Cahill, Lockheed-Georgia, and Major L. Keel, AFWAL/FIMM, for assisting with the analysis of the wind tunnel results and preparation of the final report.

# TABLE OF CONTENTS

SECTION	PAGE
I INTRODUCTION	1
II AERODYNAMIC DESIGN	3
1. Background	3
a. Two-Dimensional Design and Test	3
b. Prior Three-Dimensional Design and Test	5
2. Design Methodology	7
a. Prior Design Approaches	7
b. 2-D Equivalent Approach	7
3. Additional Drag Reduction Concepts	12
a. Swept Wing Tips	12
b. Wing Anti-Drag Bodies	13
III WIND TUNNEL TEST	15
1. Test Facility	15
2. Model and Instrumentation	15
3. Test Conditions and Schedule	16
4. Data Reduction	17
IV WIND TUNNEL DATA ANALYSIS	19
1. Modified Leading Edge Results	19
a. Chordwise Pressure Distribution Comparisons	19
b. Aerodynamic Characteristics	20
(1) Repeatability	20
(2) Lift, Drag and Pitching Moment Characteristics	20
(3) Drag Rise Characteristics	21
c. Incremental Drag and Pitching Moment	21



# TABLE OF CONTENTS (Con't)

SECTION		PAGE
	2. Aerodynamic Correlation of Leading Edge Effects	22
	a. Comparison of Theoretical and Measured Pressure Distributions - Equivalent 2-D Method	22
	b. Comparison of Theoretical and Measured Pressure Distributions - FLO-22	23
	c. Comparison of Predicted and Measured Drag Results	24
	3. Swept Tip Results	24
	4. Anti-Drag Body Results	26
V	PERFORMANCE	28
	1. Summary of Effects on C-141B Cruise Performance, Productivity and Mission Fuel for the Modified Leading Edge.	28
	2. Summary of Effects of the Swept Wing Tips on C-141B Cruise Performance	29
VI	CONCLUSIONS AND RECOMMENDATIONS	30
	REFERENCES	133

# LIST OF ILLUSTRATIONS

FIGURE		PAGE
1	C-141 Drag Characteristics	40
2	Research Airfoils - Example of the Effect of Leading Edge Region on Airfoil Drag Rise	41
3	Results from High Speed Test Evaluation of C-141 2-D Airfoil Leading Edge Modifications	42
4	Effect of Leading Edge Modification on C-141B Drag and Cruise Range Parameter at Trim $C_L = 0.46$	45
5	Comparison of $W^{12}$ and $W^{35}$ Measured and Design Ordinates at $\eta = 0.793$	46
6	Design Procedures for Leading Edge Modifications	47
7	Effect of Leading Edge Change on Airfoil Wave Drag, $\eta = 0.794$	48
8	Effect of Leading Edge Change on Airfoil Wave Drag, $\eta = 0.445$	49
9	Effect of Leading Edge Change on Airfoil Wave Drag, $\eta = 0.625$	50
10	Effect of Leading Edge Change on Airfoil Wave Drag, $\eta = 0.95$	51
11	Comparison of Basic and Modified Leading Edge Shapes	52
12	Effect of $W^{37}$ Leading Edge Modifications on Chordwise Pressure Distributions	53
13	Comparison of Spanwise Variation of the 2% Ordinate for the Basic and Modified Leading Edges	57
14	Comparison of Spanwise Variation of Wave Drag Increments for the Modified Leading Edges Relative to the Baseline	58
15	Swept Wing Tip Extension Planform	59
16	C-141 Airfoil Aft Camber Change	60

# LIST OF ILLUSTRATIONS (Con't)

FIGURE		PAGE
17	Sketch of Anti-Drag Body Locations	61
18	Photograph of the 0.044 Scale C-141B Model	62
19	Three View Sketch of the 0.044 Scale C-141B Model	63
20	Pressure Instrumentation	66
21	Effect of $W^{37}$ Leading Edge Modification on Chordwise Pressure Distributions at $M = 0.70$	67
22	Effect of $W^{37}$ Leading Edge Modification on Chordwise Pressure Distributions at $M = 0.75$	71
23	Effect of $W^{37}$ Leading Edge Modification on Chordwise Pressure Distributions at $M = 0.77$	75
24	Effect of $W^{37}$ Leading Edge Modification on Chordwise Pressure Distributions at $M = 0.79$	79
25	Effect of $W^{37}$ Leading Edge Modification on Chordwise Pressure Distributions at $M = 0.80$	83
26	Effect of $W^{37}$ Leading Edge Modification on Chordwise Pressure Distributions at $M = 0.81$	87
27	Effect of $W^{37}$ Leading Edge Modification on Chordwise Pressure Distributions at $M = 0.83$	91
28	Baseline Data Repeatability at $M = 0.60$	95
29	Baseline Data Repeatability at $M = 0.77$	97
30	Modified Wing Data Repeatability at $M = 0.77$	99
31	Lift, Drag and Pitching Moment Characteristics at $M = 0.70$	101
32	Lift Drag and Pitching Moment Characteristics at $M = 0.79$	103
33	Drag Rise Characteristics of $W^{12}$	105
34	Drag Rise Characteristics of $W^{37}$	106

# LIST OF ILLUSTRATIONS (Cont'd)

FIGURE		PAGE
35	Effect of $W^{37}$ on Drag Rise Characteristics	107
36	Incremental Drag and Pitching Moment Coefficients for $W^{37}$	108
37	Comparison of 2-D Equivalent Theory to Experimental Pressure Distributions at $M_{TEST} = 0.79$	110
38	Comparison of FLO-22 Predictions to Experimental Pressure Distributions at $M = 0.77$	113
39	Comparison of FLO-22 Predictions to Experimental Pressure Distributions	117
40	Comparison of FLO-22 Predictions to Experimental Pressure Distributions at $M = 0.79$	118
41	Comparison of Predicted and Measured Drag Increments for $W^{37}$	119
42	Effect of Swept Tip on Chordwise Pressure Distributions of $W^{37}$	120
43	Drag Rise Characteristics of $W^{37}$ Plus Swept Tip	124
44	Effect of Swept Tip on Drag Rise Characteristics	125
45	Effect of Anti-Drag Bodies on Chordwise Pressure Distributions at $M = 0.79$	126
46	Drag Rise Characteristics of $W^{37}$ and Swept Tip Plus Anti-Drag Bodies	130
47	Effect of Anti-Drag Bodies on Drag Rise Characteristics	131
48	Performance Summary for Leading Edge and Swept Tip Modifications	132

# LIST OF TABLES

TABLE	PAGE
1. Configuration Symbols	33
2. Model Dimensional Data	34
3. Wing Pressure Orifice Locations	37
4. Boundary-Layer Transition Strip Location	38
5. Test Program Summary	39

# LIST OF SYMBOLS

$A_{0,1,2,3,4}$	Coefficients of independent variable in leading edge curve fit polynomial
$B_{1,2,3,4}$	Exponents of independent variable in leading edge curve fit polynomial
BL	Butt line
b	Wing span
b/2	Wing semi-span
$C_D$	Drag coefficient
$C_{D_W}$	Wave drag coefficient
$C_L$	Lift coefficient
$C_{L_{TAIL-OFF}}$	Tail-off lift coefficient
$C_M$	Pitching moment coefficient
$C_P$	Pressure coefficient
$C_P^*$	Critical pressure coefficient for $M = 1$
c	Chord
$c_d$	Section drag coefficient
$c_l$	Section lift coefficient
FS	Fuselage station
IRAD	Independent Research and Development
L/D	Lift to drag ratio
LE	Leading edge
M	Mach number
MAC	Mean aerodynamic chord
M(L/D)	Cruise range parameter

$q$	Dynamic pressure
$R_N$	Reynolds number
WL	Water line
WS	Wing station
$X/C, x/c$	Non-dimensional chordwise location
$x$	Chordwise distance
$Y/C, y/c$	Non-dimensional ordinate
$y$	Ordinate or vertical location
2D	Two-dimensional
3D	Three-dimensional
$\alpha$	Angle of attack
$\Delta$	Incremental
$\eta$	Non-dimensional semi-span location
$\Lambda$	Sweep angle
$\Lambda_{EFF}$	Effective sweep angle based on local flow

Note: Configuration symbols are listed in Table 1.

## SECTION I

### INTRODUCTION

The aerodynamicists ability to analyze transonic flows has advanced significantly in the past decade. Transonic airfoil codes are now as accurate as subsonic airfoil codes and transonic wing codes are rapidly approaching the accuracy of subsonic wing codes. Currently effort is being directed toward extending wing codes to include body effects and the effects of other components.

These transonic codes are much more costly to run than their corresponding subsonic codes because of their non-linear formulation. This extra cost requires that specific benefits of using these codes must be identified. One way to ascertain the value of these advances is to apply these codes to the redesign of wings that were designed prior to the development of these transonic codes. The goal of such redesign efforts would be to quantify the improvement in the transonic cruise efficiency of a given aircraft due to the use of the transonic codes.

A prime candidate for such a redesign effort is the C-141 aircraft. A large part of its flying time is spent in cruising at transonic speeds, approximately  $M=0.74$ , and since the C-141 fleet consumes about 15 percent of the total Air Force's jet fuel annually, a small improvement in cruise efficiency could net a significant savings in fuel.

The Flight Dynamics Laboratory's, FDL, interest in transonic codes and their application to the redesign of an existing aircraft's wing merged nicely with Lockheed-Georgia's ongoing effort to reduce the creep drag of the C-141 aircraft. Under IRAD work they had isolated the creep drag problem of the C-141 to the airfoil profile. They had also done



some basic cut and try experimental work to determine the effect of the leading edge shape on the airfoil's creep drag. Based on this work FDL and Lockheed-Georgia formulated an effort to use transonic airfoil and wing codes to optimize the C-141 wing.

Under contract to FDL, Lockheed-Georgia produced leading edge modifications to the C-141 wing to reduce its cruise drag. These modifications were restricted to the first twelve percent chord due to the position of the wing's front spar. The two resulting designs were tested at Arnold Engineering and Development Center (AEDC) 16-foot Transonic Tunnel and the results are documented in Reference 5. Reference 5 also contains background on these efforts, a description of the procedures used to design the wing leading edge modifications, and a description of two other wing modifications tested, a wing swept tip extension and trailing edge anti-drag bodies. Due to inaccuracies in model construction, the test results were not totally satisfactory and FDL and Lockheed-Georgia entered into a cooperative program to design, build, and test a third leading edge modification. That effort and its results are the subject of this technical report.

## SECTION II

### AERODYNAMIC DESIGN

#### 1. BACKGROUND

The C-141 exhibits an increase in drag with increasing Mach number throughout the subsonic Mach number range in wind tunnel tests and in flight. Figure 1 shows this creep drag and drag rise for the C-141A. Figure 1 also shows that a subsonic drag rise, of the same order of magnitude as that of the airplane, has been measured on the wing alone and on the basic airfoil.

##### a. TWO-DIMENSIONAL DESIGN AND TEST

Previous studies by Lockheed-Georgia have attempted to isolate the source of the C-141 creep drag and drag rise. These studies indicated that the problem was not related to either induced drag changes or premature flow separation as Mach number increases. Based on these results they then focused on the more likely source of increased profile drag due to viscous and pressure losses. IRAD studies were initiated at Lockheed-Georgia in an effort to understand more fully the relationships between pressure distributions and the drag rise phenomena as they occur on 2-D airfoils such as that of the C-141A.

Initial efforts compared the drag rise characteristics of conventional airfoil shapes such as the C-141 airfoil to a number of supercritical airfoils. Two geometric characteristics emerged as important factors in airfoil drag rise performance. They were the trailing edge cusp region and leading edge contour. An example of the effect of leading edge contour is shown in Figure 2. The two research airfoils in this test were essentially the same except for the forward 15 percent of the chord.

Moving the leading edge of the airfoil upward results in a moderate pressure peak on the first 10 percent of the upper surface with a weaker shock development which is further aft than the shock on the original airfoil. This influence of the leading edge suction (or pressure) peak is evident throughout the Mach number range, causing improved creep drag as well as delayed drag divergence performance.

Based on these results, Lockheed expanded its IRAD studies to include the design, test, and analysis of a series of leading edge modifications to a two-dimensional C-141 airfoil. For the C-141, the location of the wing spar restricted the extent of modification to the forward 12% chord, thus limiting the amount of drag reduction which might be achieved. An existing 2-D model of a C-141 airfoil at  $\eta = 0.389$  was cut at the 12% chord location and modified to accept removable leading edges. To provide a baseline for comparison a replacement leading edge was constructed using the original airfoil ordinates.

Manual iteration of the viscous airfoil theory of Bauer, et al<sup>(1)</sup> was used to develop a number of designs. Also, one design was determined during a cooperative effort between Lockheed-Georgia and NASA/Ames using the 2-D CONMIN method<sup>(2)(3)</sup> of optimization. This latter design procedure was also used to verify the previous manual designs.

Results for the baseline and two of the modified leading edges are summarized in Figure 3. The 2-D CONMIN leading edge, LE6, uses the existing lower surface shape and is thus a more practical modification. Several larger perturbations, such as LE 3A, were included to provide a range of leading edge shapes. Figure 3(b) illustrates relative changes of the flow over the leading edges and demonstrates that weaker shock formations were achieved with the modifications. The drag rise data of

Figure 3(c) shows the substantial improvement of both LE6 and 3A over the baseline. Although the expected reductions in creep drag at the low and intermediate Mach numbers ( $M < 0.65$ ) did not materialize, creep drag is reduced for  $M > 0.65$  and an increase in drag divergence Mach number of approximately 0.02 is achieved. At  $M_{2D} = 0.73$ , corresponding to a cruise Mach number of 0.775, a drag reduction of 11 counts was indicated. LE6 proved to be as good or better than any of the others, thus verifying the capability of the CONMIN design approach and also emphasizing that the modification may be applied to the upper surface only.

At the section lift coefficients, which correspond to the equivalent 2-D local lift coefficients at cruise on the mid and outer span portions of the C-141 wing, drag reductions of 11 to 16 counts were typical. Since 15 counts of drag represents about 6 percent of the total C-141 cruise drag, a design goal of 5 to 7 percent drag reduction at cruise for the wing was adopted as a standard for the 3-D wing aerodynamic design.

#### b. PRIOR THREE-DIMENSIONAL DESIGN AND TEST

The two-dimensional results discussed above were presented to Flight Dynamics Laboratory personnel. This application of transonic aerodynamic codes to improving on existing airfoil and wing designs fit nicely into FIMMs External Aerodynamics Group's charter. Thus an effort was contracted for Lockheed-Georgia to extend their 2-D work to a 3-D design that would be tested at AEDC's 16T wind tunnel.

Three leading edge modifications were designed from which two were selected for model fabrication and testing in conjunction with the basic C-141 leading edge. The first modification was designed using a Lockheed-Georgia version of 2-D CONMIN extended to permit a wider range of design

variables. A 3-D numerical optimization scheme under development by Hicks<sup>(4)</sup>, similarly extended in scope, was employed to obtain a second leading edge. The third was based on the best of the 2-D modifications tested in the Lockheed-Georgia CFWT. The 2-D and 3-D CONMIN designs showed close similarities in ordinates, theoretical pressure distributions and drag coefficients; therefore, only the 3-D CONMIN wing,  $W^{35}$ , was tested and not the 2-D. The second wing tested,  $W^{36}$ , was based on the earlier 2-D work.

An existing model of the C-141B, 0.044 scale, was modified for this test. The wing was cut at 12% chord to remove the leading edge. Three new sets of leading edges were fabricated, one set to replace the baseline C-141 leading edge,  $W^{12}$ , and two modified sets,  $W^{35}$  and  $W^{36}$ , for evaluation.

The results of this test, as documented in References 5, 6, and 7, were disappointing in terms of drag reduction measured. The best leading edge, according to the AEDC test data, was the  $W^{35}$  for which a drag reduction at cruise of approximately 5 to 9 counts (2.0 to 3.6%) was obtained, Figure 4. Measurement of the model after the test revealed inaccuracies in the construction of the basic and modified leading edges, Figure 5. These errors were such that the geometric differences between the manufactured  $W^{35}$  and  $W^{12}$  were much less than they should have been. Subsequent analysis of these measured ordinates by the transonic codes used in the design process revealed drag levels in excellent agreement with the test results. Based on this correlation it was concluded that the target drag reduction goal of between 5 and 7 percent would have been obtained with the proper leading edge ordinates.

This effort was successful in demonstrating the capabilities of the transonic codes to modify an existing wing to obtain a cruise drag

reduction. The target drag reduction of 6% was not achieved due to model manufacturing inaccuracies. However, the increase in leading edge suction did occur and this net thrusting effect tended to reduce creep drag and increase the drag divergence Mach number as predicted.

The results were promising enough that the Flight Dynamics Laboratory and Lockheed-Georgia decided to continue the effort on a cooperative basis. A new leading edge would be designed and built based upon the knowledge gained from this effort. FDL would then provide the funding for an AEDC 16T wind tunnel test. This effort is documented in this report.

## 2. DESIGN METHODOLOGY

Four different design methodologies have been used during this effort. These methodologies were used to evaluate the relative benefits and penalties of using each. Three (2-D CONMIN, 2-D Airfoil, and 3-D CONMIN) were used in designing the leading edges for the first three-dimensional test at AEDC. The fourth method (2-D equivalent) was used to design the leading edges for this entry at AEDC.

### a. PRIOR DESIGN APPROACHES

For the first entry three leading edges were designed but only two tested. The leading edge designed by using the 2-D CONMIN method was so close geometrically to the 3-D CONMIN leading edge that it was not built or tested. The other leading edge tested was based on the best of the earlier 2-D airfoils from the Lockheed IRAD. A summary of these design procedures is shown in block diagram form in Figure 6. Details of the individual design methods are given in References 6 and 7.

### b. 2-D EQUIVALENT APPROACH

This approach was developed after the AEDC 16T wind tunnel test in April 1978. It was based on the experience gained in using the three design

approaches mentioned earlier. Several important lessons were learned or reinforced from these previous design and test efforts. These lessons include:

(1) 2-D and 3-D numerical optimization give similar results for high-aspect-ratio, moderately swept clean wings.

(2) Numerical optimization using inviscid theory produced a design which performed as well as a more costly design based on viscous theory. This result can be expected where the design changes do not significantly affect the boundary layer properties.

(3) Very tight control of model fabrication tolerances is required when minor leading edge contour changes are being evaluated.

The first two lessons above combined to make a 2-D equivalent, inviscid approach in the optimization process desirable in terms of holding down computer costs. Use of a 3-D viscous code was limited to analysis of the final wing design. The third lesson impacted the model manufacturing process which is discussed in Section III.2.

The equivalent 2-D airfoil at each control station was obtained using simple sweep theory to convert from 3-D to 2-D and vice versa. The equivalent 2-D airfoils and conditions are defined by:

$$(y/c)_{2D} = (Y/c)_{\text{streamwise}} \times \frac{1}{\cos \Lambda_{\text{EFF}}}$$

$$M_{2D} = M_{\text{streamwise}} \times \cos \Lambda_{\text{EFF}}$$

$$C_{P2D} = C_{P3D} \times \frac{1}{\cos^2 \Lambda_{\text{EFF}}}$$

where  $\Lambda_{\text{EFF}}$  = Sweep at Upper Surface Shock

For this design effort the number of control stations was five;  $\eta = 0.118, 0.445, 0.625, 0.815, \text{ and } 0.95$ . The root station,  $\eta = 0.118$ , was held as the unmodified basic airfoil and the other four were optimized.

The 2-D CONMIN<sup>(8)</sup> code was again used for the optimization but it was linked to Jameson's full potential inviscid transonic airfoil code<sup>(9)</sup> rather than the Bauer code used in the earlier 2-D CONMIN approach. The function to be minimized was wave drag at each span station. The final design produced by this 2-D equivalent approach was analyzed using a viscous version of the Bauer code<sup>(1)</sup>.

The choice of design conditions was a critical step for this effort, as the leading edge shape was found to be very sensitive to design lift coefficient. The design cruise Mach number for this effort was selected as  $M = 0.79$  for two reasons. First, this Mach number provides a strong shock wave and hence greater resolution in the sensitive calculations made during the minimization process. Second, the cruise range parameter,  $M(L/D)$ , from the previous AEDC test of the modified leading edge was optimum at  $M = 0.79$ . The appropriate 2-D lift coefficient for the transonic program was selected by matching the upper surface leading-edge pressures with the previous AEDC test data at each control station. Because of the higher than expected loss in lower surface loading due to fuselage/wheel-pod overpressures measured in the AEDC test, the 2-D section lift coefficients are somewhat higher than those used in the previous 2-D design.

The leading edge shape was defined as a fourth-order polynomial,  
$$y = A_0 + A_1 x^{B_1} + A_2 x^{B_2} + A_3 x^{B_3} + A_4 x^{B_4}$$
 where the A's and B's are independent design variables. Both ordinate and slope continuity were enforced at the match points on the wing box.  $A_3$  and  $A_4$  were selected to satisfy these match conditions, thus leaving seven design variables.



Additionally, angle of attack,  $\alpha$ , was used as a "dummy" design variable to provide the required lift coefficient. Starting values for the A's and B's were determined by curve fitting the basic C-141 leading edge. The airfoil chord was held fixed.

A great amount of detail design and analysis was done with the  $\eta = 0.794$  station and the results, summarized in Figure 7, demonstrate the important aspects of this design effort. Figure 7 is a convenient means of visualizing the amount of change in ordinate at 2-percent chord and its corresponding effect on wave drag. Two types of theoretical wave drag are shown, one for a viscous code analysis and the other for an inviscid code. The similarity in the curves validates the use of an inviscid code in the optimizer. The first three data points shown are for airfoils from the basic wing,  $W^{12}$ , the 3-D CONMIN wing,  $W^{35}$ , and a wing designed using this 2-D equivalent approach,  $W^{39}$ . Airfoils,  $W^{40}$  and  $W^{41}$ , with greater amounts of modification than the optimized airfoil,  $W^{39}$ , were determined by a manual iteration of the curve fitting process. These results substantiate the existence of a drag bucket and show the eventual drag rise as a reflex in surface curvature on the upper surface occurs due to the 12 percent chord match point. Relaxation of this match point constraint to 17 percent chord produced the  $W^{37}$  airfoil, which is a substantial improvement over the earlier designs.

Relaxation of the match point to 17 percent chord was also used at the  $\eta = 0.95$  station after initial modification efforts using the 12% match point failed to produce a drag reduction. At  $\eta = .625$  and  $\eta = .445$  the match point was moved back to 12 percent chord. At the  $\eta = .445$  station, the optimized airfoil differed little from the basic airfoil and offered no aerodynamic improvement over it. The upper surface contour at

$\eta = 0.794$  was duplicated at the  $\eta = 0.445$  station and the analysis program showed the improvements noted in Figure 8 for the  $W^{37}$  configuration.

Figures 9 and 10 show the results at  $\eta = 0.625$  and  $\eta = 0.95$ . The basic,  $W^{12}$ , airfoils and modified,  $W^{37}$ , airfoils are compared in Figure 11. These airfoils were selected for testing in this effort.

The theoretical pressure distributions for the basic and modified airfoils are shown in Figure 12. These predictions are from the Bauer<sup>(1)</sup> program. Comparisons of these pressure distributions reveal remarkable improvements in shock formation considering the limited extent of the modification. There are also significant changes in the upper surface pressures before the shock. The major change is the creation of a pressure peak on the first 12% of the upper surface but the influence of this peak does carry over all the way to the shock. On the lower surface the change in pressure coefficients is much less with the largest effect being at the two outboard stations.

A comparison of  $W^{37}$  to  $W^{35}$  shows the difference in results between the two optimizations and the basic wing. Figure 13 summarizes the spanwise variation of the  $y/c$  ordinate at 2 percent chord for the three wings. The increasing deflection spanwise for the modified wings effectively removes some of the existing large leading-edge camber as the tip is approached. Figure 14 shows the resulting wave drag reductions across the wing span for these modifications. Integration of these curves shows a reduction in wave drag of 8 counts for  $W^{37}$  and 5 counts for the  $W^{35}$  design. In the AEDC test of the incorrectly fabricated  $W^{35}$  the measured drag reduction was about 9 counts which indicates that the 3-D drag improvements may be substantially higher than indicated in Figure 14. Thus the

expected drag reduction for  $W^{37}$  was approximated at 14 to 16 counts at  $M = 0.79$ . The primary reasons for the greater leading edge deflection and a corresponding greater reduction in drag for  $W^{37}$  versus  $W^{35}$  are relaxation of the 12 percent constraint on the outboard wing and use of higher 2-D design lift coefficients.

### 3. ADDITIONAL DRAG REDUCTION CONCEPTS

Two additional wing modifications from Lockheed-Georgia's IRAD were included in the wind tunnel test portion of this study to evaluate additional drag reduction potential for the C-141 aircraft. These two modifications were: swept wing tips (extended span), and a series of wing trailing edge bodies called anti-drag bodies spaced across the wing. The necessary model components for these configurations were provided at the expense of the Lockheed-Georgia Company and the test time for the earlier AEDC entry was included in the FDL funded test program. For this entry Lockheed-Georgia Company funded the test time for these items while FDL funded the leading edge test time.

During the earlier test entry these two concepts were tested individually on the basic wing. For this test they were tested together on the modified wing to see if the drag savings from the individual concepts were additive.

#### a. SWEPT WING TIPS

There are two reasons for trying swept wing tips on the C-141. First, the obvious increase in aspect ratio reduces the induced drag for a given wing lift coefficient while the wing loading reduction for a given total lift should reduce shock losses on the wing. Second, sweeping of the tip should counter the tendency for the isobars on the present wing to

become unswept at the tip. The amount of extension and sweep for this modification was based on experience with a similar application on the C-5A wing. The planform of the swept wing tip extension is shown in Figure 15.

b. WING ANTI-DRAG BODIES

Lockheed-Georgia experience with development tests on the C-5A flap-track fairings indicated that such fairings could be designed to provide a net drag reduction notwithstanding the increased profile drag due to the fairings themselves. Analysis of the C-5A results show that the major effect at cruise speeds must be a reduction in shock strength due to an effective change in camber. For application to the C-141 wing, an approach to design a set of anti-drag bodies, similar to flap-track fairings, was devised.

Assuming that a favorable change in 2-D camber could be applied to the 3-D wing by means of properly sized anti-drag bodies, use was made of the 2-D Bauer<sup>(1)</sup> airfoil analysis program to determine the effects of changes in camber. To increase the aft camber in a manner which could be approximately represented by isolated bodies at the trailing edge, a lower surface modification was devised as shown in Figure 16(a). The lower surface ordinates were modified by the addition of thickness which varied from zero at  $X/C = 0.65$  to 2 percent at the trailing edge. Figure 16(b) shows the effect on the theoretical pressure distribution. In comparison with the basic airfoil, the higher aft loading permits a reduction in section angle of attack from 2.7 degrees to 0.9 degrees. This results in a decrease in upper surface shock strength coupled with a rearward shock movement, which reduces the section compressibility drag from 24 counts to 5 counts.

The increase in lower surface trailing edge thickness of 2 percent chord was converted into a spanwise cross-sectional area distribution at the trailing edge. To ensure a reasonable representation of this distribution with adequate spacing to prevent local channel flow interference effects, a total of eight bodies on each wing was chosen, with the most outboard body located at the inboard edge of the aileron. Figure 17 shows a sketch of the body locations on the wing.

### SECTION III

#### WIND TUNNEL TEST

##### 1. TEST FACILITY

The Arnold Engineering Development Center Propulsion Wind Tunnel (16T) is a variable density, continuous-flow closed circuit tunnel capable of being operated at Mach numbers from 0.2 to 1.5, stagnation pressures from 120 to 4000 psfa, and Reynolds numbers from 0.5 to 5.5 million per foot. The test section is 16 ft square by 40 ft long and is enclosed by 60-degree inclined-hole perforated walls of six percent porosity.

##### 2. MODEL AND INSTRUMENTATION

A 0.044 scale C-141B model, Figure 18, was used in this test. The wing and empennage are constructed of 4340 steel and the fuselage is aluminum. The other model components are made from combinations of metal, plastic and fiberglass. A list of the model components with identification symbols is in Table 1 and model dimensional data is given in Table 2. A three view sketch of the model is shown in Figure 19.

The forward 12% of the wing, full span, is removable. Modeler's putty was used to extend the modification to 17% chord near the wing tip. Two leading edge configurations were investigated during this entry; the basic C-141 wing,  $W^{12}$ , and the 2-D equivalent approach wing,  $W^{37}$ .

A total of 118 static pressure orifices were located on the right-hand wing, upper and lower surfaces, at four spanwise stations as illustrated in Figure 20 and listed in Table 3. All the orifices were connected to and recorded from a four-module, 48-port scanivalve assembly located in the model nose section. In addition, internal cavity pressure and differential across the balance were measured from two single orifices located fore and aft in the blade cavity and a single orifice located aft of the balance.

The model was mounted on a Task 3500-B MK-I-3.5 inch internal balance supported by a blade-sting system. This is a six-component, force type, strain gage balance. Its design limits and calibration are discussed in Reference 10. A forward blade support attached to the balance along the fuselage's forward lower centerline was used to minimize support interference effects on the aft fuselage. The blade lower section was attached to a sting adapter and the AEDC PWT 16T "A" sting.

The sting pitch and roll angles were sensed from synchrotransmitters. The model attitude was obtained from a combination of sting attitude and sting-balance deflections under aerodynamic loads. In addition, an angular position indicator mounted in the model was used as a back-up pitch indicator.

Boundary layer transition was fixed on the model by means of Ballotini glass beads applied in strips. The transition strip location, width, and bead diameter for each model component are shown in Table 4.

### 3. TEST CONDITIONS AND SCHEDULE

All configurations were run at a Reynolds number of 4.8 million per foot. (4.69 million based on model wing MAC) and a nominal freestream Mach number range from  $M = 0.60$  to  $0.83$ . Six-component force and pressure measurements were obtained at zero yaw over an angle-of-attack range from  $-4$  to  $+4$  degrees. Flow visualization photos of fluorene sublimation were obtained to verify transition fixing. A summary of the test program is shown in Table 5.

#### 4. DATA REDUCTION

Force and moment measurements were normalized to coefficient form in the body and stability axis system using the following dimensions:

Wing area, ft <sup>2</sup>	6.247
Mean aerodynamic chord (MAC), in	11.724
Span, in	84.302
Reference Moment Center, in	FS 40.605
	WL 10.428
	BL 0.00

The balance output data were reduced to coefficient form based on incompressible dynamic pressure and AEDC's balance calibration prior to the test. Blockage and tunnel wall effects were assumed to be negligible due to the small model-tunnel size ratio and porous walls of the test section. No corrections for effects of blade-sting tare and interference, nacelle internal drag or flow angularity were applied, as the objective of this test was to identify drag increments between the basic and modified configurations.

Pressure data were recorded from the  $\pm 12.5$  psid transducers contained in the 48 SGM scanivalve module unit and reduced to coefficient form

$$C_p = \frac{P_m - P_s}{q}$$

where

$C_p$  = Pressure coefficient

$P_m$  = Model pressure

$P_s$  = Freestream or reference static pressure

$q$  = Freestream dynamic pressure.



During the acquisition of pressure data, computer evaluation of the pressure rate-of-change was used and the transducer output was not acquired for computational purposes until either the rate of change was within AEDC's acceptable limits or a maximum time delay was reached.

## SECTION IV

### WIND TUNNEL DATA ANALYSIS

#### 1. MODIFIED LEADING EDGE RESULTS

##### a. CHORDWISE PRESSURE DISTRIBUTION COMPARISONS

Chordwise pressure distributions at the four spanwise pressure stations for the base,  $W^{12}$ , and modified,  $W^{37}$ , wings are compared in Figures 21 through 27 for  $M = 0.7, 0.75, 0.77, 0.79, 0.80, 0.81$ , and  $0.83$ . An angle of attack of approximately  $1.5^\circ$  was chosen for these comparisons to correspond to the C-141 cruise condition.

Comparison of the pressure distributions at the two inner stations,  $\eta = 0.193$  and  $0.418$ , at any of the Mach numbers show very little improvement for the  $W^{37}$  wing over the  $W^{12}$ . There is a slight increase in leading edge suction but not enough to give a significant drag reduction. At the outer stations,  $\eta = 0.637$  and  $0.793$ , there is a definite increase in leading edge suction for the  $W^{37}$  wing. This increase in leading edge suction is the type of improvement sought and is the major source of drag reduction demonstrated in this test.

The leading edge modification had a secondary goal of weakening the shock strength and moving it aft. This never occurred experimentally. The only time the shock was weakened was at  $\eta = 0.793$  and  $M = 0.77$ ; however, the shock had moved forward rather than aft. The shock moved aft only at high Mach numbers;  $M = 0.81$  and  $0.83$  for  $\eta = 0.793$ ; and  $M = 0.79, 0.80$ , and  $0.81$  for  $\eta = 0.637$ ; however, the shock strength remained unchanged. At  $M = 0.75$  and  $0.77$  the shock moved forward. At  $M = 0.70$  a leading edge shock formed on the modified wing and this produced a drag increase.

Favorable effects on the chordwise pressure distributions occurred primarily on the outer half of the wing with no significant changes inboard. Changes in shock position were detrimental for  $M = 0.77$  and below and just slightly favorable for  $M = 0.79$  and up.

The lack of shock movement on the wing contrasts sharply with the shock movement found in the 2-D tests. This indicates that 3-D effects are the dominating influence on shock position and strength on the wing.

#### b. AERODYNAMIC CHARACTERISTICS

##### (1) Repeatability

Repeat runs were made during this test for each configuration. One set of data was taken near the start of the test of a configuration and the second set at the end of the test. Figures 28 and 29 show these runs for  $W^{12}$  at  $M = 0.60$  and  $0.77$ ; Figure 30 shows  $W^{37}$  at  $M = 0.77$ . The repeatability is excellent with the drag being within  $\pm 3$  counts throughout the range. This accuracy of drag measurement was very important for this effort where small increments between configurations are to be measured. The accuracy of the data acquisition is discussed in detail in the report documenting the test by Brown of AEDC<sup>(10)</sup>.

##### (2) Lift, Drag, and Pitching Moment Characteristics

The lift, drag and pitching moment characteristics for all four configurations tested are shown in Figures 31 and 32 for Mach numbers of  $0.7$  and  $0.79$ . In this section only the  $W^{12}$  and  $W^{37}$  data will be discussed. The swept tip and anti-drag body data will be discussed in sections IV.3 and IV.4.

At  $M = 0.7$ , Figure 31, there are no measurable differences in the lift curves for the two leading edge shapes. The pitching moment

change, -0.003, associated with this change is considered insignificant, as it represents less than 0.1 of a degree of stabilizer trim change for the C-141. The drag polar, however, shows a drag penalty of 8 counts at the equivalent cruise  $C_L$  of 0.5. This drag penalty is due to the formation of a leading edge shock on the modified wing as shown in Figure 21.

At  $M = 0.79$ , Figure 32, the lift and pitching moment curves are the same up to the cruise  $C_L$  of 0.50. However, the drag polar shows a 20 count drag reduction for  $W^{37}$  at  $C_L = 0.50$ . This is a drag reduction of 7.4% at the design cruise point and it exceeds the target drag reduction of 14 to 16 counts.

### (3) Drag Rise Characteristics

Drag rise summaries for  $W^{12}$  and  $W^{37}$  are shown in Figures 33 and 34 for a range of lift coefficients. These curves are the result of an interpolation of the wind tunnel data at constant lift coefficients. Since the model was tested tail-off and untrimmed, the cruise lift coefficient is approximately 0.5, corresponding to a trimmed airplane lift coefficient at cruise of 0.46. A comparison of the drag rise for both wings at three lift coefficients near the cruise value is made in Figure 35. A small drag penalty for  $W^{37}$  is evident at speeds below  $M = 0.75$ . At  $M = 0.75$  the drag levels are identical. Above  $M = 0.75$  the modified wing  $W^{37}$  has a definite drag advantage. The creep drag is reduced and drag divergence is delayed.

#### c. INCREMENTAL DRAG AND PITCHING MOMENT

Incremental drag and pitching moment coefficients for the modified wing are summarized in Figure 36 for constant values of tail-off untrimmed lift coefficient. These data are increments interpolated directly from the test data. Scatter, amounting to  $\pm 0.0001$  in  $C_D$  and  $\pm 0.001$  in  $C_M$ , have

been faired out in generating these curves. At a typical cruise point for the C-141, approximately  $M = 0.77$  and  $C_{L_{TAIL-OFF}} = 0.5$ , the  $W^{37}$  modification reduces drag by about 7.5 counts. This increases to over 20 counts of drag reduction at  $M = 0.79$ . Pitching moment changes are less than  $\pm 0.004$  over the cruise range and are considered insignificant.

## 2. AERODYNAMIC CORRELATION OF LEADING EDGE EFFECTS

### a. COMPARISON OF THEORETICAL AND MEASURED PRESSURE DISTRIBUTIONS - EQUIVALENT 2-D METHOD

In order to compare the 3-D test results to the 2-D theory the 3-D results must be converted to 2-D by means of the relationships discussed in section II.2.b. Thus data at the 3-D design point of  $M = .79$  is compared to the 2-D theory at  $M = .73$  and the pressure coefficients are ratioed to their 2-D counterparts for comparison. Figure 37 shows this comparison for  $\eta = 0.418, 0.636$  and  $0.793$ .

At  $\eta = 0.418$ , 2-D viscous theory is shown and the agreement in shock position is good. The leading edge pressure peak predicted for  $W^{37}$  did not occur and this may be due to the spanwise influence of the unmodified inboard leading edge or to the influence of the fuselage. The discrepancy in lower surfaces pressures is due to the interference of the wheel well fairings and pylons and nacelles.

At  $\eta = 0.636$  and  $\eta = 0.793$  the agreement between theory and experiment for both wings is very good for the leading edge pressures. This is the critical area for matching with the 2-D equivalent approach used in the design and it confirms the soundness of the design approach. Experimentally the shock wave is further forward than predicted. This is due to the use of an inviscid code for the design.

b. COMPARISON OF THEORETICAL AND MEASURED PRESSURE DISTRIBUTIONS -  
FLO-22

The basic and modified wings were analyzed using a 3-D transonic wing code, FLO-22, for purposes of comparison. The predictions of this theory are compared to the experiment in Figure 38. The theoretical predictions are least accurate on the inboard wing since the body, wheel well pods and pylons/nacelles are not modeled in the theory. At  $\eta = 0.193$  the pressure distributions do not compare very well but the shock position and strength are predicted correctly. At  $\eta = 0.418$  the upper surface pressures match very well for the basic wing, however, the shock position is not as well predicted as it is for the rest of the wing. For the W<sup>37</sup> wing at  $\eta = 0.418$  the predicted pressure peak does not occur and the correlation of upper surface pressures is not good. The disagreement in lower surface Cp's for both wings is due to the interference of the wheel well pods and pylon/nacelles. These results underline the inadequacy of wing only codes to design the inboard portion of wings. At  $\eta = 0.636$  and  $\eta = 0.793$  the correlation between experiment and theory is excellent in all aspects. It should be noted that FLO-22 runs were made at a Mach Number 0.01 above the test correlations. Figures 39 and 40 show this same correlation at  $\eta = 0.793$  using the 0.01 Mach Number shift at test Mach Numbers of 0.78 and 0.79.

Contrasting Figures 37 and 38 gives an indication of the adequacy of using 2-D inviscid theory for wing designs. In this case where we were only modifying the leading edge and looking for changes in wave drag it was barely adequate. However, more extensive modifications would call for the use of 3-D codes which give superior pressure and shock correlations.

Figure 38 also highlights the limitation of the wing alone code whenever interference effects from the body, etc. are significant.

### c. COMPARISON OF PREDICTED AND MEASURED DRAG RESULTS

The incremental drag difference between  $W^{37}$  and  $W^{12}$  experimentally is compared to the theoretical predictions in Figure 41. This comparison is at the untrimmed cruise lift coefficient of 0.5. The two- and three-dimensional theories agree well with each other with the most significant difference being at  $M = 0.80$  which is well into the drag rise. The experimental data correlates very well for  $0.75 \leq M \leq 0.79$  and this substantiates the design technique used in the effort. At  $M = 0.80$  the experimental drag increment is over twice that predicted by theory, however, this is into the drag rise area where neither theory is considered accurate. At  $M = 0.70$  neither theory predicted the formation of a leading edge shock wave which produced the drag increase shown experimentally.

### 3. SWEPT TIP RESULTS

The addition of the swept wing tip to the modified wing has very little effect on the chordwise pressure distributions as shown in Figure 42 for  $M = 0.79$  and  $\alpha = 1.0$  degrees. At the two outboard span stations there is a slight rearward shift in the shock which indicates a favorable effect on the tip isobars.

Figures 31 and 32 compare the lift, pitching moment and drag characteristics tip on (triangle symbol) to tip off (circle symbol) at  $M = 0.70$  and  $M = 0.79$ . All of these coefficients are based on a wing area of 6.247 square feet and the added area due to the wing tip is ignored. The addition of the wing tip increases the lift at a given angle of attack and as Figure 32 indicates may delay the break in the lift curve slope. The

additional lift at  $\alpha = 1.0^\circ$ , approximately  $\Delta C_L = 0.015$ , is primarily concentrated at the tip as the pressure data in Figure 42 shows. This additional lift is located behind the center of gravity of the airplane and creates the additional nose down pitching moment shown in Figures 31 and 32. At  $C_L = 0.5$ , the pitching moment increment is  $\Delta C_M = -0.025$  which corresponds to approximately one-half degree of stabilizer trim change for the C-141. The expected large savings in wing induced drag due to the 9.5 percent increase in wing span were realized as shown in the drag polars in Figures 31 and 32.

The drag rise characteristics for the modified wing with the swept tip are shown in Figure 43 and are compared in Figure 44 with data for the modified wing without the swept tip. At  $C_L = 0.5$  and for Mach numbers below 0.76, the induced drag reduction amounts to about 17 counts. At  $M = 0.79$  the drag reduction increases to 25 counts, indicating a reduction in compressibility drag of 8 counts. This reduction in compressibility drag indicates that the swept tips are improving the shock losses over the wing, especially at the tip where the isobars become unswept on the wing without the swept tip.

These changes in aerodynamic characteristics are identical to those observed in the earlier test<sup>(5)</sup> where the swept tip was added to the basic wing rather than the modified wing. This indicates that the effects of the leading edge and the swept tip modifications are independent and additive as we had expected them to be.

Because the wing loading in the region of the tip is altered by the swept tip modification, the center of pressure for the wing is shifted outboard a significant amount. In the earlier report<sup>(5)</sup> this incremental shift



in the center of pressure at cruise was found to be 2.3 percent of the wing semi-span. This change in center of pressure could be reduced or eliminated by uprigging the ailerons.

#### 4. ANTI-DRAG BODY RESULTS

The anti-drag bodies, eight per side, were added to the  $W^{37}$  wing with the swept tips installed to evaluate the combined effects of all three modifications. The earlier entry<sup>(5)</sup> had tested the anti-drag bodies on the basic wing,  $W^{12}$ , only.

The effect of the anti-drag bodies on the chordwise pressure distributions is shown in Figure 45. The increase in aft loading and the aft shock movement clearly indicate that the design objective of increasing camber was achieved with the anti-drag bodies. Station  $\eta = 0.793$  is outboard of the last anti-drag body; however, the influence of the anti-drag bodies is very evident on the upper surface indicating good carry-over. The lift, drag and pitching moment characteristics for this configuration are shown by the plus symbol on Figures 31 and 32. This data can be compared to the  $W^{37}$  plus swept tip data, triangle symbols, to get the incremental effect due to the addition of the anti-drag bodies. The angle of attack needed to produce a cruise lift coefficient is almost a degree less due to the camber effect. The nose down pitching moment increases by  $-0.015$  at  $C_L = 0.5$  and this would require approximately  $0.3$  degree of stabilizer trim change. The drag polars show a definite drag penalty at low lift coefficients and a slight drag reduction at lift coefficients above  $0.5$ .

The drag rise characteristics for the anti-drag bodies are shown in Figure 46. Figure 47 shows the effect of the anti-drag bodies on the drag rise of the modified wing with swept tip. This modification only provides

a drag reduction above  $M = 0.79$  at the design cruise lift of  $C_L = 0.5$ .

These drag results are not quite as good as the results<sup>(5)</sup> when the anti-drag bodies were tested on the basic wing. Thus the drag effects of the anti-drag bodies do not appear to be totally additive to the effects of the leading edge and swept tip modifications.

SECTION V  
PERFORMANCE

1. SUMMARY OF EFFECTS ON C-141B CRUISE PERFORMANCE, PRODUCTIVITY AND MISSION FUEL FOR THE MODIFIED LEADING EDGE.

The baseline configuration for the performance evaluation in this study is the C-141B aircraft as flight tested in FY80. Performance improvements for the leading edge modification were added incrementally to the performance for this aircraft. No corrections were applied to the tested drag increments between the  $W^{12}$  and  $W^{37}$  configurations.

The cruise lift coefficient for the C-141 is typically 0.46, trimmed, and this has been chosen for the cruise summary comparisons. This value corresponds to approximately  $C_L = 0.5$  for the tail-off untrimmed test results reported herein. Figure 48 summarizes the effect of the leading edge modification on the C-141B drag rise and range parameter,  $M(L/D)$ , for this cruise condition. Two conclusions can be drawn from these results. First, an increase in the range parameter is indicated above  $M = 0.74$ . Second, the drag decrease improves substantially as the Mach number is increased to the design point,  $M = 0.79$ .

The performance curve for the leading edge modification only was put into the C-141B performance deck to determine relative specific range values for the basic and modified configurations. The differences in cruise speeds resulted in changes in cruise altitude and specific fuel consumption (SFC) which offset the fuel savings due to the drag reductions obtained so that net mission fuel remained the same. This result was very disappointing since from a fuel savings standpoint, the increased cruise speed was not beneficial. However, the increased cruise speed could be utilized to

increase the productivity of the C-141 fleet.

2. SUMMARY OF EFFECTS OF THE SWEPT WING TIPS ON C-141B CRUISE PERFORMANCE.

The effect of the swept wing tips added to the C-141B with a modified leading edge is also shown in Figure 48. The effects of these two modifications have been shown to be additive, thus the effect of the swept tips can be extracted from the  $M(L/D)$  vs.  $M$  data shown. The swept tip offers a substantial improvement in  $M(L/D)$  over the entire Mach number range tested,  $0.70 \leq M \leq 0.83$  and increases the Mach number for best  $M(L/D)$  to  $M = 0.79$ . This can be attributed primarily to the 9.5 percent increase in wing span.

## SECTION VI

### CONCLUSIONS AND RECOMMENDATIONS

An analytical and wind tunnel test program has been completed on a leading edge modification to the C-141B wing in order to evaluate cruise drag reduction. Two additional drag reduction concepts, swept wing tips and anti-drag bodies, were tested. The principal conclusions follow.

a. A successful application of a low cost 2-D transonic numerical optimization method (CONMIN) to design an improved leading edge contour for the C-141B wing has been demonstrated. For this unique problem where only the forward 17 percent of the wing was modified the use of a low cost 2-D code instead of the more costly 3-D code was found to be adequate for prediction of leading edge pressures but not to be adequate for shock prediction. The correlation of leading edge pressures on the outboard half of the wing was excellent. The correlation at  $\eta = 0.418$  was not good; however, this station is between the engines and even current 3-D codes would not be expected to give accurate results here.

b. The advantages of a 3-D transonic wing code over the 2-D code is shown in the accurate prediction of shock strength and location at all four span stations. The correlation of  $C_p$ 's are excellent for the outboard span stations.

c. The need for body and pylon/nacelle modeling is shown by the lack of pressure correlation at the two inboard span stations. The differences between the wing code predictions and experiment can be attributed directly to aerodynamic interference from these components.

d. The creation of a leading edge pressure peak did reduce the creep drag for this aircraft. Comparison of the experimental pressure distributions reveals that the change in leading edge pressures is the only

significant difference between the two wings; therefore, this must be the reason for the drag reduction.

e. The increased cruise speed capability provides a potential benefit with respect to productivity of the C-141. By taking advantage of the higher cruise speed, mission time is decreased, which either reduces flight hours for the fleet or increases the total fleet productivity capability.

f. Substantial drag reduction was measured at the design Mach number of 0.79. This resulted in increases in aerodynamic cruise efficiency,  $M(L/D)$ , and in the Mach number for maximum  $M(L/D)$ . However increases in engine SFC as Mach number increases negate the expected fuel savings.

g. The effect of the swept wing tip was confirmed as being additive to the effects of the leading edge modification since the changes due to adding the swept tip to the modified wing were virtually identical to the changes when it was added to the basic wing.

h. The effect of adding the anti-drag bodies to the modified wing with swept tips was not as great as the effect of adding them to the basic wing. This was expected since the design of the anti-drag bodies was based on the basic airfoil and wing shapes.

2. In view of the above discussion and conclusions, the following is recommended.

a. Future work on leading edge modifications should address the cruise speed range of  $0.74 \leq M \leq 0.76$  to avoid detrimental changes in engine SFC.

b. A different design objective should be chosen for the CONMIN optimizer. This effort used minimum wave drag as the design objective. Other quantities such as total drag or leading edge suction could be

utilized.

c. Active consideration of low speed performance (take-off, landing, and air-drop) should be part of any future leading edge design since this wing is the result of considerable compromise between low speed and cruise requirements.

d. A 3-D wing/body code should be used for redesign of the in-board half of the wing. At 40% semi-span the need for pylon/nacelle modeling is very evident.

e. The swept wing tip should be studied further. A load alleviation scheme using up rigged ailerons should be demonstrated. These results should then be compared to a winglet designed for the C-141B and the relative benefits and penalties should be clearly identified.

TABLE 1  
CONFIGURATION SYMBOLS

<u>SYMBOLS</u>	<u>COMPONENT</u>
$B^{12}$	FUSELAGE - C-141B Base; Basic C-141A Fuselage with 280 inch Full Scale Extensions
$K^{19}$	PYLONS - Engine Nacelles
$N^8$	NACELLES - Flow Through, with Inlet Spinners
$W^{12}$	WING - Basic High/Low Speed $W^{12}$ Steel Wing with Removable Leading Edges (Forward 12% $C_w$ ). 3 Panels L.E. Each Semi-Span
$W^{37}$	WING - $W^{12C}$ With 2-D Equivalent Approach Leading Edge
$Z^{f1}$	ANTI-DRAG BODIES - Flap Track Fairing Type, Wing Trailing Edge; 8 per Semi-Span
$Z^{G21}$	WHEEL WELL FAIRING
$Z^{t6}$	WING TIP - Swept; Chord/Span Ratio = 1.33/1
$Z^{W7A}$	WING-FUSELAGE FILLET - C141A Pro- duction Fillets



TABLE 2  
MODEL DIMENSIONAL DATA

FUSELAGE - B<sup>12</sup>

Length, Inches	82.350
Max. Frontal Area, Ft <sup>2</sup>	0.305
Max. Equiv. Diameter, Inches	7.480
Fineness Ratio (L/D)	11.009
Nose Location, FS	3.098
Fuselage Reference Line (FRL), WL	8.800

PYLONS - K<sup>19</sup>

	<u>INBOARD</u>	<u>OUTBOARD</u>
Area, Ft <sup>2</sup>	0.090	0.093
Span, Inches	1.453	1.517
MAC, Inches	8.800	8.800
Thickness, Streamwise, % Chord	8.000	8.000
Sweep of Leading Edge, Degrees	73.000	73.000

NACELLES - N<sup>8</sup>

Area, Side per Nacelle, Ft <sup>2</sup>	0.168
Length, Inches	8.256
Max. External Diameter, Inches	2.900
Internal Diameter, Inches - Inlet	2.244
- Exit	1.940
Internal Area, In <sup>2</sup> - Inlet	3.954
- Exit	2.956
Fineness Ratio, (L/D) Ext.	2.843
Toe-In, Degrees - Inboard	2.0
- Outboard	1.0
Location of Inlet $\epsilon$ - INBOARD, FS	29.104
WL	8.479
BL	12.272
- OUTBOARD FS	32.709
WL	8.163
BL	20.103

TABLE 2 (CONT'D)

<u>WING</u> - $W^{12}$		
Area, $Ft^2$ (S)		6.247
Span (Equiv.), Inches/Ft(b)		84.302/7.025
Aspect Ratio (A)		7.9
Taper Ratio ( $\lambda$ )		0.373
Thickness Ratio ( $t/c$ ) - Root (BL 0.00)		0.130
	- Inboard Break (BL 17.804)	0.112
	- Outboard Break (BL 18.778)	0.110
	- Tip	0.100
	- Mean	0.113
Sweep of 25% chord, Degrees	- Inboard	23.734
	- Outboard	25.025
Sweep of Leading Edge, Degrees		
	- Inboard	28.253
	- Outboard	27.285
Dihedral, Degrees	- Inboard	-0.941
	- Outboard	-1.195
Incidence, Degrees from FRL @ BL 0.00 (i)		4.891
Twist, Degrees	- Root (BL 0.00)	0.00
	Inboard Break (BL 17.804)	-2.201
	Outboard Break (BL 18.778)	-2.279
	Tip (BL 42.151)	-5.584
Chord Lengths (Projected), in.- Root ( $c_r$ ) BL 0.0		17.547
	MAC ( $\bar{c}$ ) BL 17.309	11.724
	Inbd. Brk. BL 17.804	10.591
	Outbd. Brk. BL 18.778	10.379
	Tip ( $c_t$ ) BL 42.151	5.803
Chord Locations - Root (L.E.) FS		28.545
	WL	13.045

BL	0.00
(MAC (25%) FS	40.605
WL	11.629
BL	17.309
TIP(L.E.) FS	50.531
WL	10.219
BL	42.151

\*NOTE: Wind Tunnel data based on projected wing planform with root chord @ 0° incidence and aero L.E. and 100% chord T.E.  
Aero data analysis based on area measured from L.E. to T.E., and 25% MAC location referenced to wing reference plane.  
W.T. Data 25% MAC location = 24.1% MAC Aero Analysis Data.

WHEEL WELL FAIRINGS - Z<sup>G21</sup>

Length, Inches	17.776
Max. Frontal Area Per Side, Inches	7.480
Max. Equiv. Diameter, Inches	3.086
Fineness Ratio	5.760
Leading Edge Location, FS	34.936

TABLE 3  
WING PRESSURE ORIFICE LOCATIONS

BL 8.127  
 $\eta = 0.193$

BL 17.634  
 $\eta = 0.418$

BL 26.825  
 $\eta = 0.637$

BL 33.437  
 $\eta = 0.793$

(X/C's FOR ORIFICE LOCATIONS)

<u>UPPER</u>	<u>LOWER</u>	<u>UPPER</u>	<u>LOWER</u>	<u>UPPER</u>	<u>LOWER</u>	<u>UPPER</u>	<u>LOWER</u>
0.0	0.02	0.0	0.02	0.0	0.02	0.0	0.02
0.015	0.05	0.015	0.05	0.015	0.05	0.015	0.05
0.03	0.10	0.03	0.10	0.03	0.10	0.03	0.10
0.05	0.20	0.05	0.15	0.05	0.15	0.05	0.15
0.07	0.30	0.07	0.20	0.07	0.20	0.07	0.20
0.09	0.40	0.09	0.30	0.09	0.30	0.09	0.30
0.11	0.50	0.11	0.40	0.11	0.40	0.11	0.40
0.20	0.63	0.15	0.50	0.15	0.50	0.15	0.50
0.30	0.80	0.20	0.65	0.20	0.65	0.20	0.65
0.40	0.95	0.25	0.85	0.25	0.85	0.25	0.85
0.50		0.30		0.30		0.30	
0.63		0.37		0.35		0.35	
0.80		0.40		0.40		0.40	
0.95		0.45		0.45		0.45	
1.0		0.50		0.50		0.50	
		0.60		0.60		0.60	
		0.70		0.70		0.70	
		0.80		0.80		0.80	
		0.90		0.90		0.90	
		0.95		0.95		0.95	
		1.00		1.00		1.00	

Table 4

## Boundary-Layer Transition Strip Location

Component	Location (In. from Leading Edge)	Width (In.)	Bead Diam. (In.)
Wing Upper Surface	0.70	0.05	0.0031
Wing Lower Surface	0.70	0.05	0.0031
Fuselage	0.90	0.10	0.0045
Pylons	0.20	0.05	0.0038
Nacelles (External)	0.80	0.05	0.0038

- Notes: 1) All measurements along body x-axis.  
2) After RN 315 the bead diameter of the wing upper surface was increased to 0.0031.

TABLE 5  
TEST PROGRAM SUMMARY

a) Model Configurations

RN No. START	RN No. END	CONF.	CONFIGURATION
315	342	1	B12, W37, ZW7, ZG21, K19, N8, ZT6, ZF1
347	352	3	B12, W37, ZW7, ZG21, K19, N8, ZT6
359	368	5	B12, W37, ZW7, ZG21, K19, N8
381	398	10	B12, W12, ZW7, ZG21, K19, N8

b) Test Program

Description & Configuration	PWT RN @ Indicated Mach Number								
	.600	.700	.750	.770	.780	.79	.80	.81	.830
I. SUBLIMATION Conf 1						315 317			
II. Force & Pressure Conf 1		337 321	338 322	339		340		341	342
Conf 3		347	348	349		350		351	352
Conf 5	359	360	361	368 362	363	364	365	366	367
Conf 10	381 383	384	385	392 386	387	388	389	390	391
III. SUBLIMATION Conf 10						395 398			

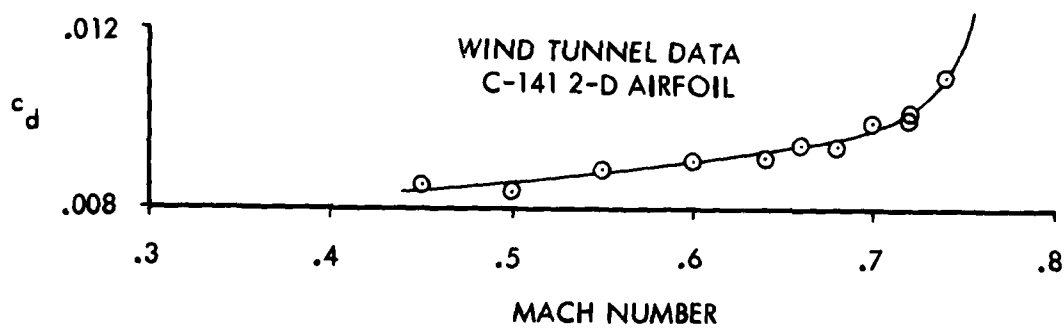
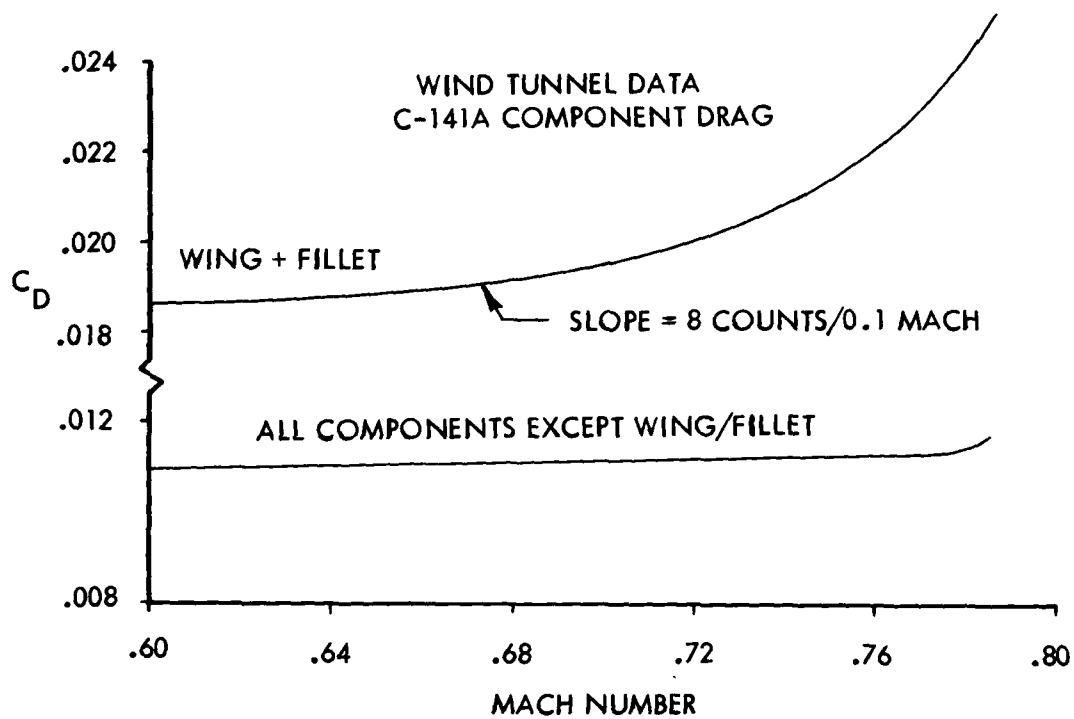
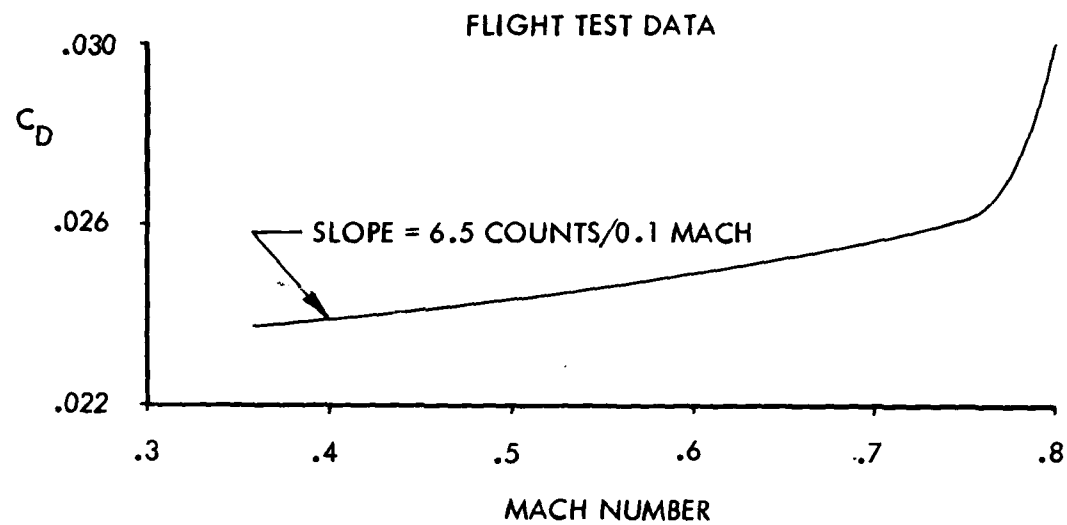


Figure 1 . C-141A Drag Characteristics

# IMPORTANCE OF LEADING EDGE REGION

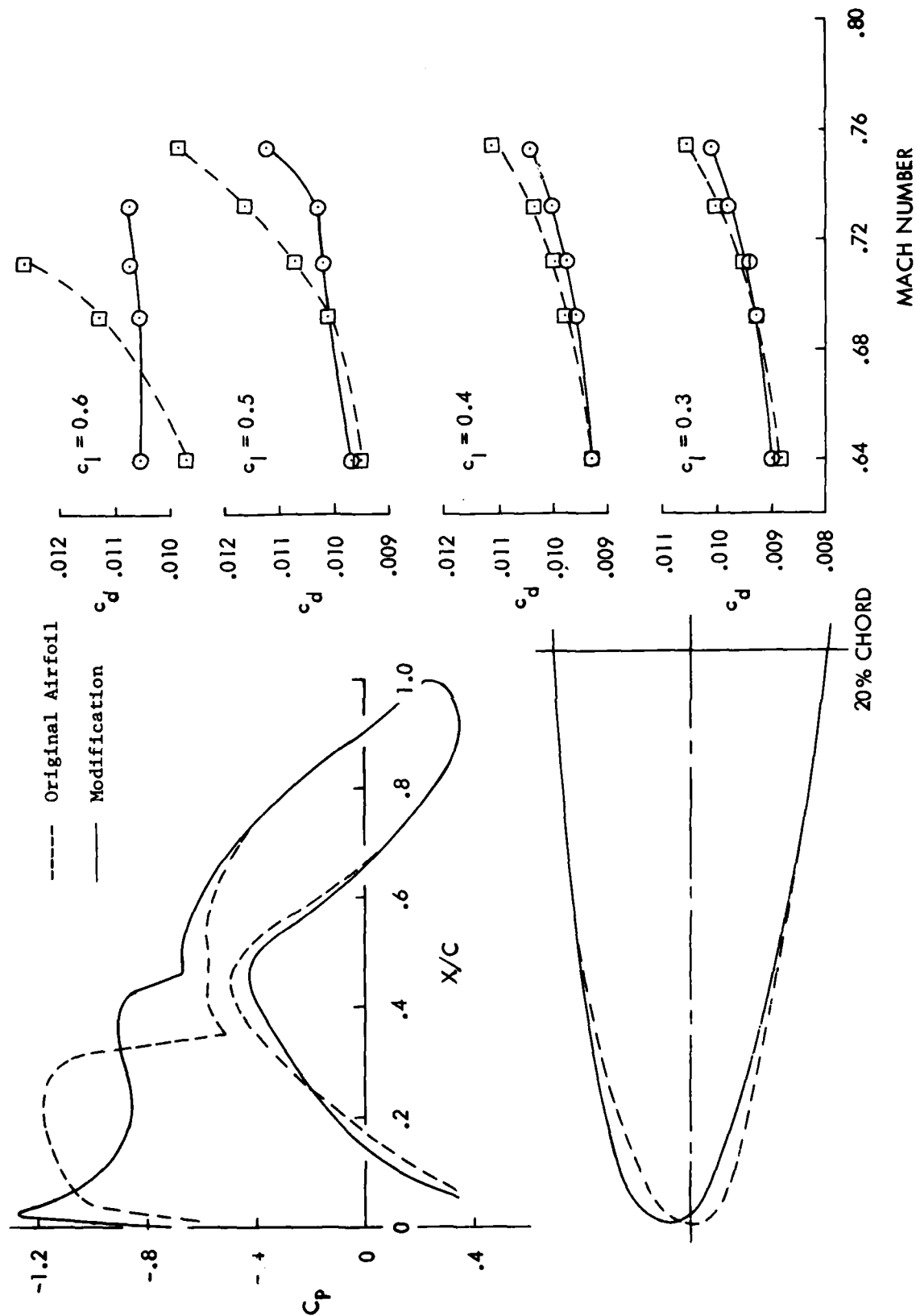
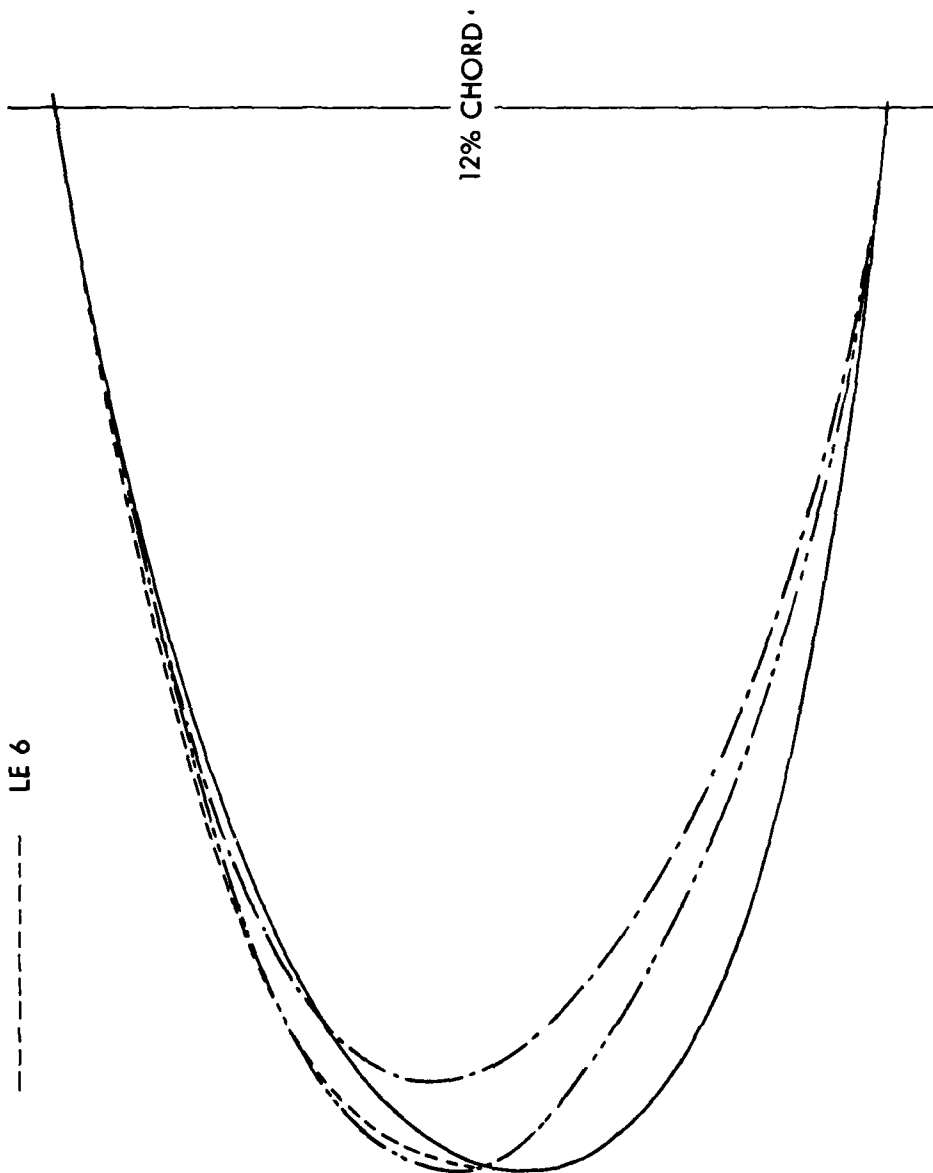


Figure 2. Research Airfoils—Example of the Effect of Leading Edge Region on Airfoil Drag Rise

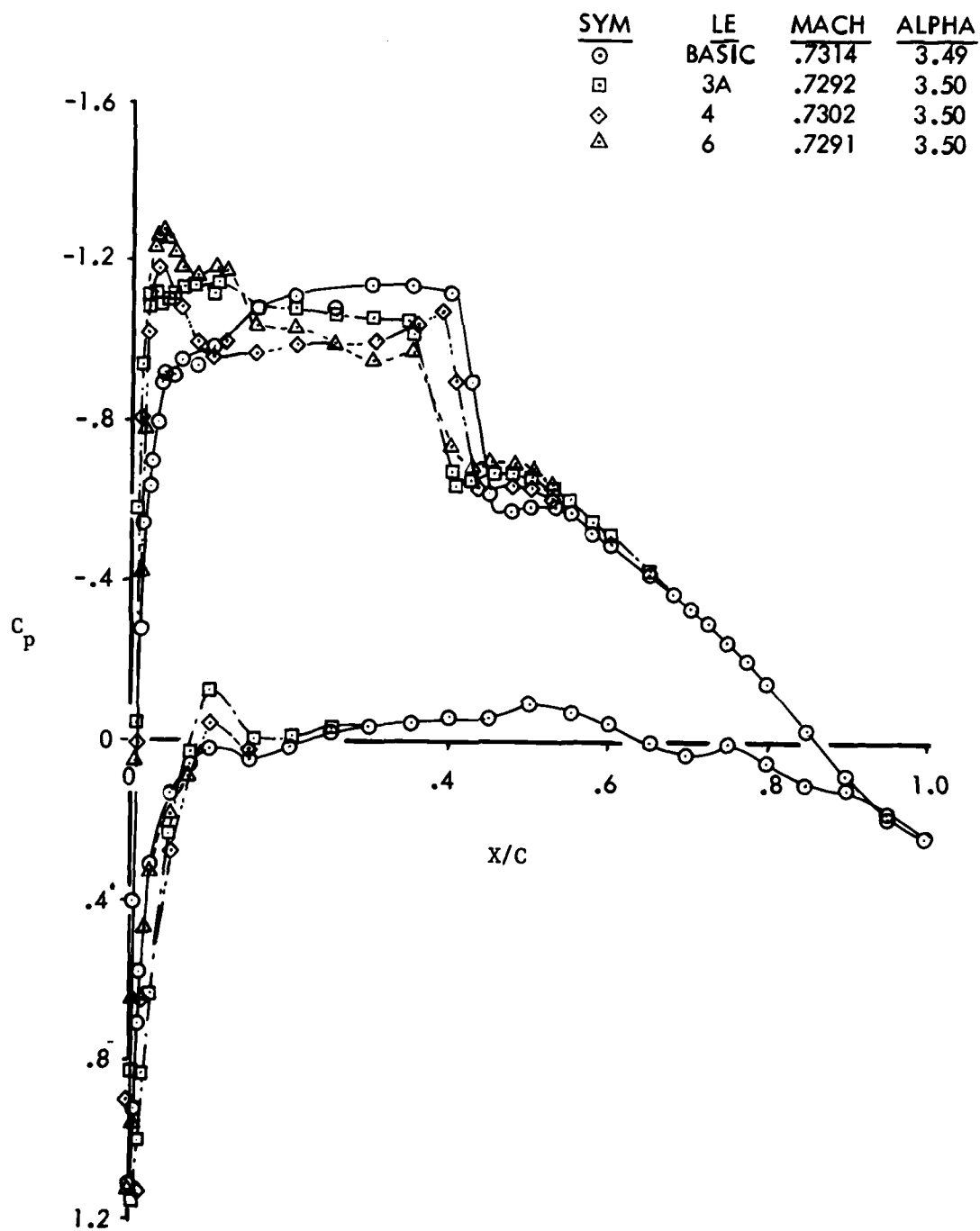


BASIC C-141  
LE 3A  
LE 4  
LE 6



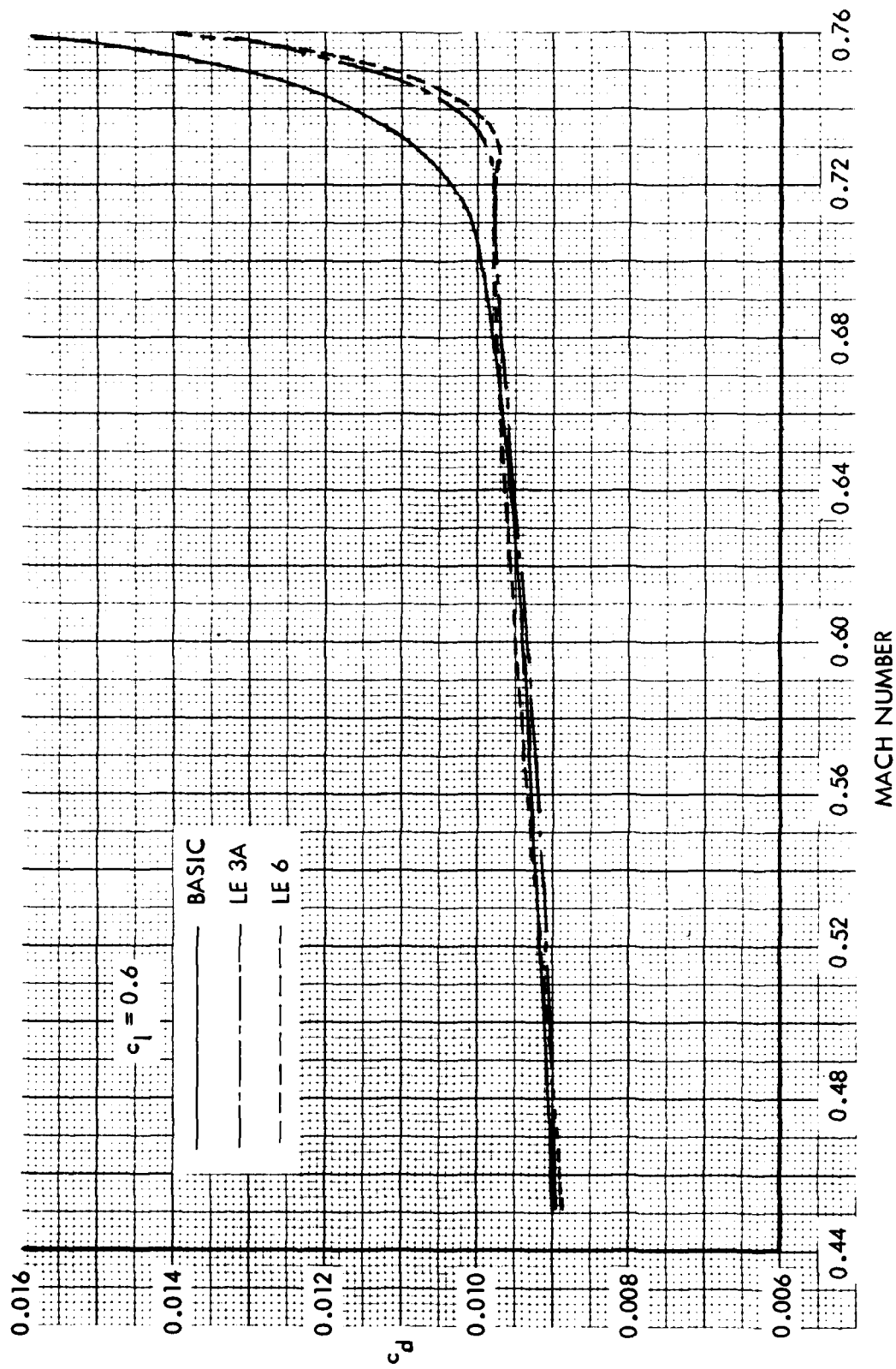
a. Leading Edge Shapes

Figure 3. Results From High Speed Test Evaluation of C-141 2-D Airfoil Leading Edge Modifications



b. Comparison of Experimental Pressure Distributions

Figure 3. Continued



c. Comparison of Drag Rise Characteristics

Figure 3 . Concluded

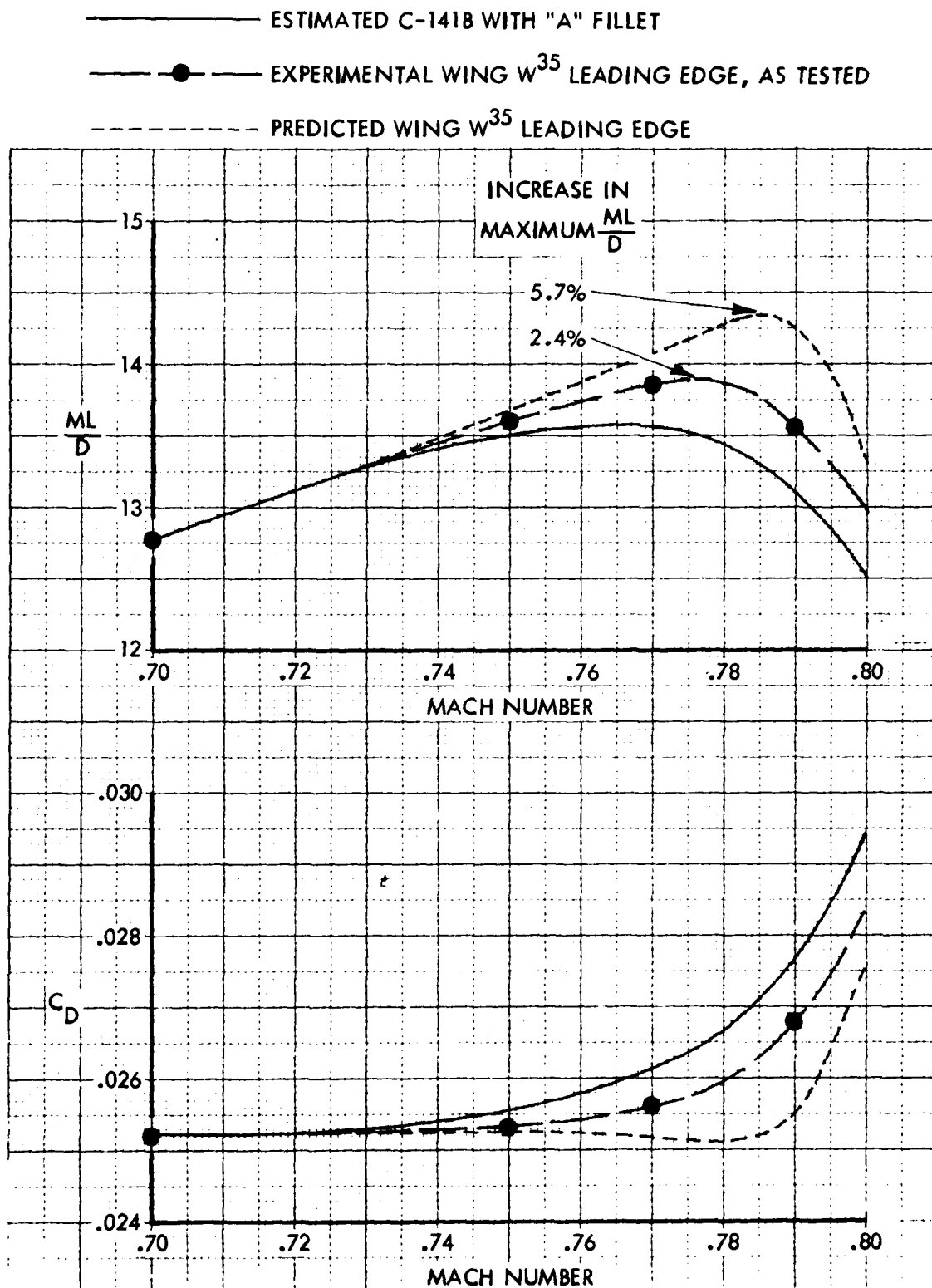


Figure 4. Effect of Leading Edge Modification on C-141B Drag and Cruise Range Parameter at Trim  $C_L = 0.46$

COMPARISON OF DESIGN AND MEASURED  
MODEL ORDINATES

$\eta = 0.793$

$W^{12}$  DESIGN ORDINATES  
 $W^{12}$  MEASURED MODEL ORDINATES  
 $W^{35}$  DESIGN ORDINATES  
 $W^{35}$  MEASURED MODEL ORDINATES

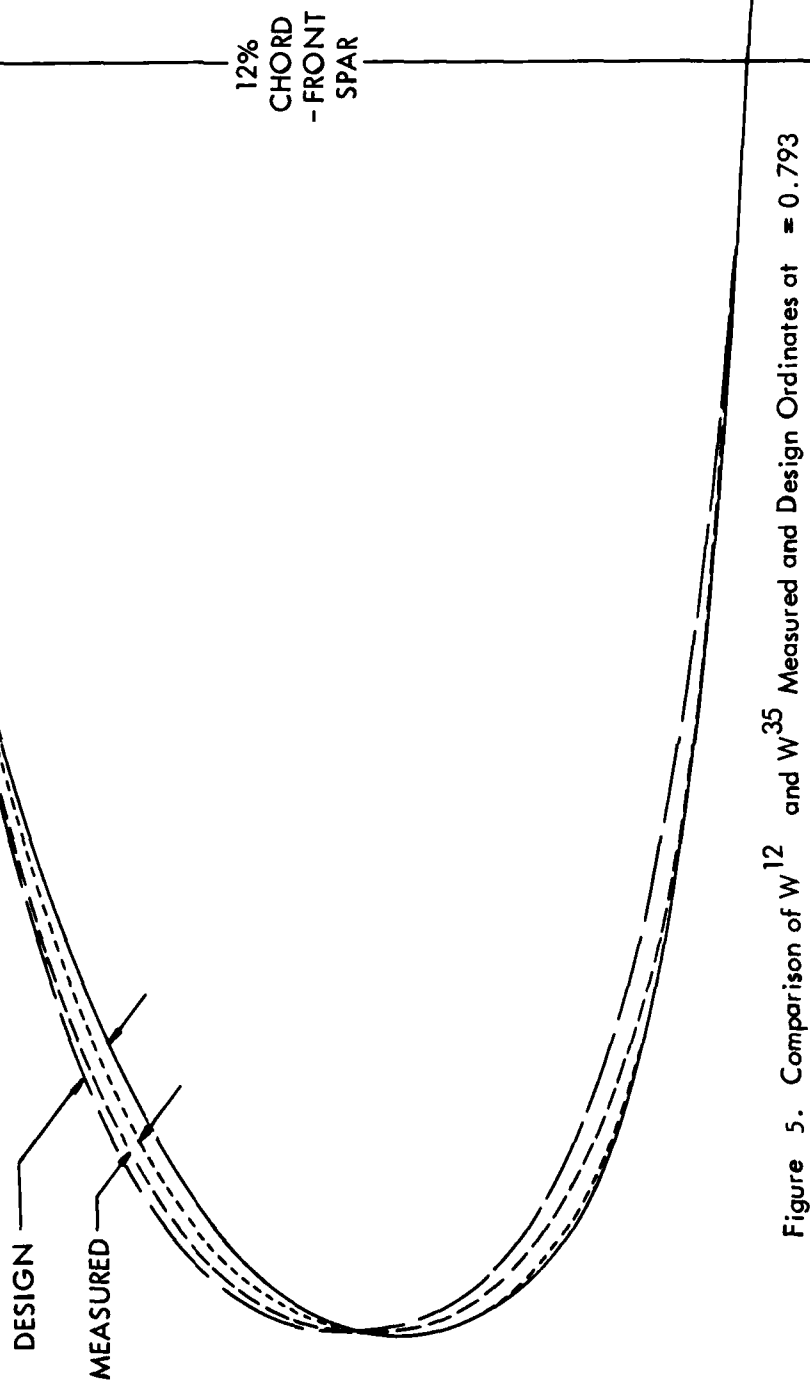


Figure 5. Comparison of  $W^{12}$  and  $W^{35}$  Measured and Design Ordinates at  $\eta = 0.793$



$$\eta = .794$$

$M = .73$   
 — INVISCID,  $C_L = .85$   
 - - - VISCOUS,  $C_L = .75$   
 Δ CONMIN AIRFOIL

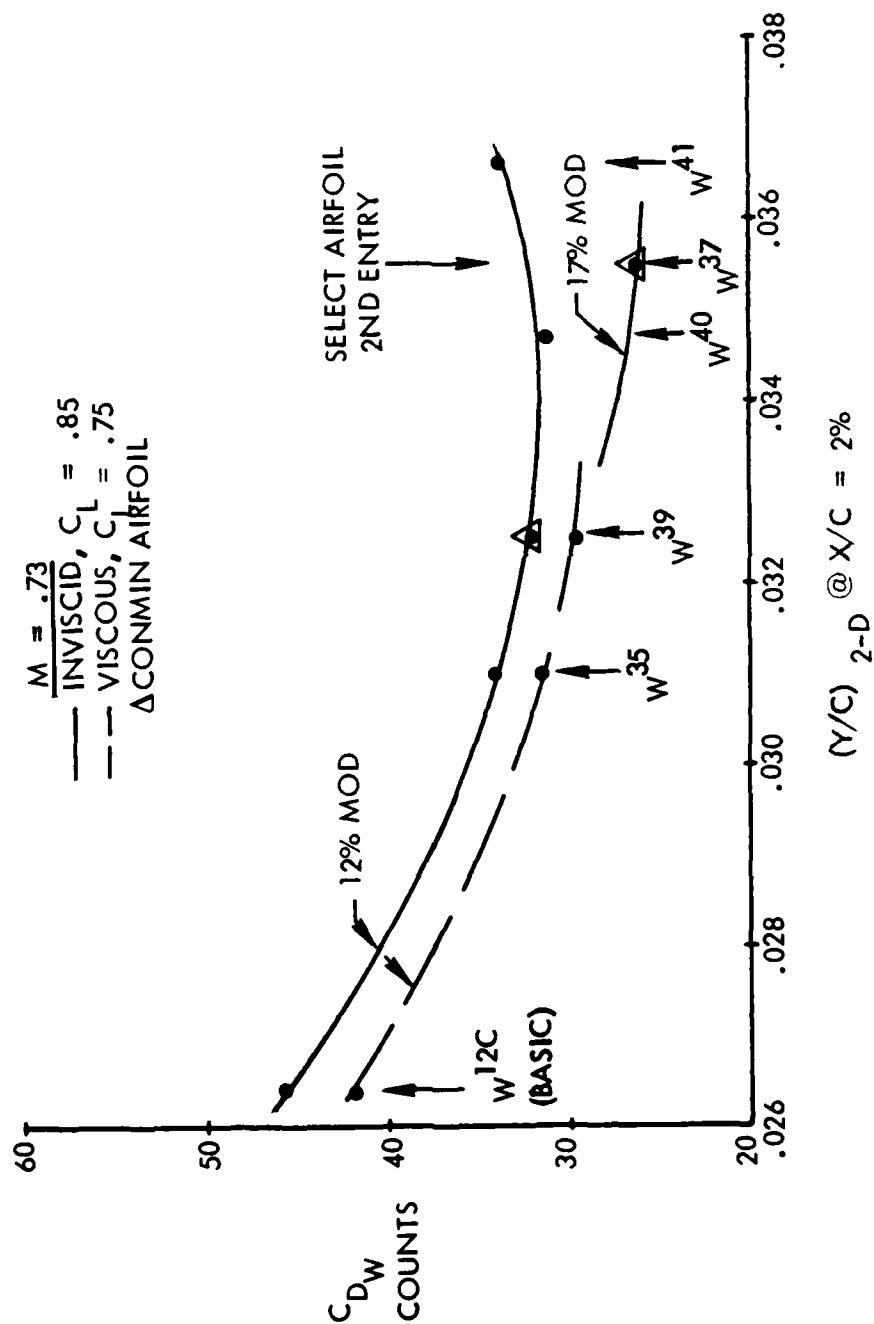


Figure 7. Effect of Leading Edge Change on Airfoil Wave Drag,  $\eta = 0.794$

$$\eta = .445$$

$$M = .73$$

— INVISCID ,  $C_L = 0.85$

— VISCOUS ,  $C_L = .75$

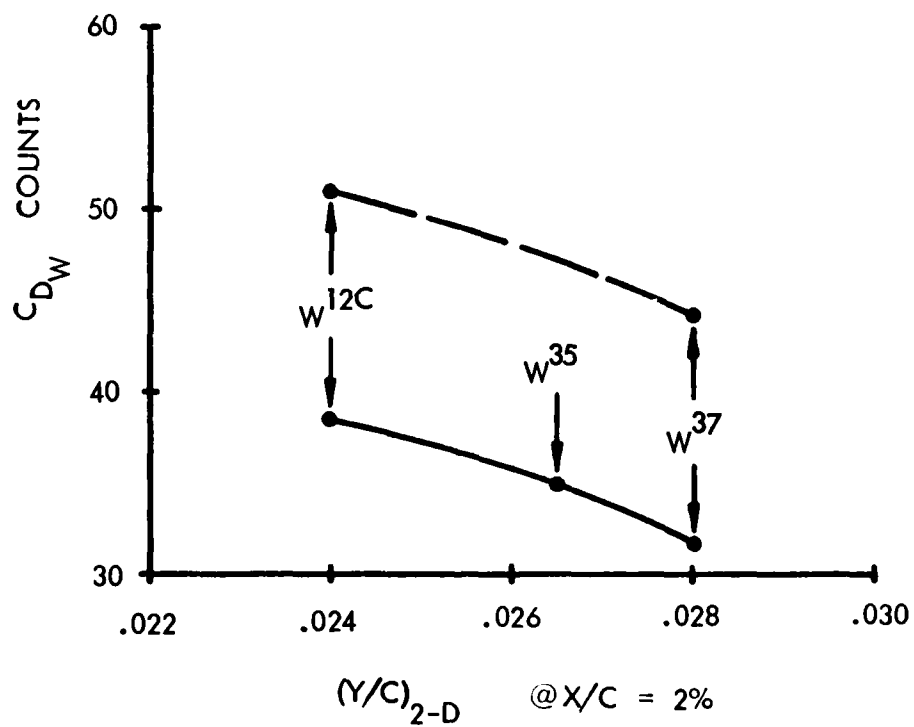


Figure 8. Effect of Leading Edge Change on Airfoil Wave Drag,  
 $\eta = 0.445$



$$\eta = .625$$

$$M = .73$$

$$\text{INVISCID } C_L = .85$$

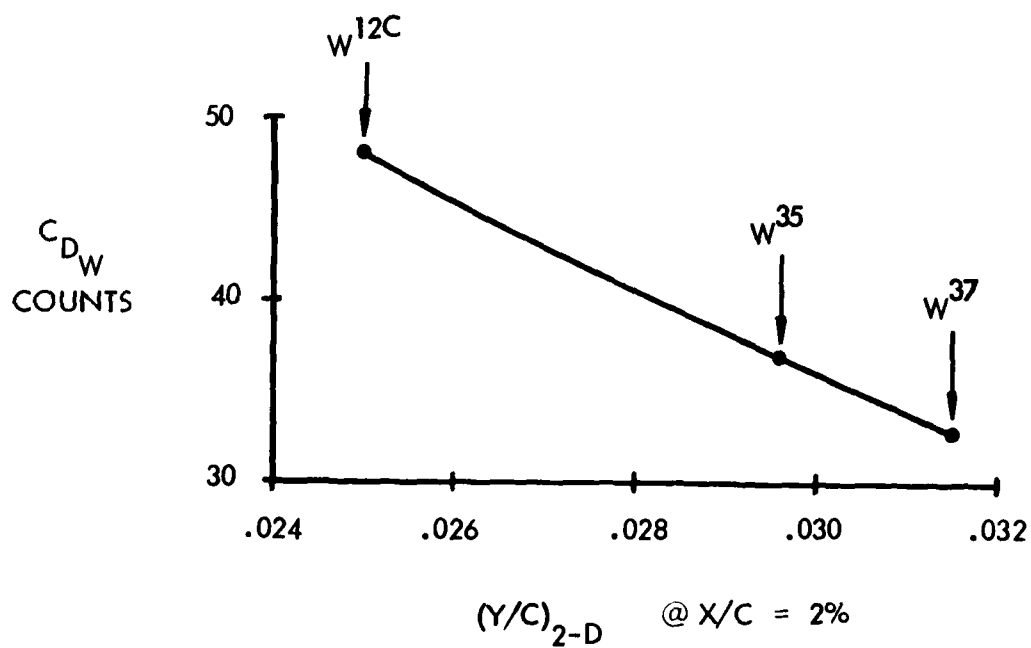


Figure 9. Effect of Leading Edge Change on Airfoil Wave Drag,  $\eta = 0.625$

$$\eta = .95$$

$$M = .73$$

$$\text{VISCOUS, } C_L = .65$$

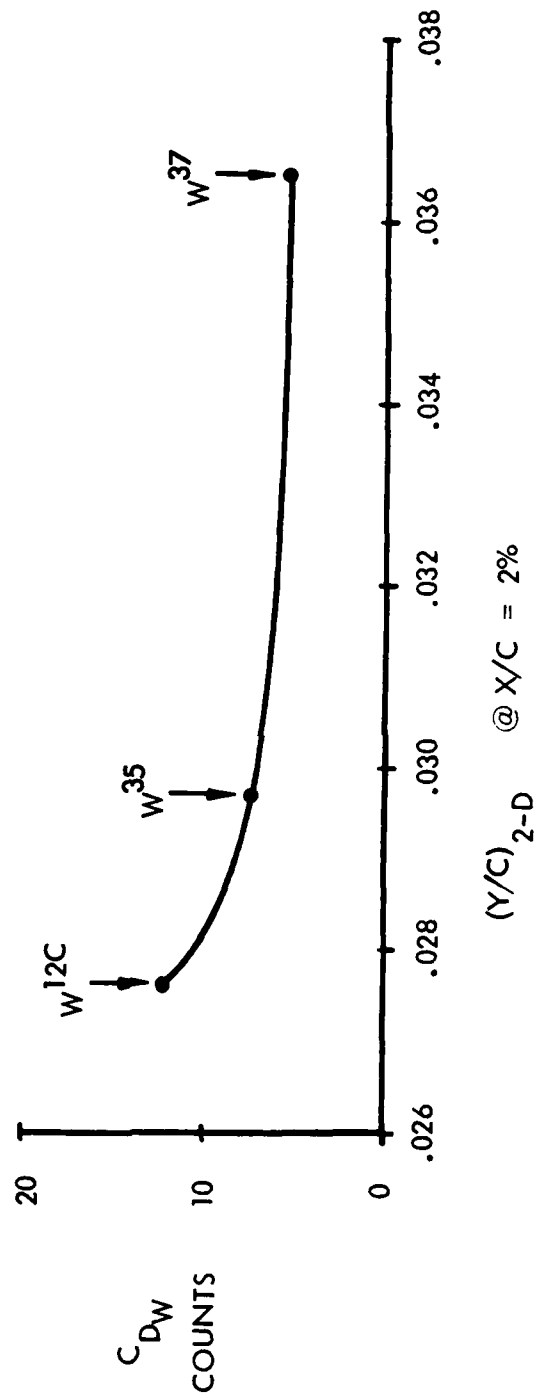


Figure 10. Effect of Leading Edge Change on Airfoil Wave Drag,  $\eta = 0.95$

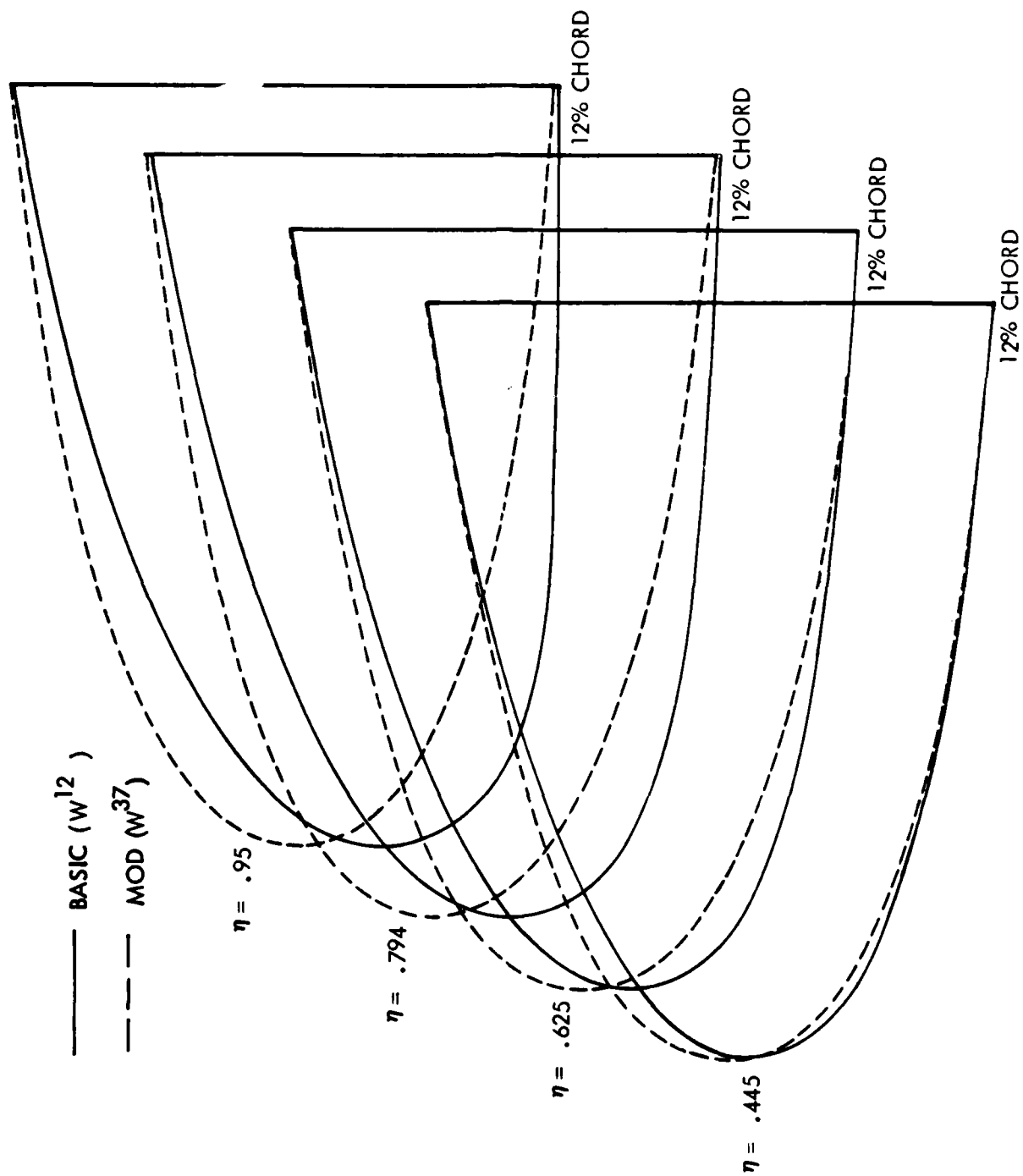


Figure 11. Comparison of Basic and Modified Leading Edge Shapes

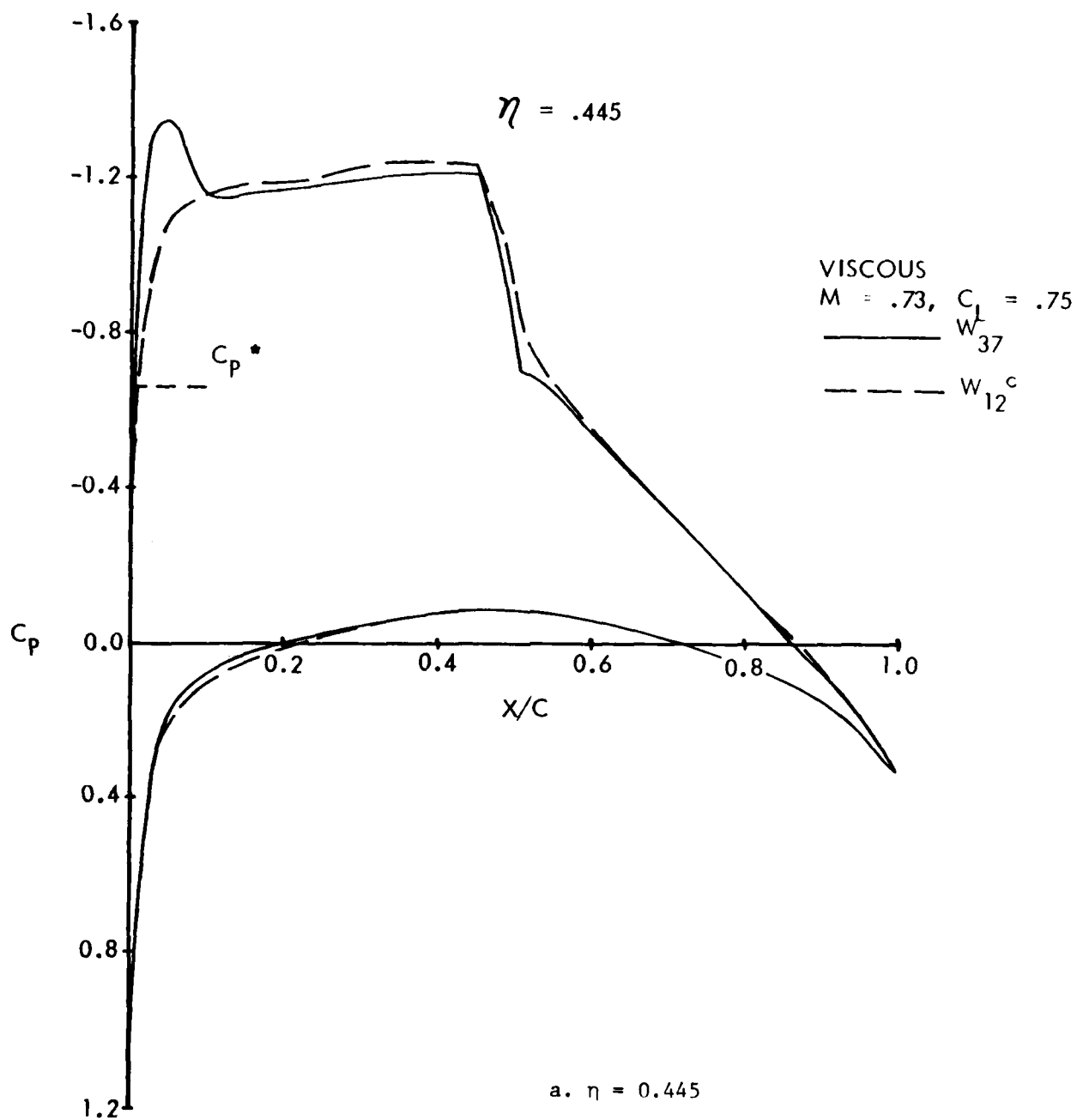
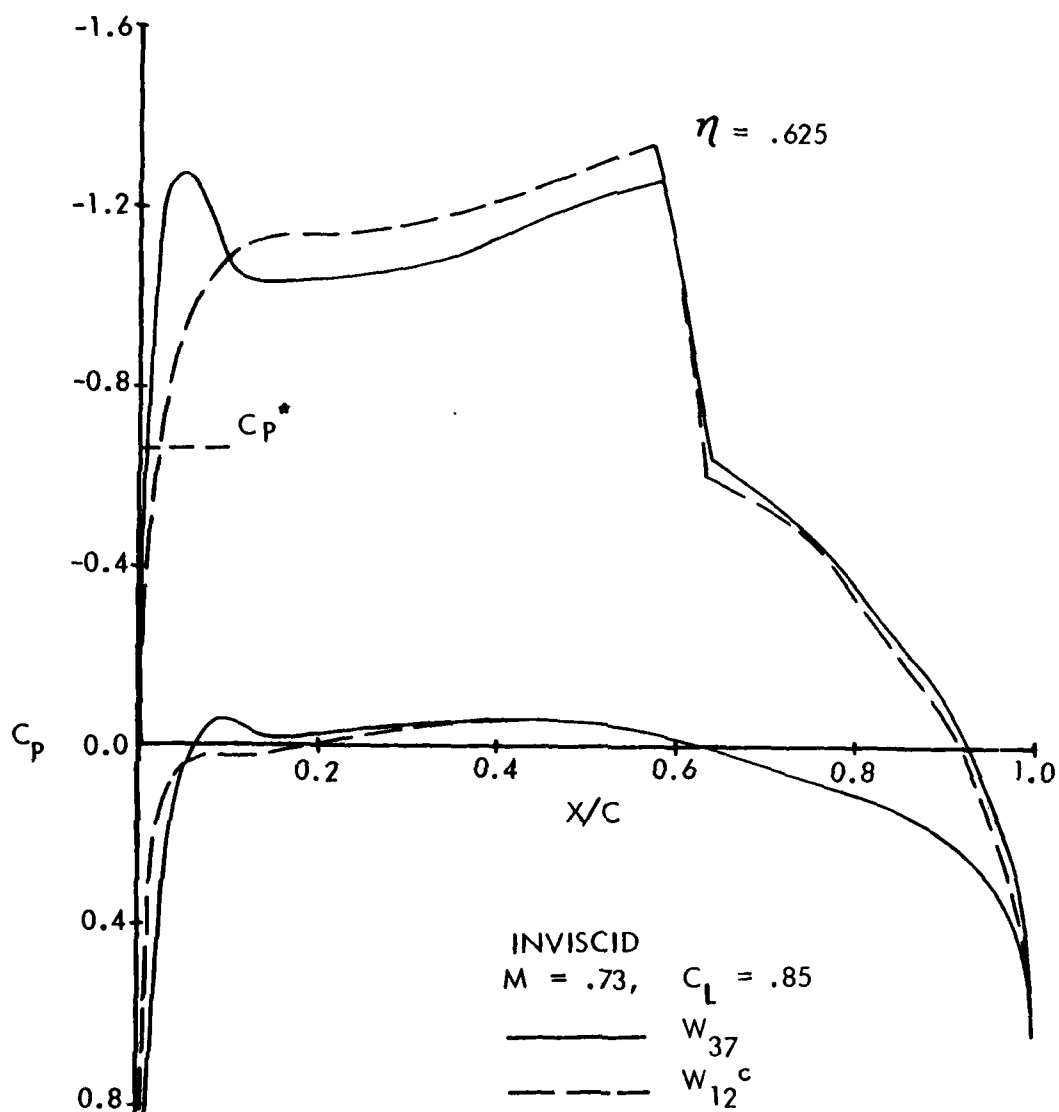
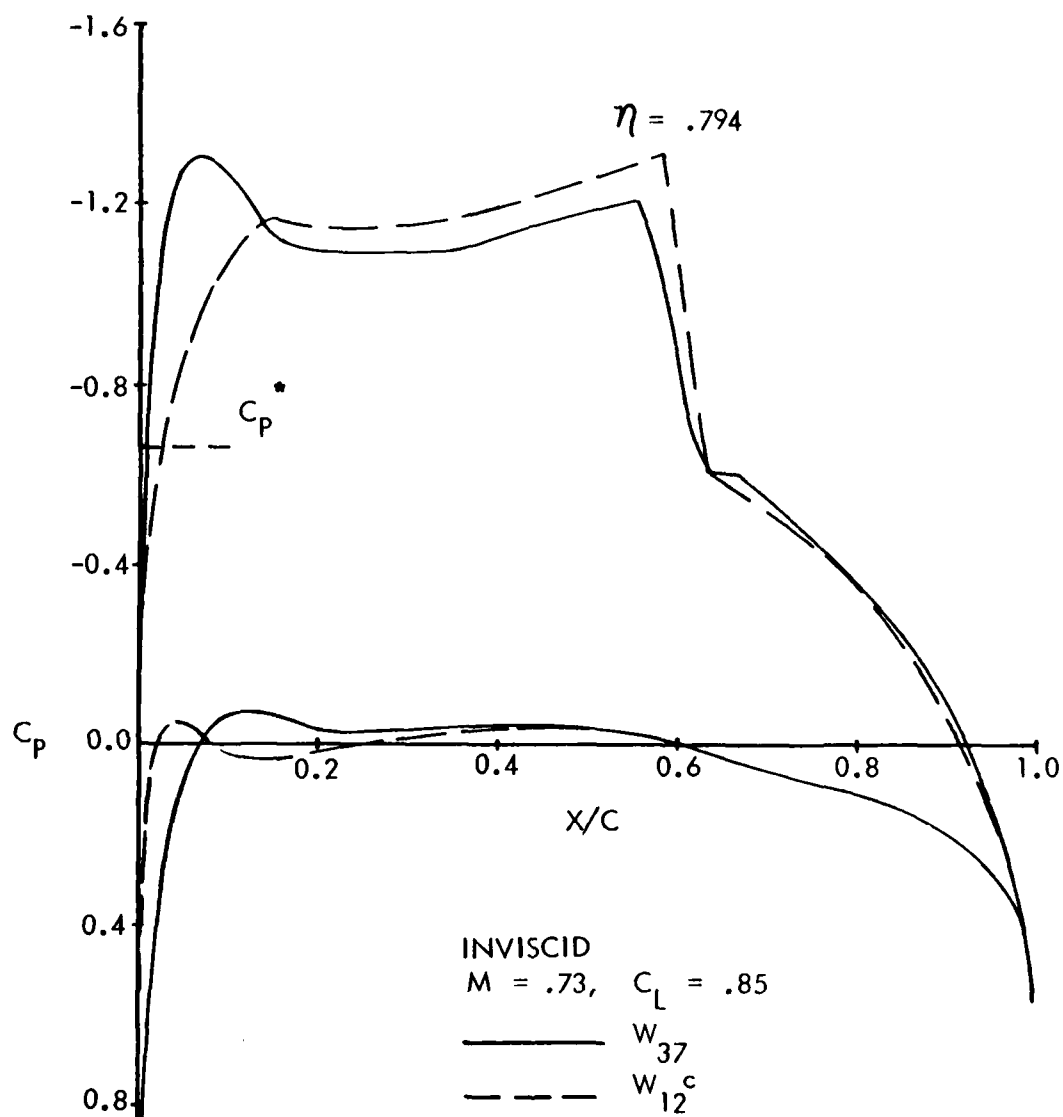


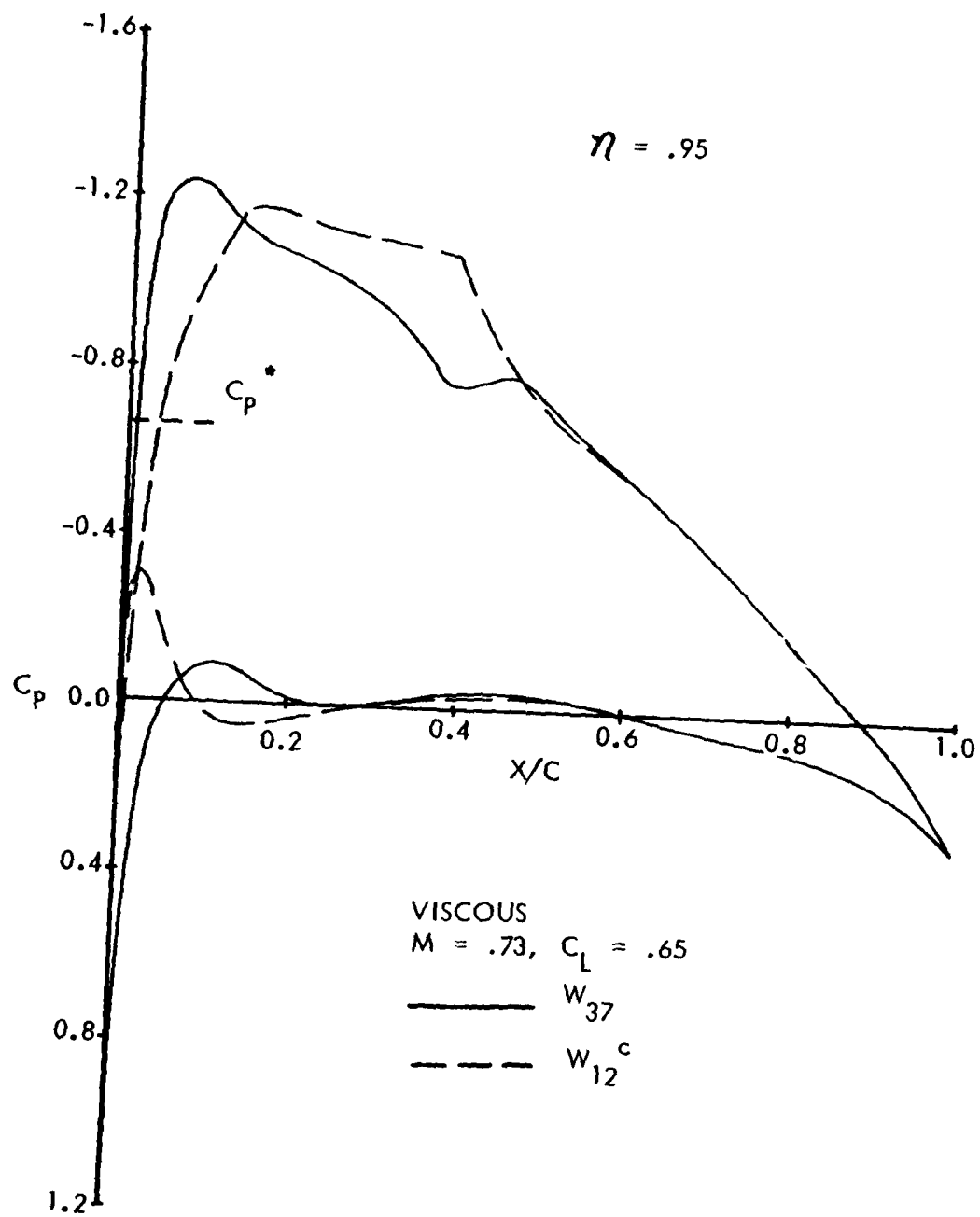
Figure 12. Effect of  $W^{37}$  Leading Edge Modifications on Chordwise Pressure Distributions



b.  $\eta = 0.625$   
 Figure 12. Continued



$c. \eta = 0.794$   
 Figure 12. Continued



d.  $\eta = 0.95$   
 Figure 12. Concluded

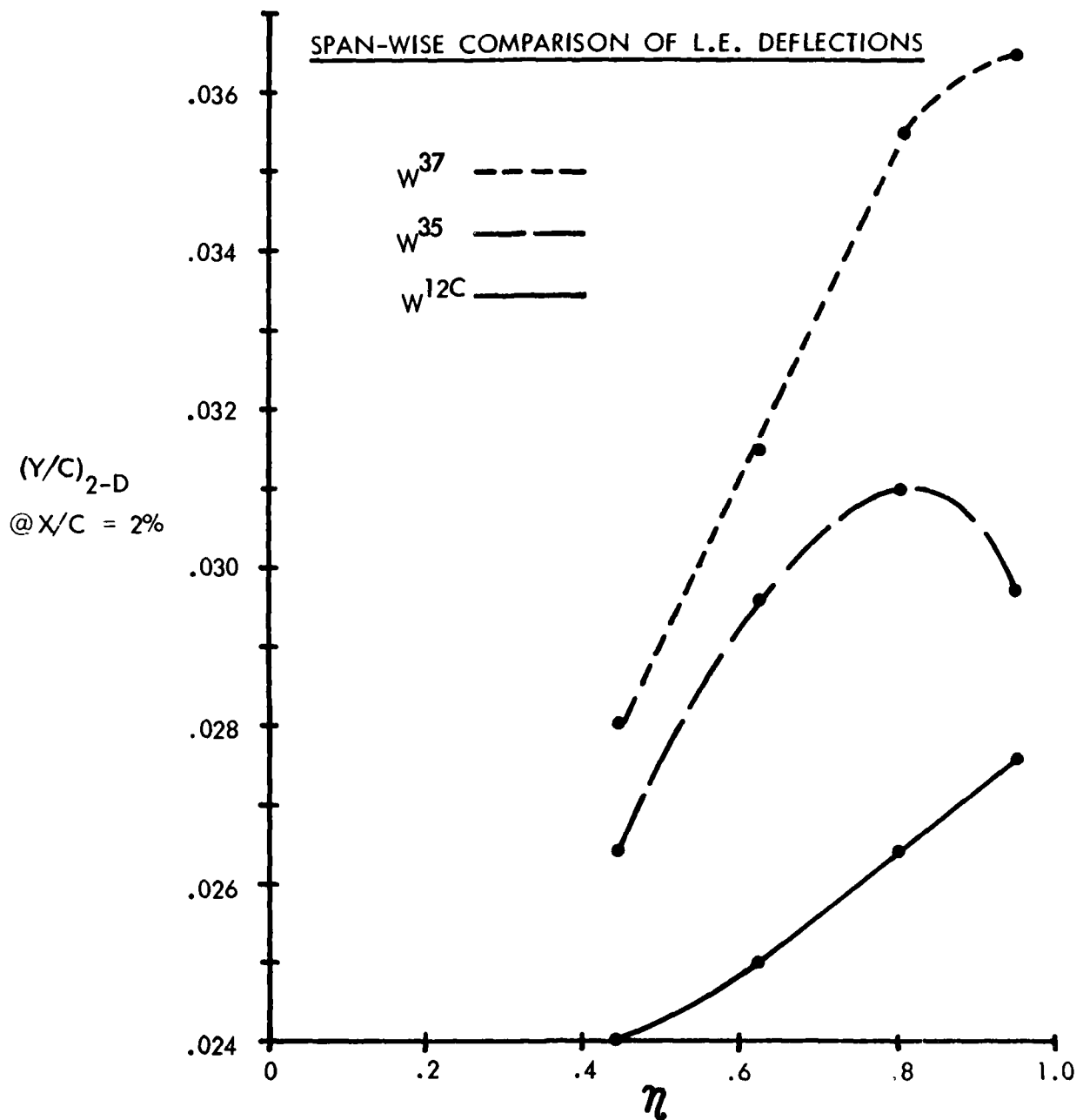


Figure 13. Comparison of Spanwise Variation of the 2% Ordinate for the Basic and Modified Leading Edges



$M_{2-D} = .73$ ,  $M_{3-D} = .79$   
 CRUISE  $C_L = .5$

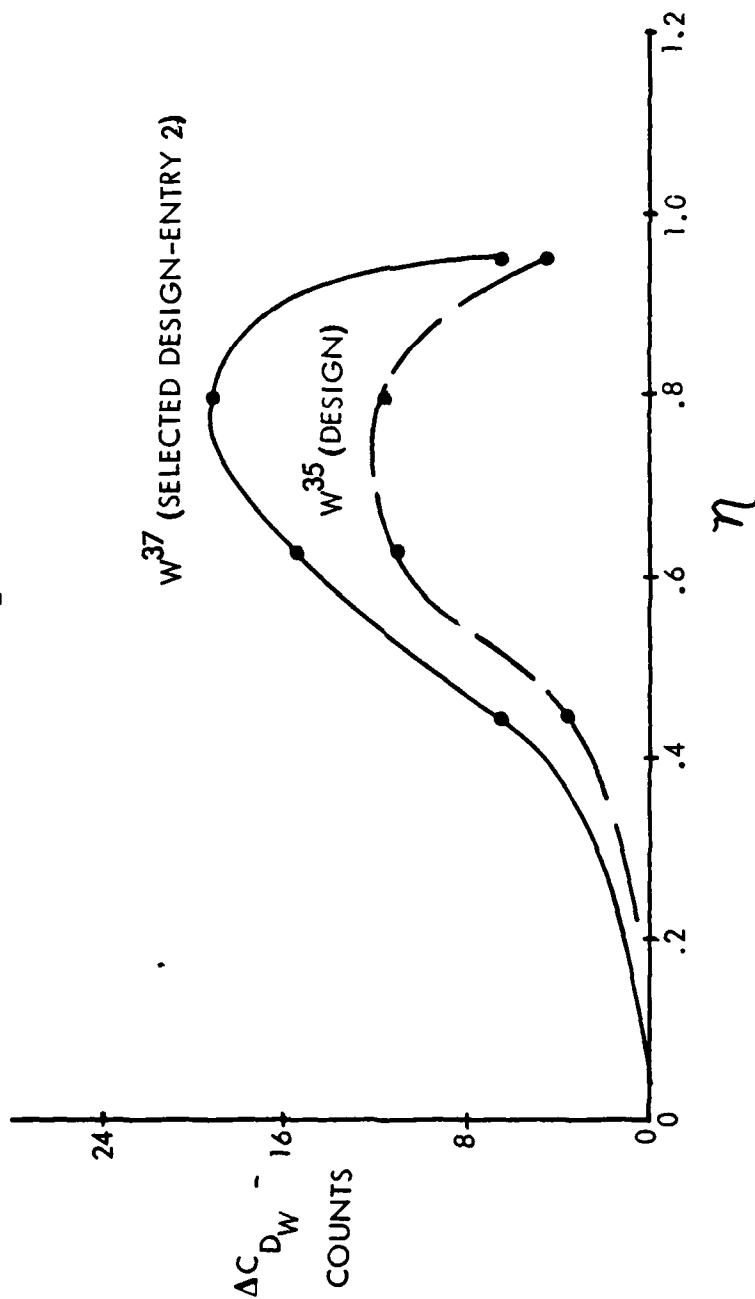


Figure 14. Comparison of Spanwise Variation of Wave Drag  
 Increments for the Modified Leading Edges  
 Relative to the Baseline

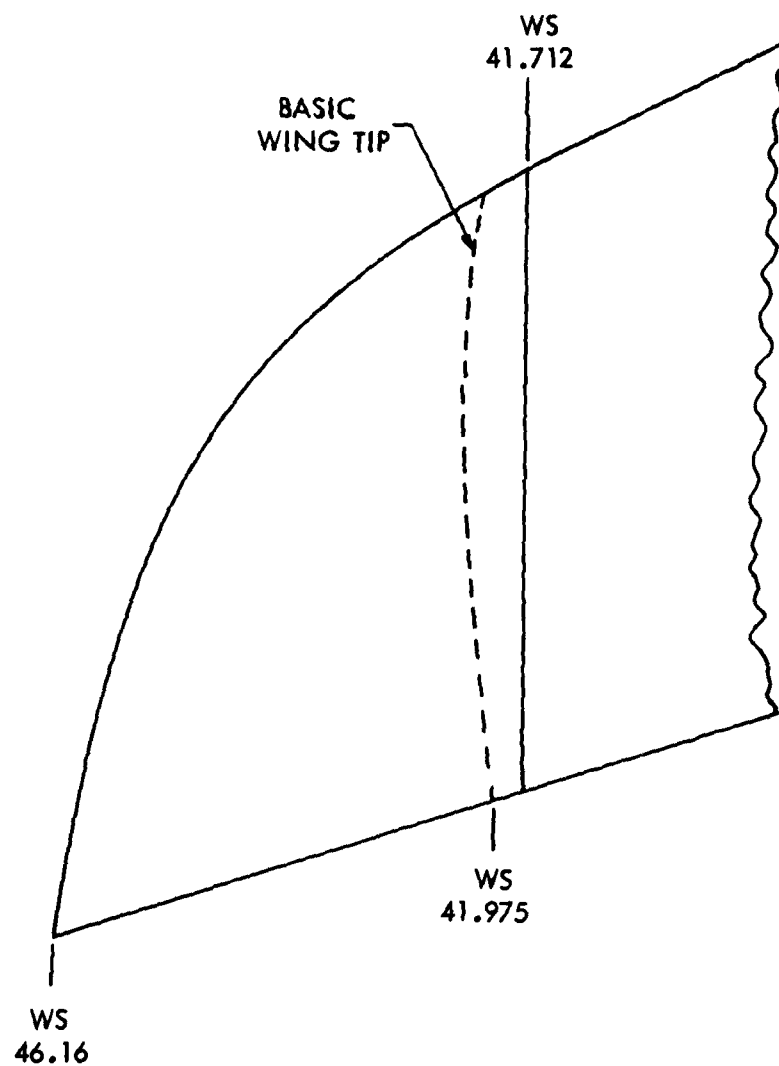
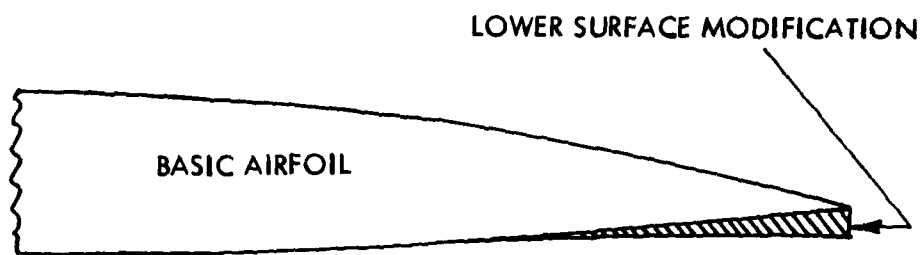
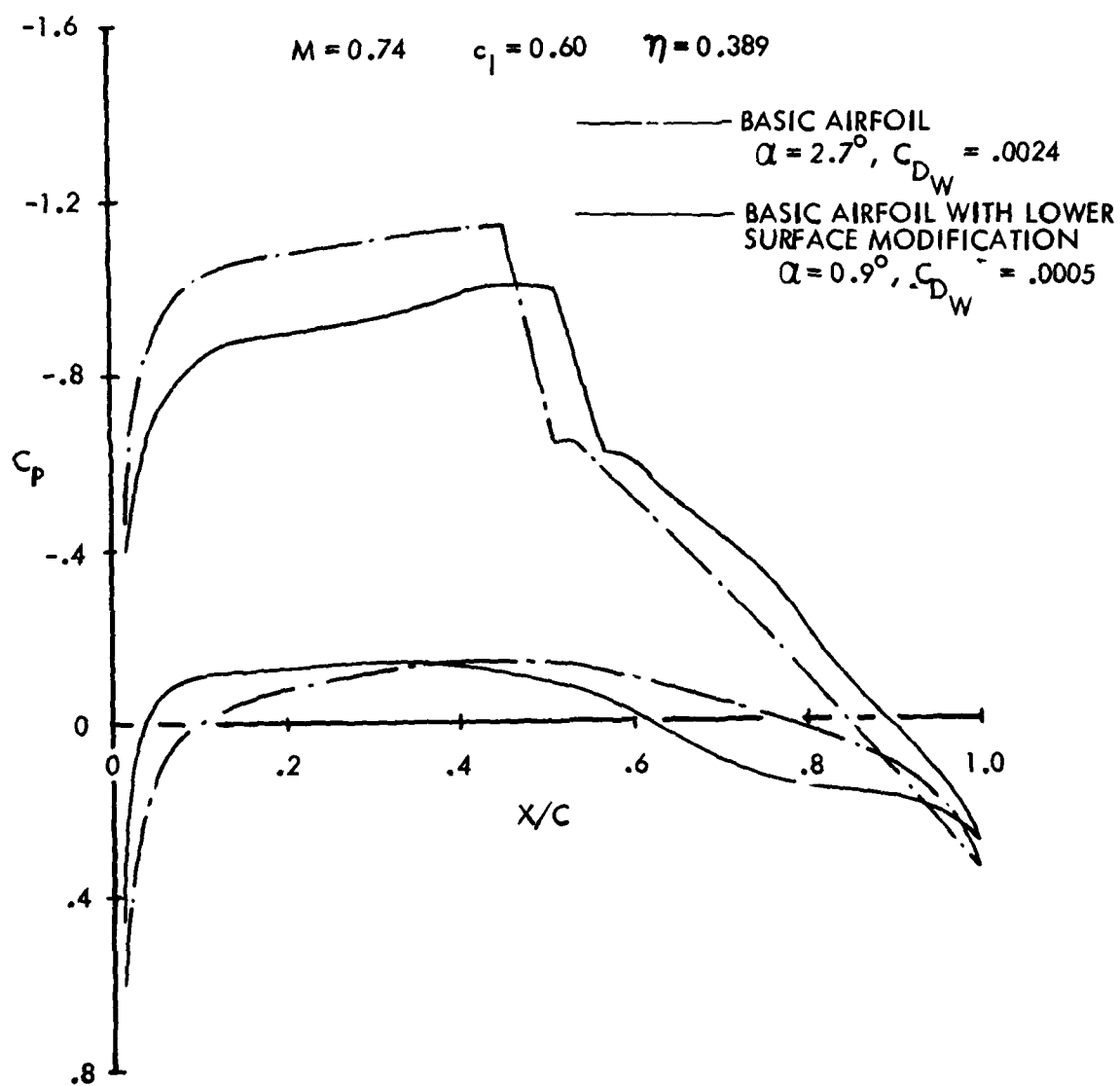


Figure 15 . Swept Wing Tip Extension Planform



a. Sketch of Lower Surface Modification



b. Effect on Theoretical Pressure Distribution

Figure 16 . C-141 Airfoil Aft Camber Change

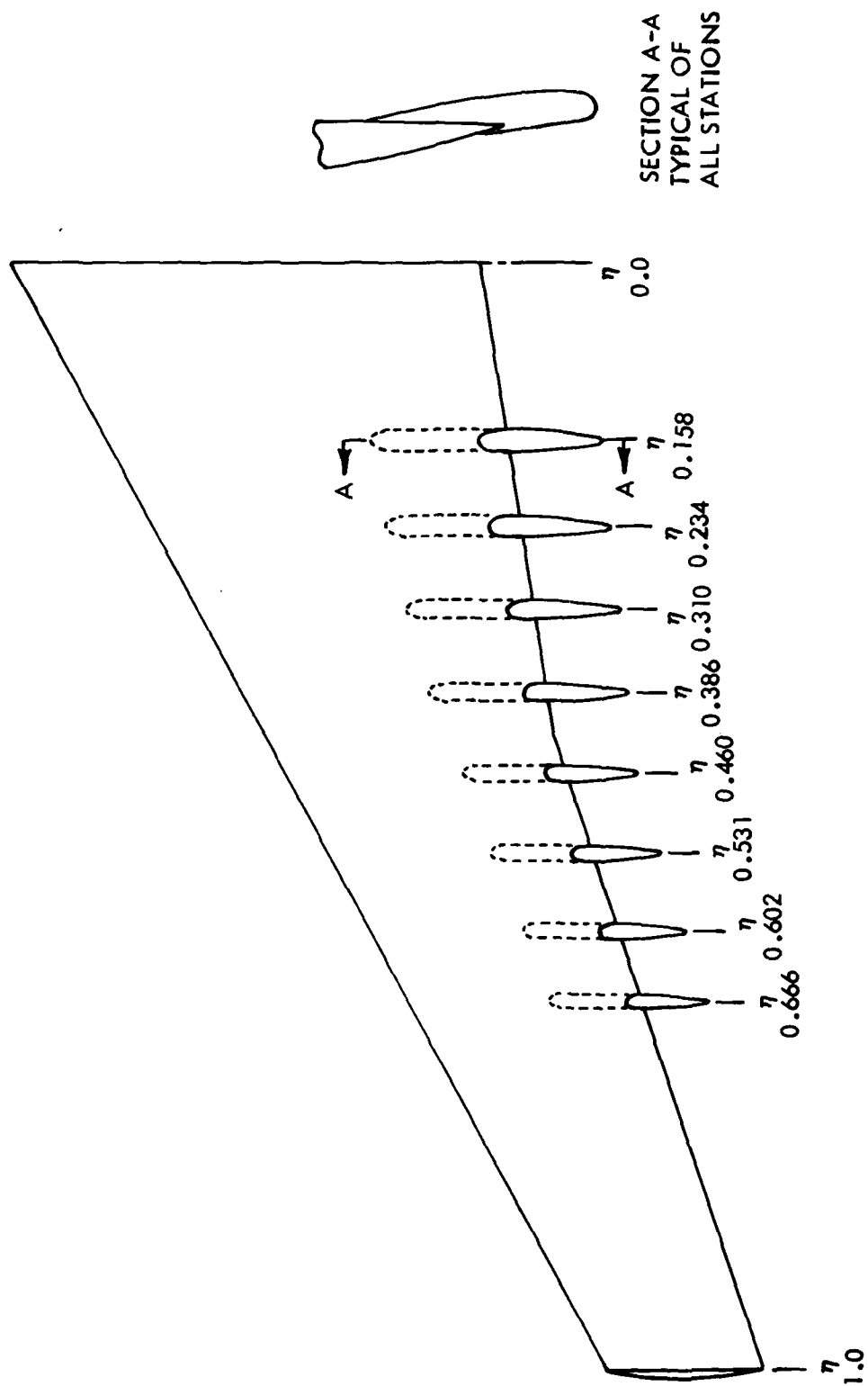


Figure 17 . Sketch of Anti-Drage Body Locations

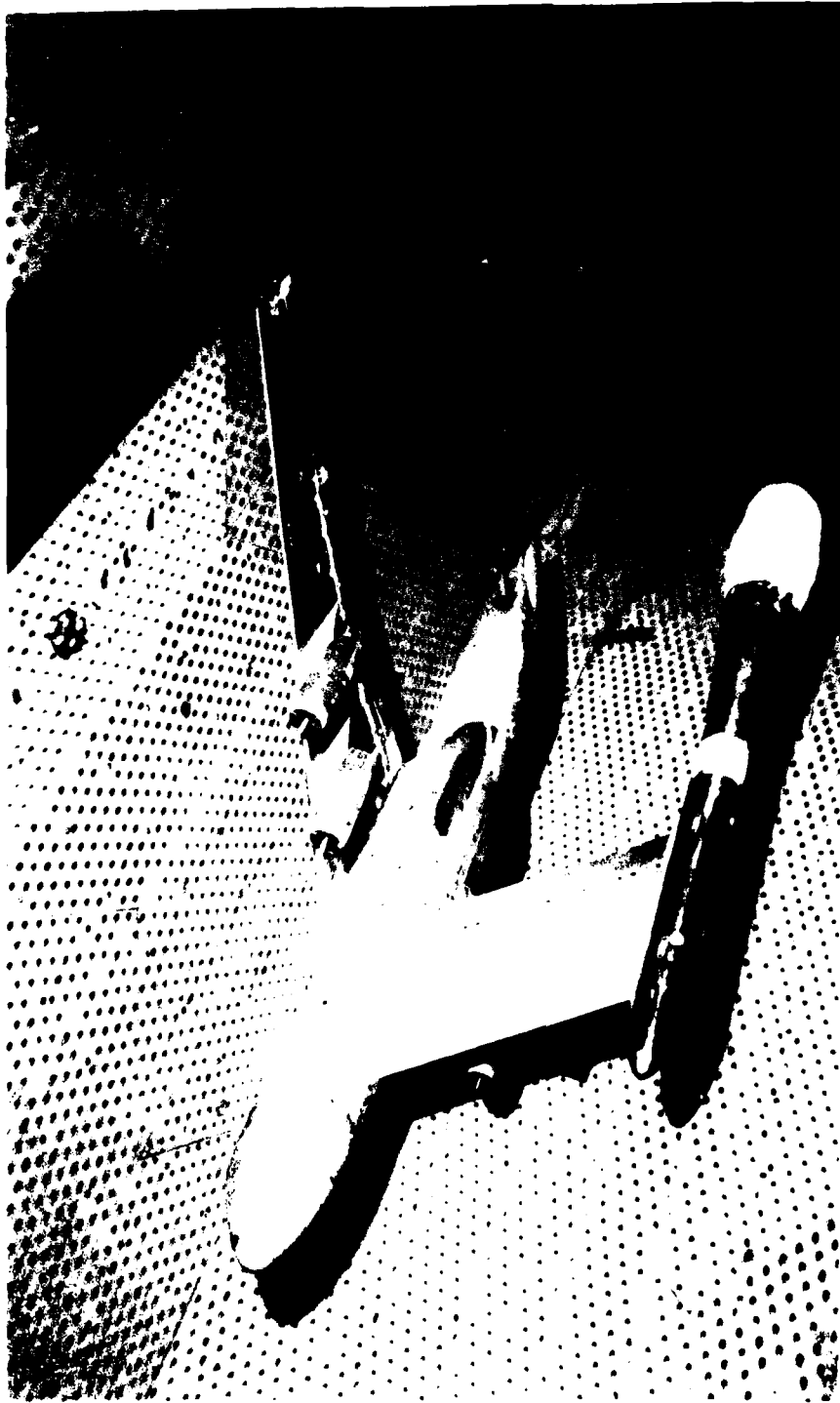
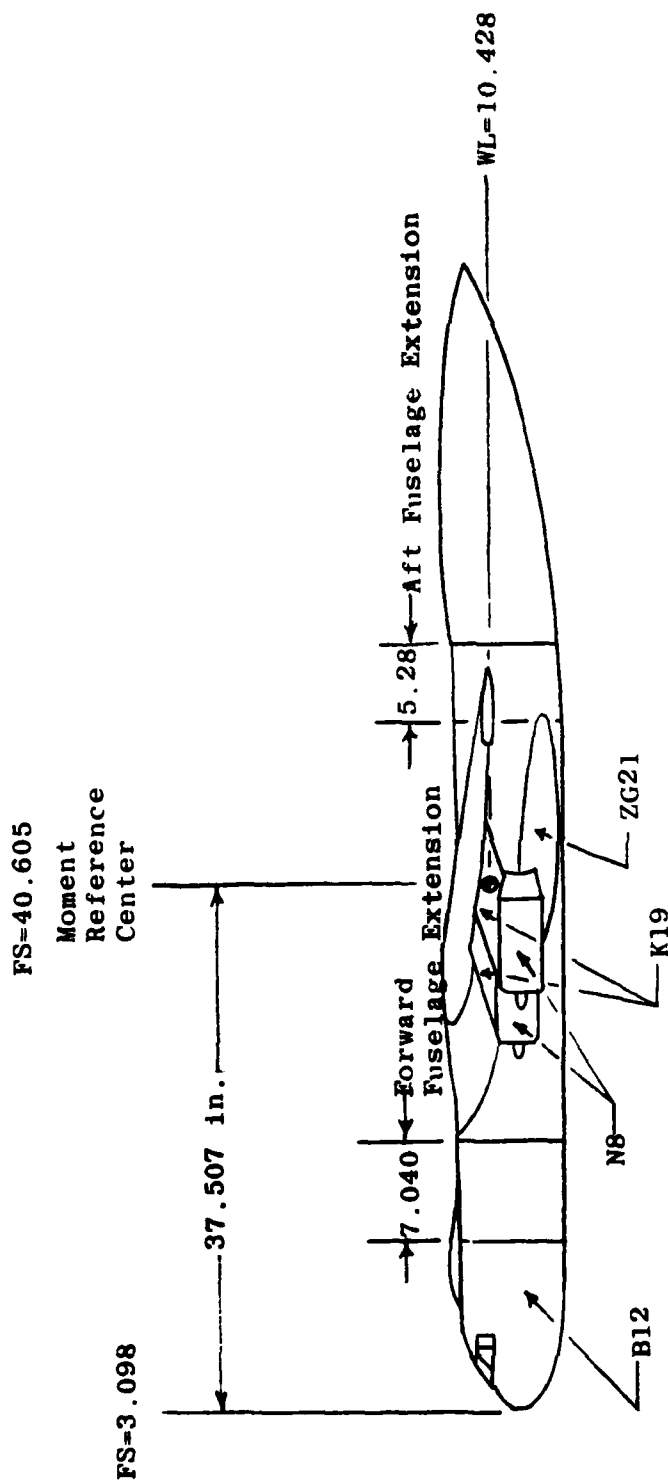


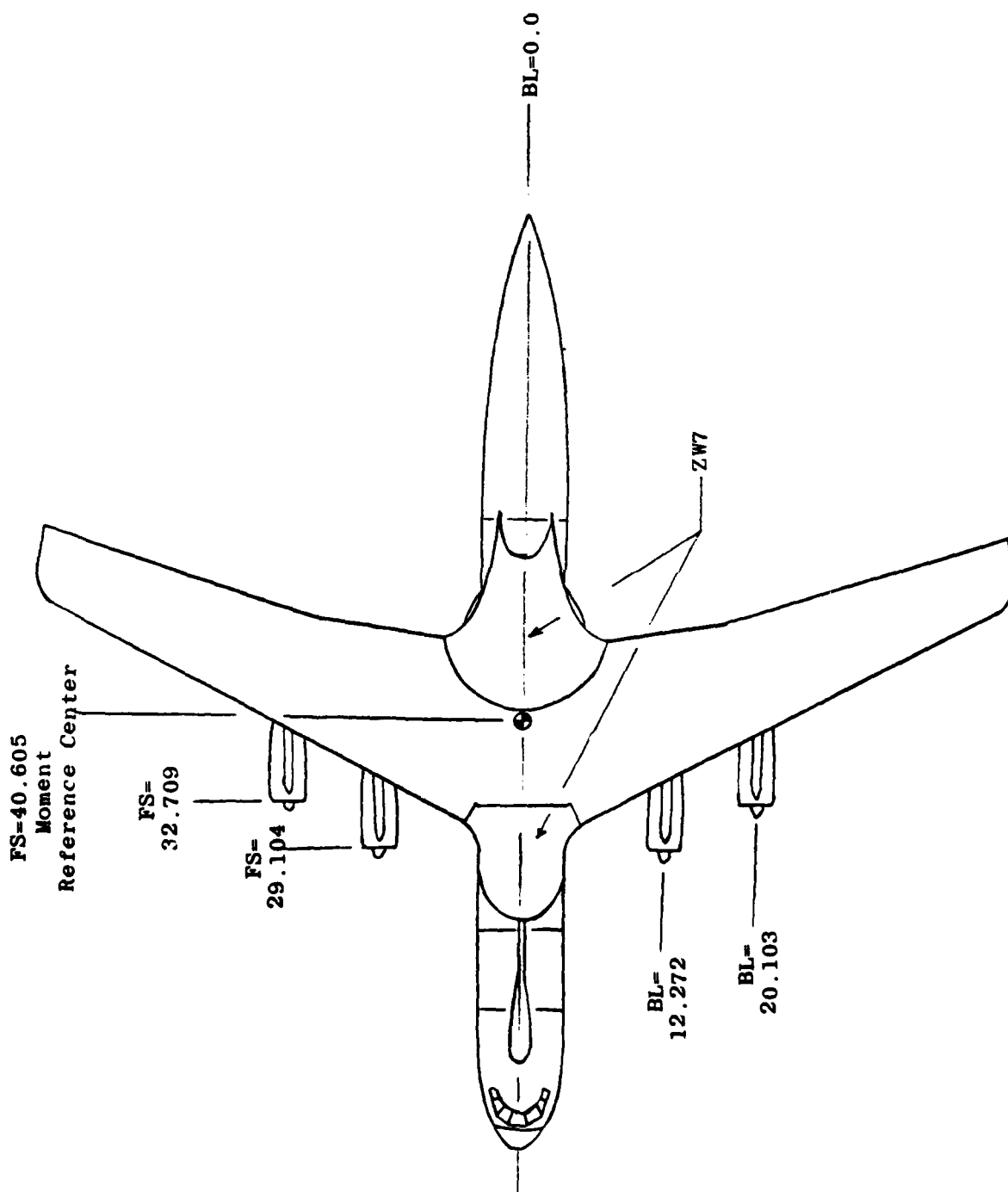
Figure 18. Photograph of the 0.044 Scale C-141B Model  
Installed at AEDC 16T



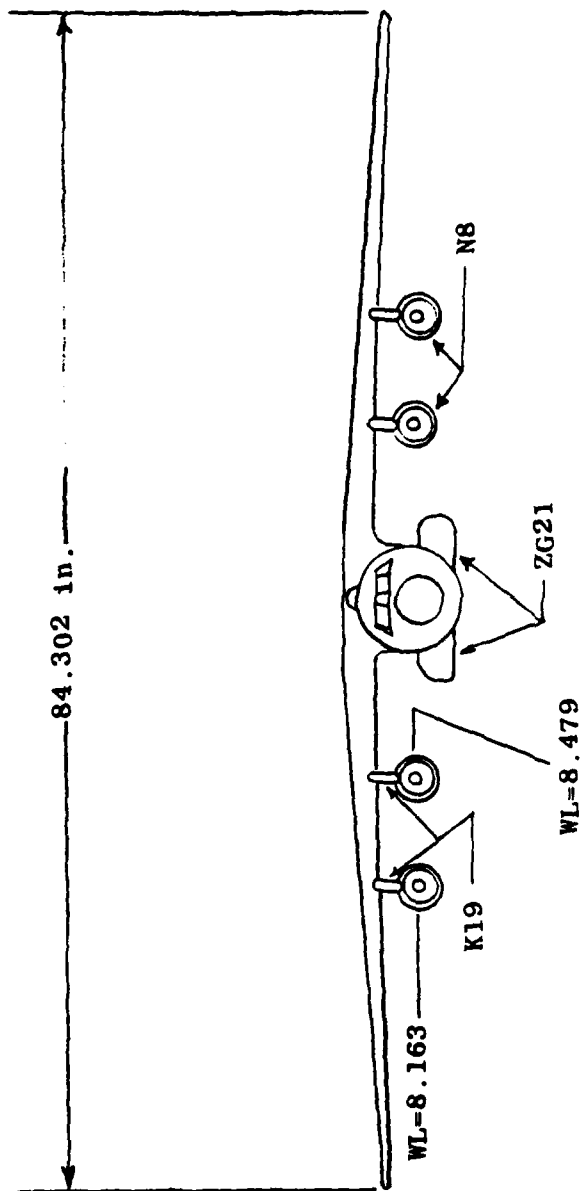
All Dimensions in Inches,  
Model Scale

a. Side View

Figure 19. Three View Sketch of the 0.044 Scale C-141B Model



b. Top View  
Figure 19. Continued



All Dimensions in Inches,  
Model Scale

c. Front View  
Figure 19. Concluded



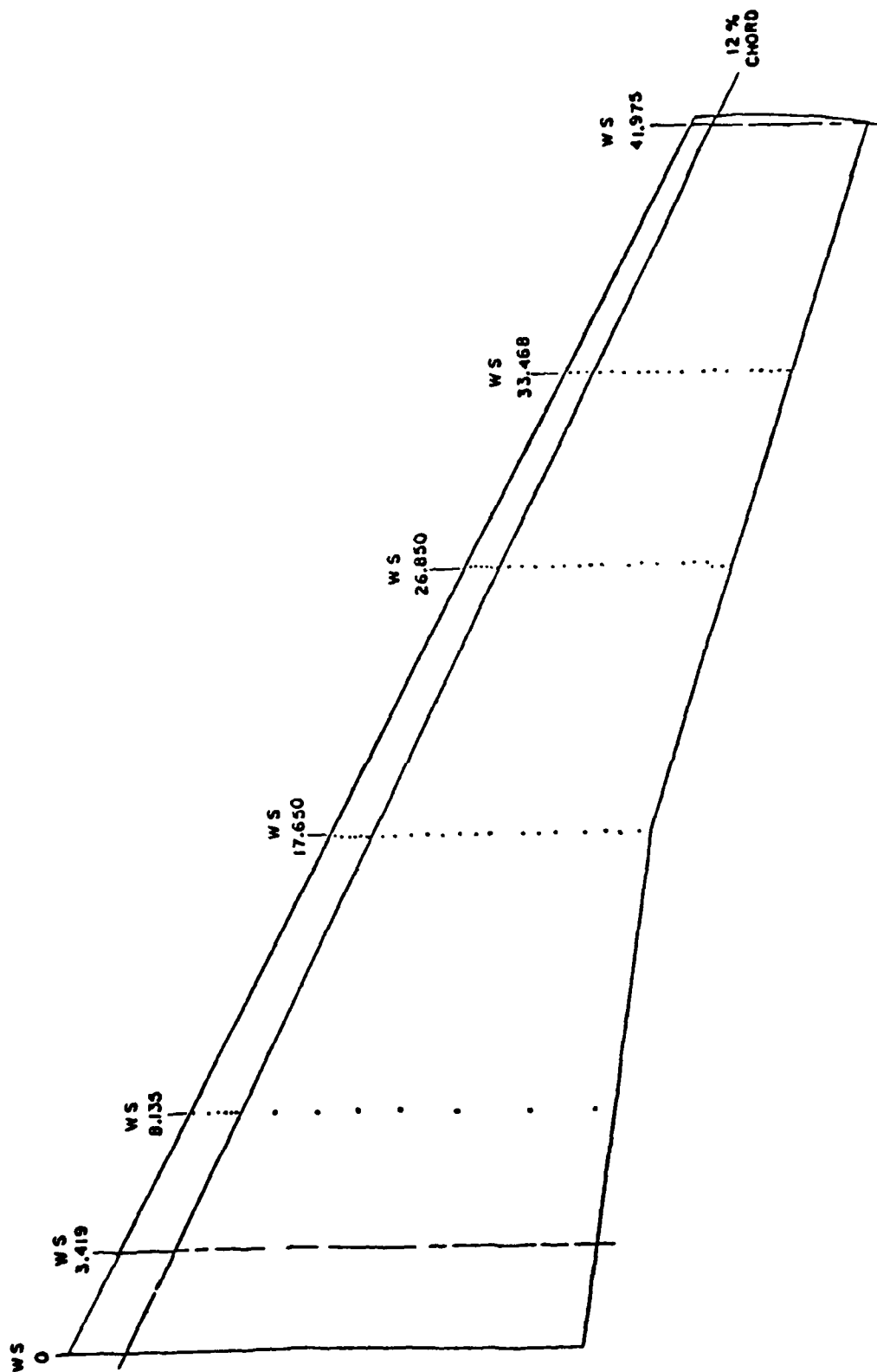
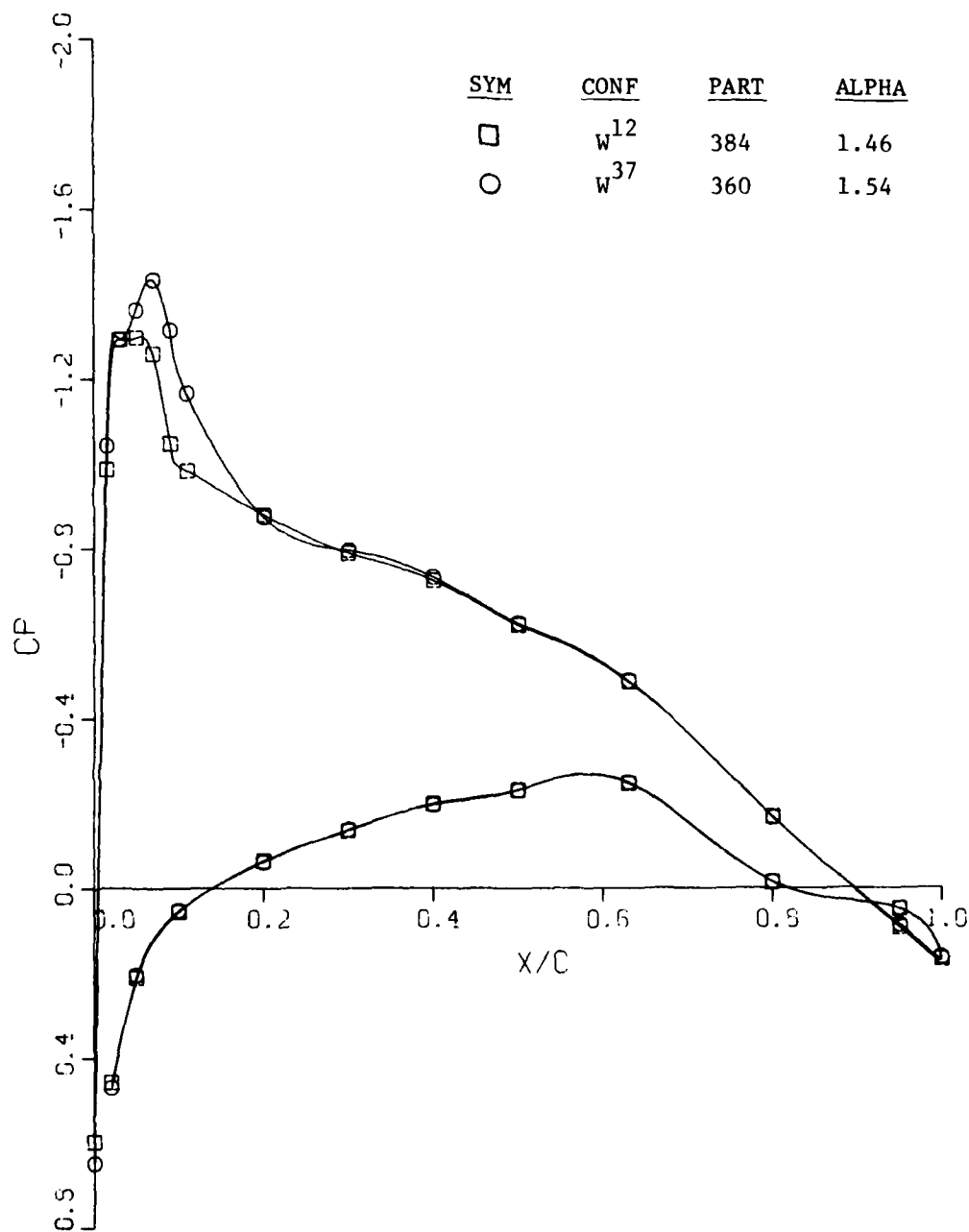
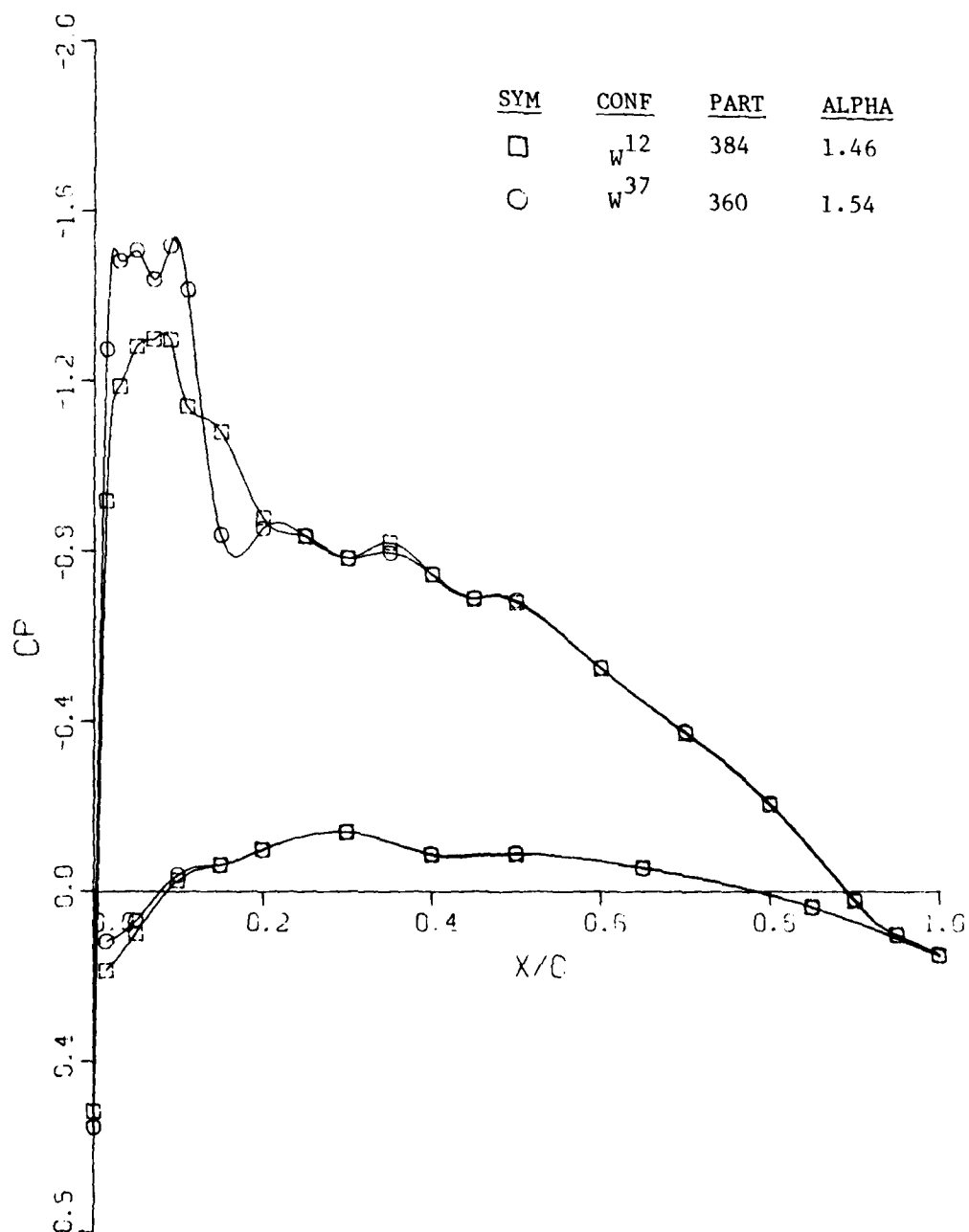


Figure 20. Pressure Instrumentation



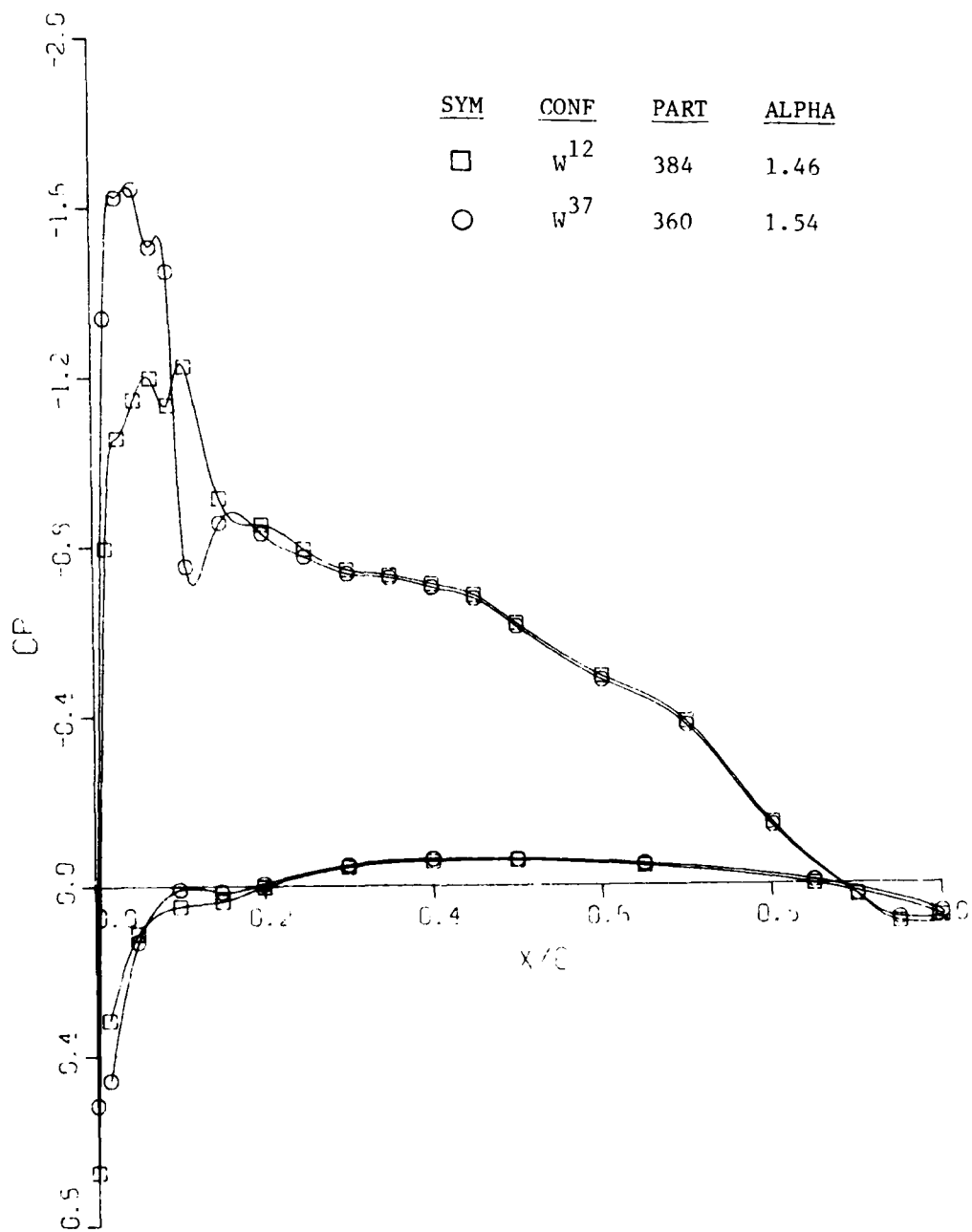
a.  $\eta = 0.193$

Figure 21. Effect of W<sup>37</sup> Leading Edge Modification on Chordwise Pressure Distributions at M = 0.70



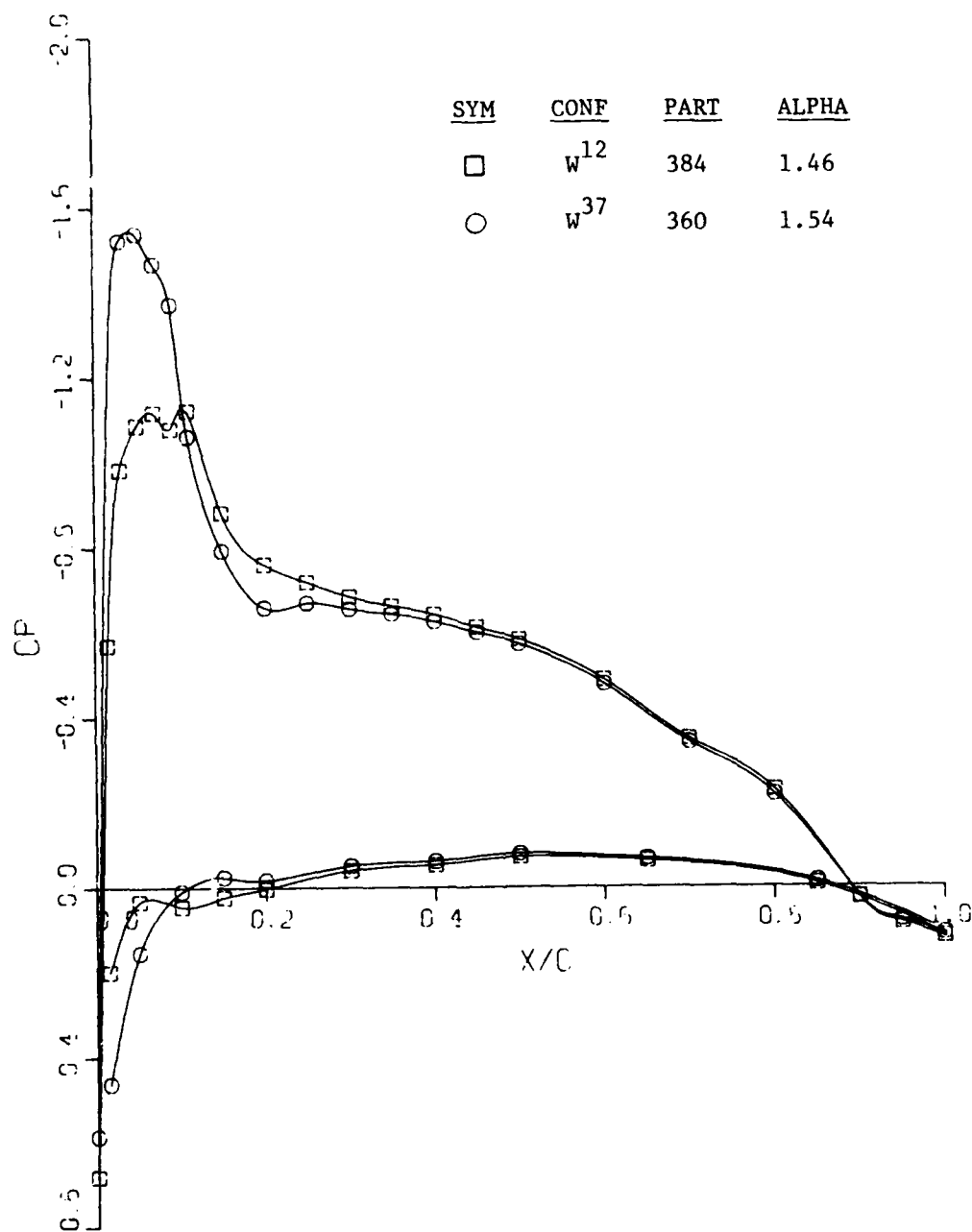
b.  $\eta = 0.418$

Figure 21. Continued



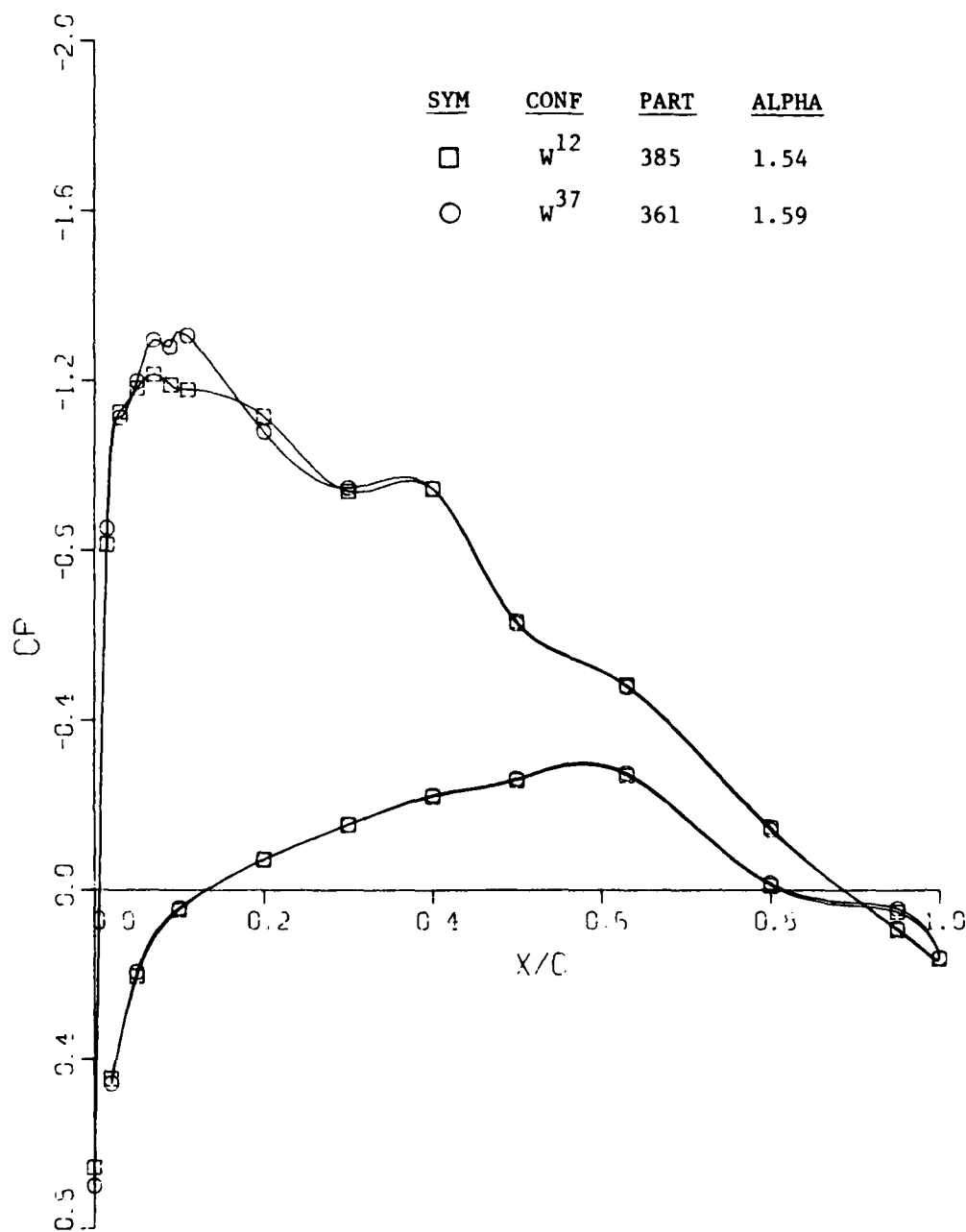
c.  $\eta = 0.636$

Figure 21. Continued

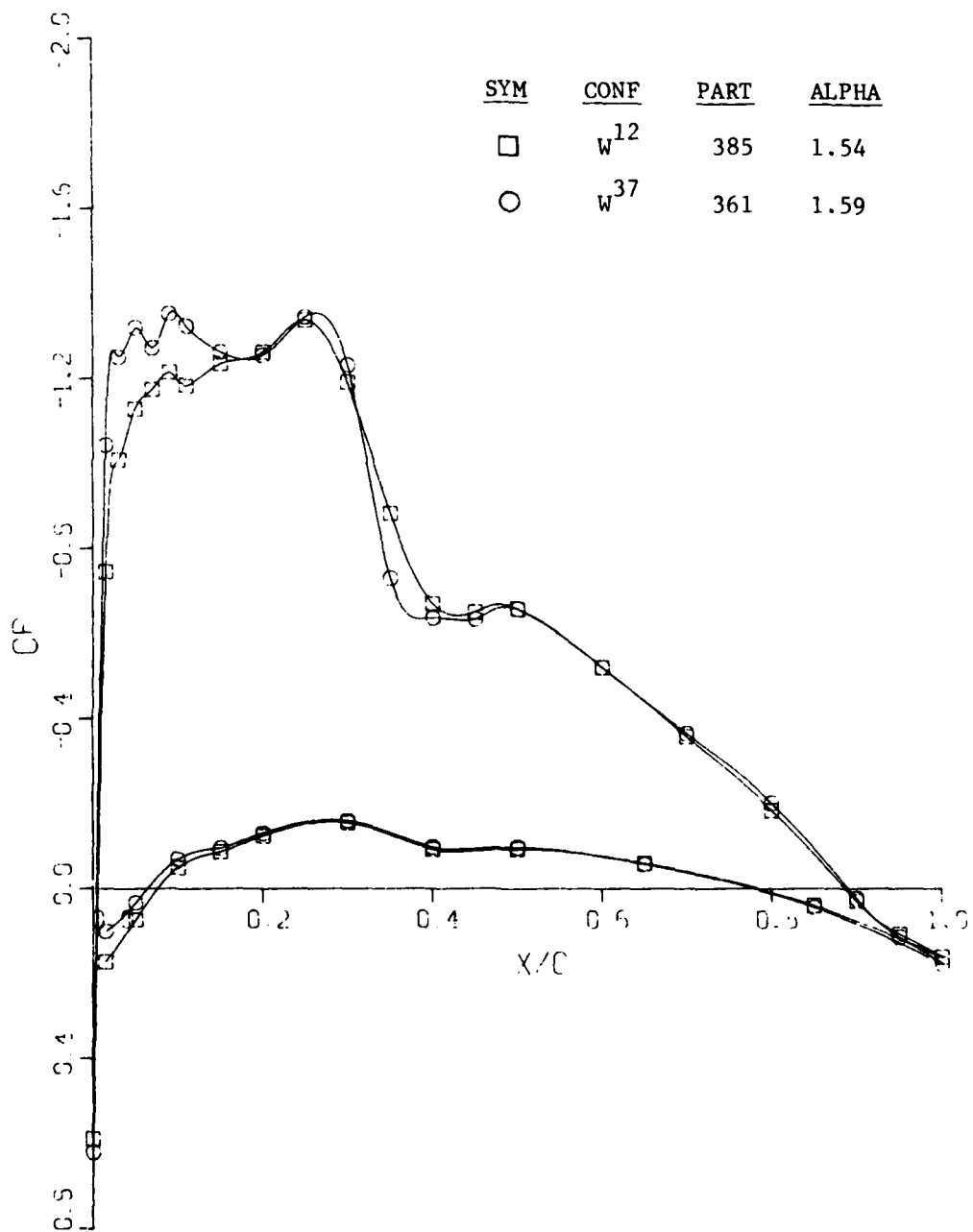


d.  $\eta = 0.793$

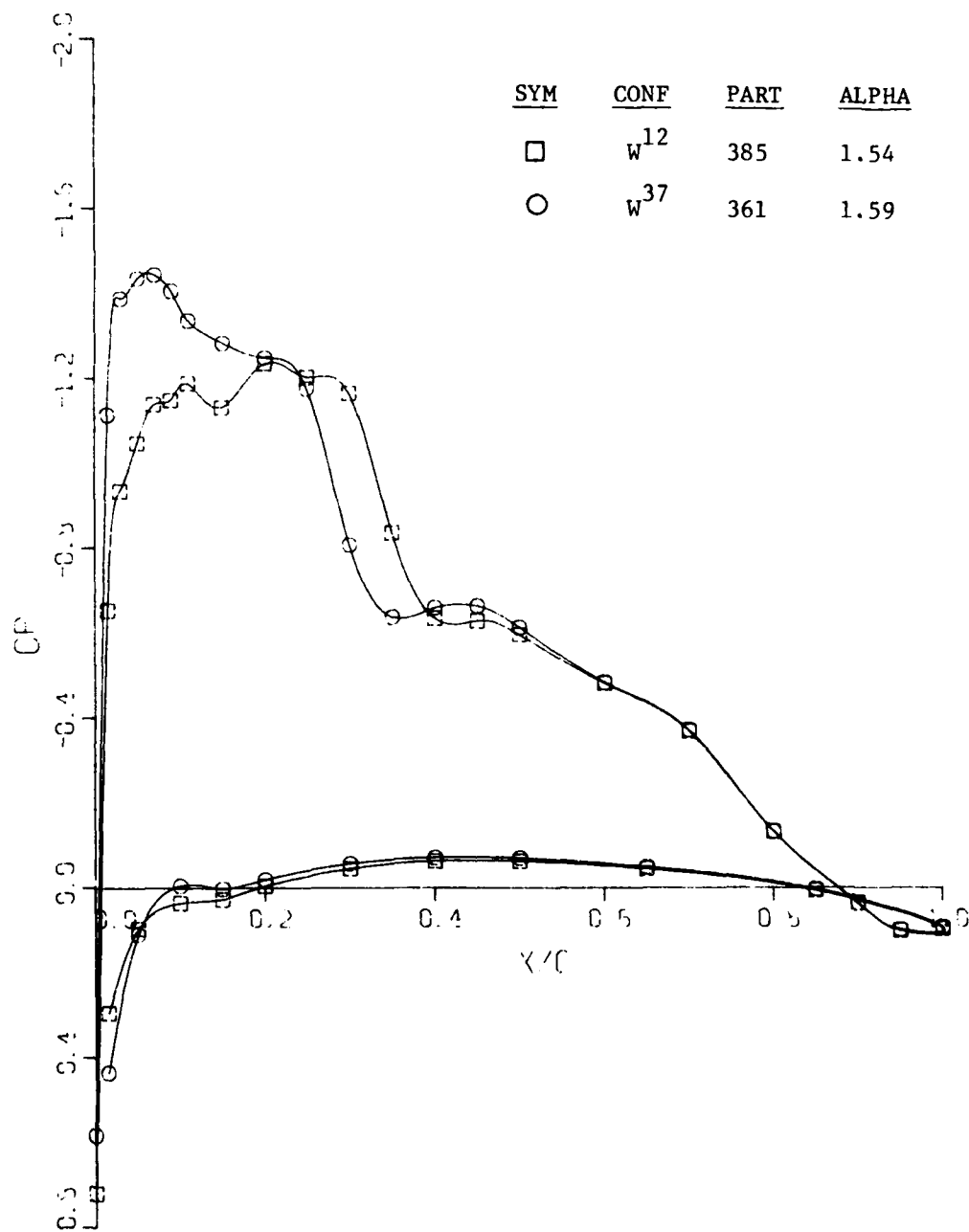
Figure 21. Concluded



a.  $\eta = 0.193$   
 Figure 22. Effect of  $W^{37}$  Leading Edge Modification  
 on Chordwise Pressure Distributions at  
 $M = 0.75$

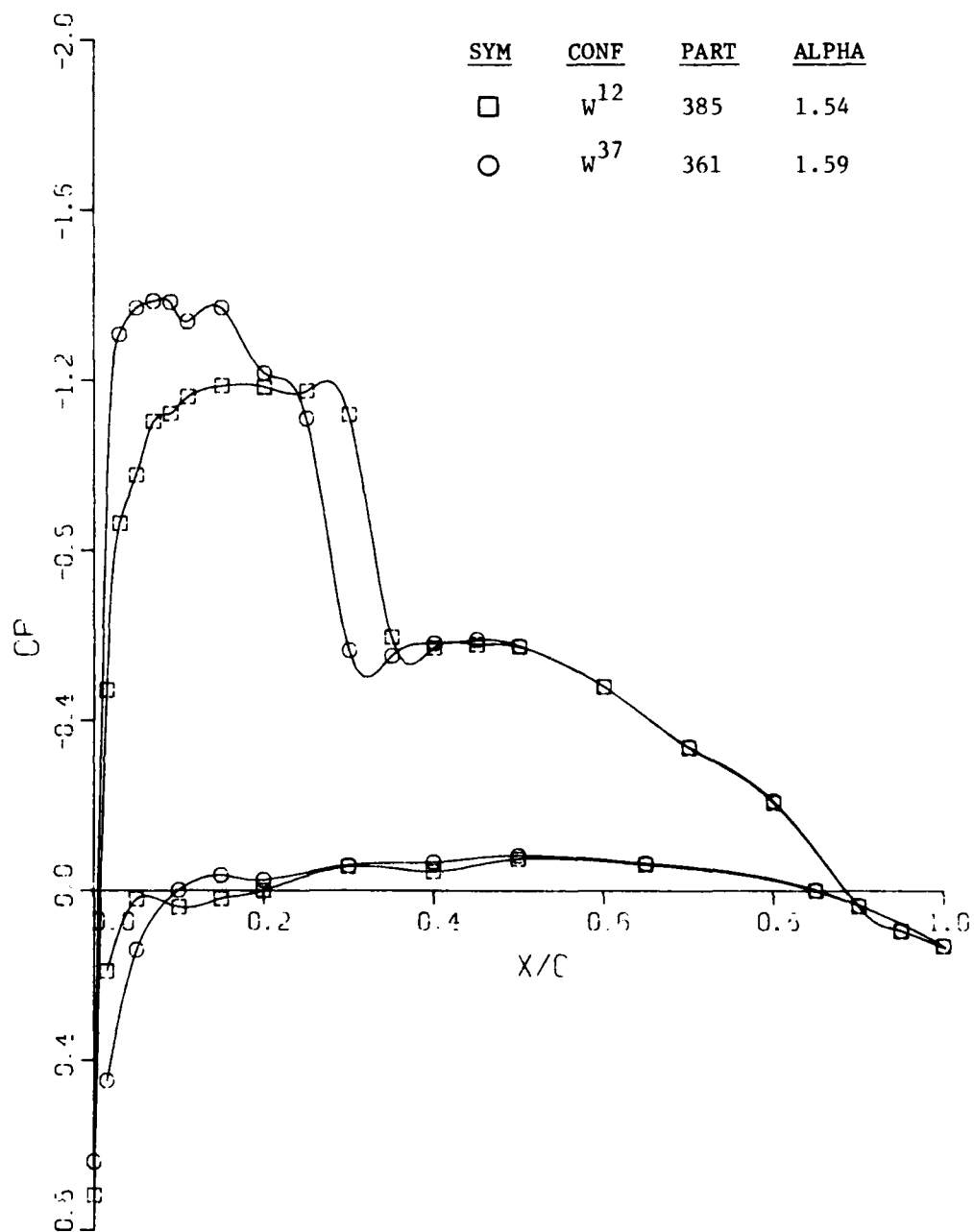


b.  $\eta = 0.418$   
Figure 22. Continued



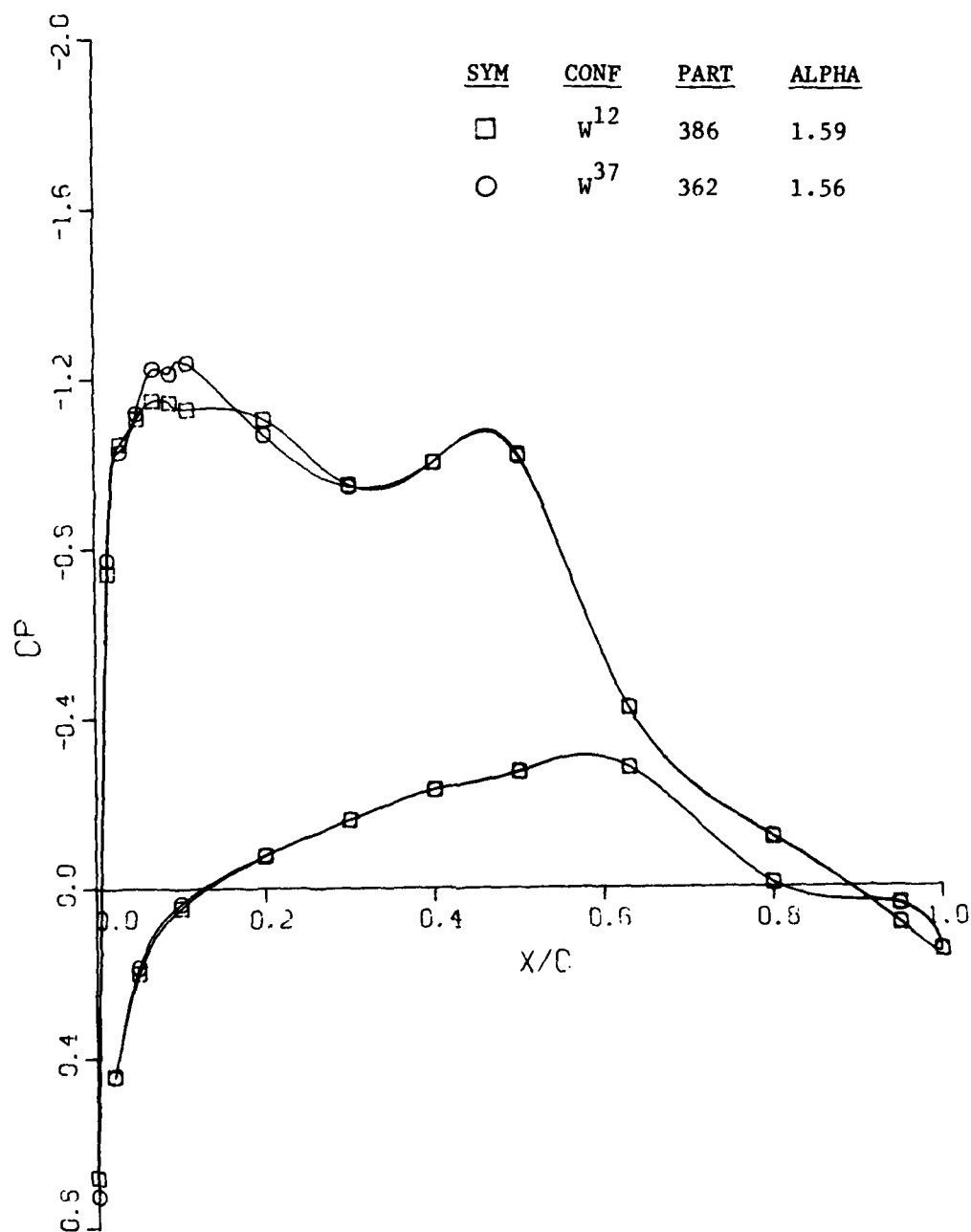
c.  $\eta = 0.636$   
Figure 22. Continued





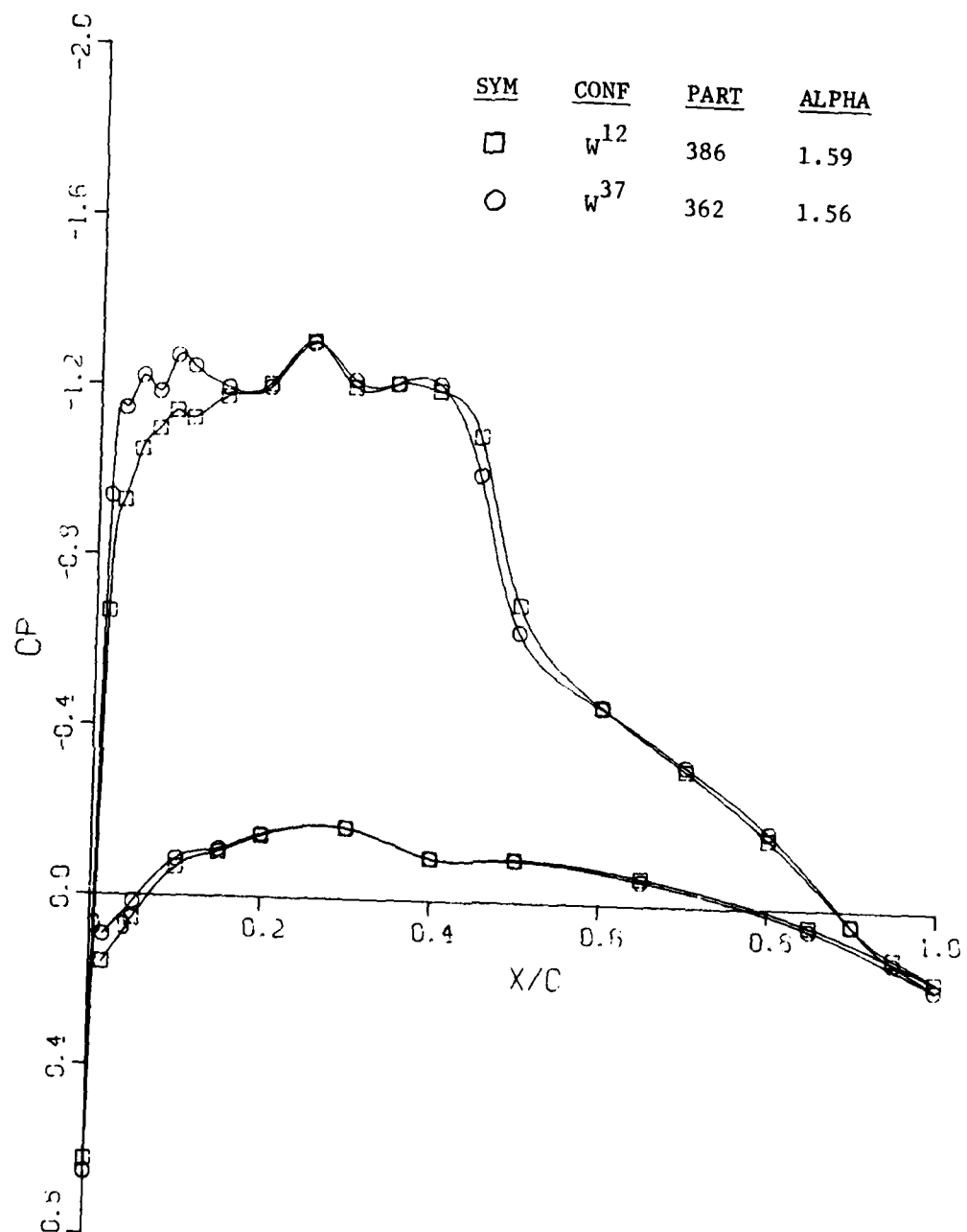
d.  $\eta = 0.793$

Figure 22. Concluded



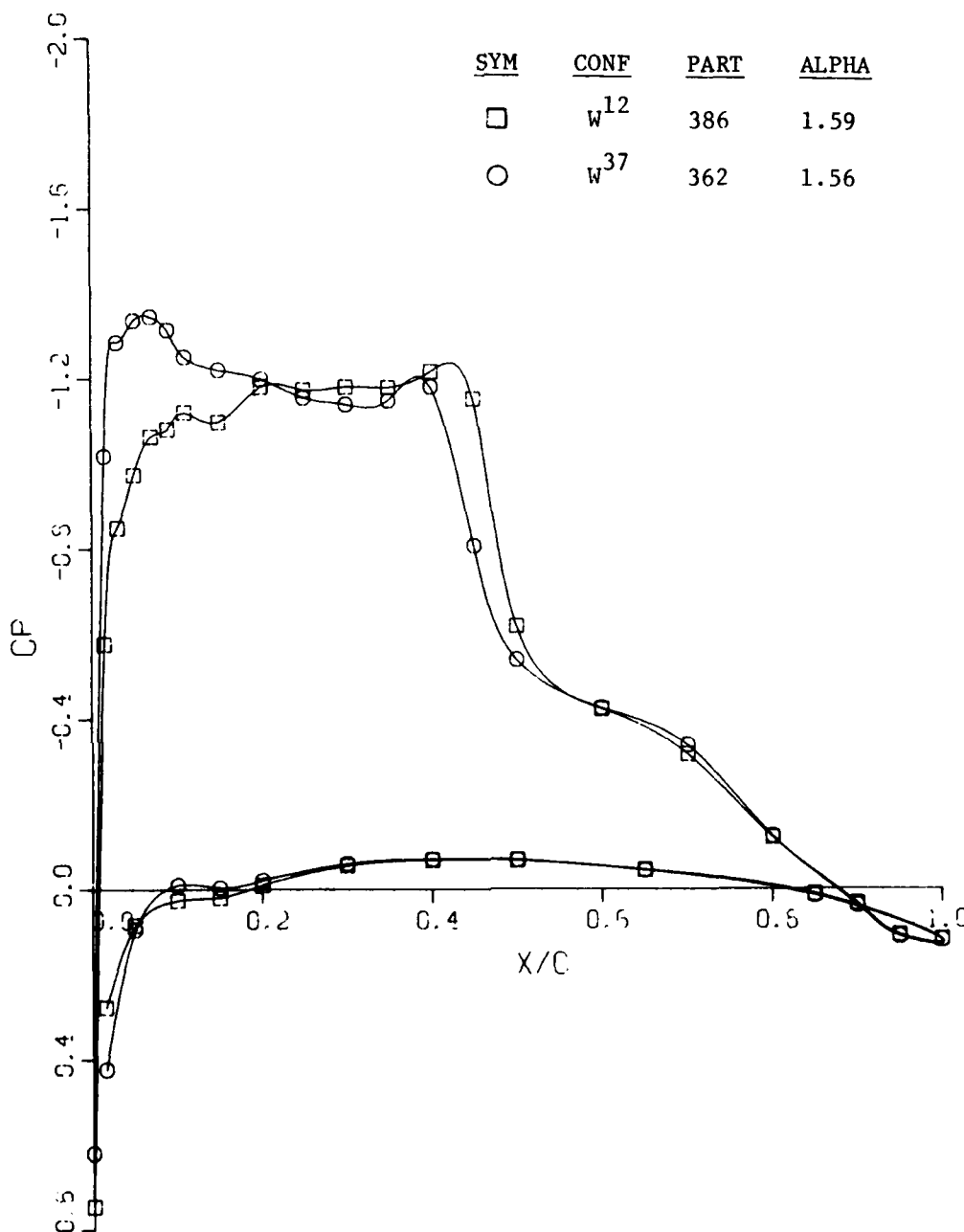
a.  $\eta = 0.193$

Figure 23. Effect of  $W^{37}$  Leading Edge Modification on Chordwise Pressure Distributions at  $M = 0.77$



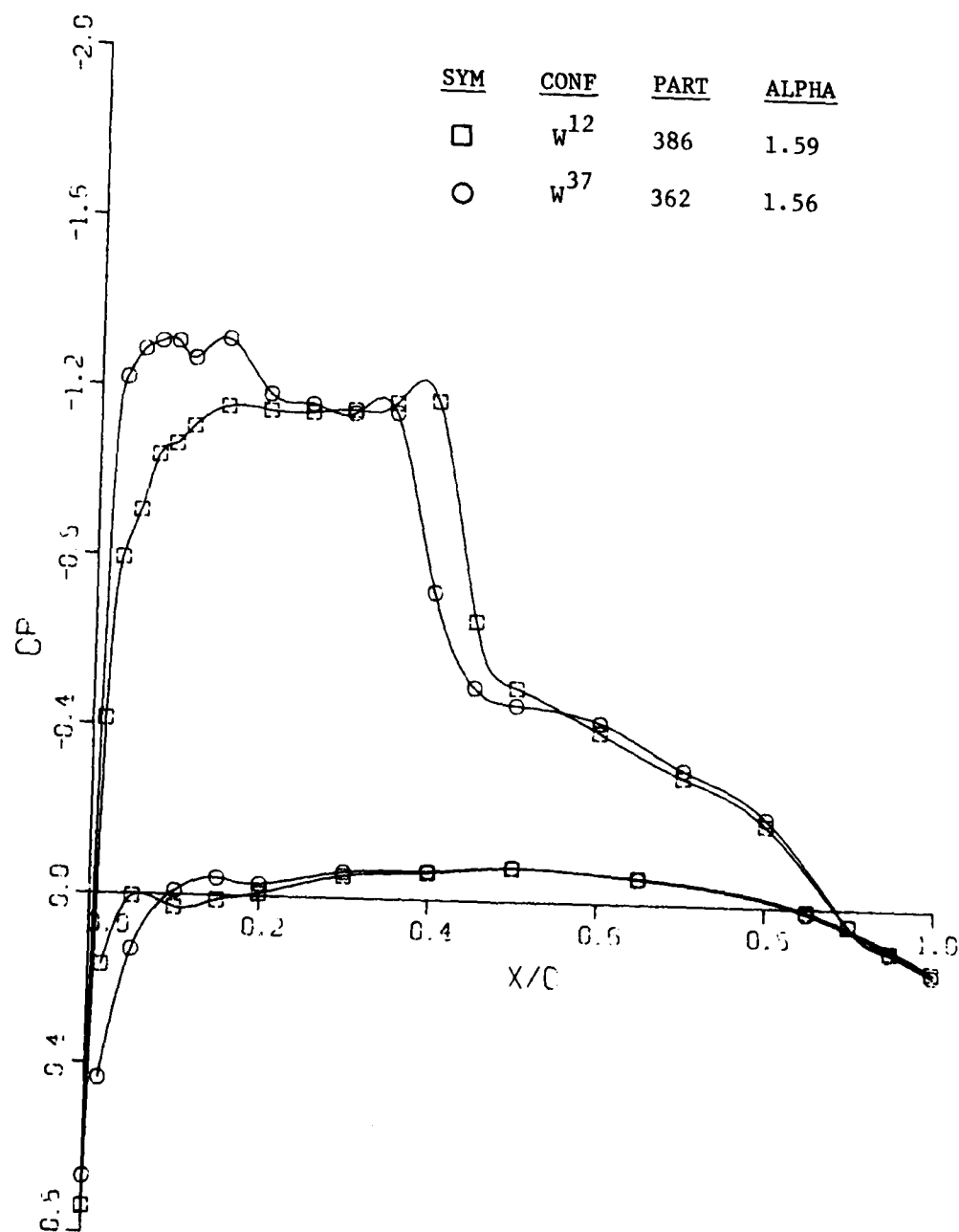
b.  $\eta = 0.418$

Figure 23. Continued

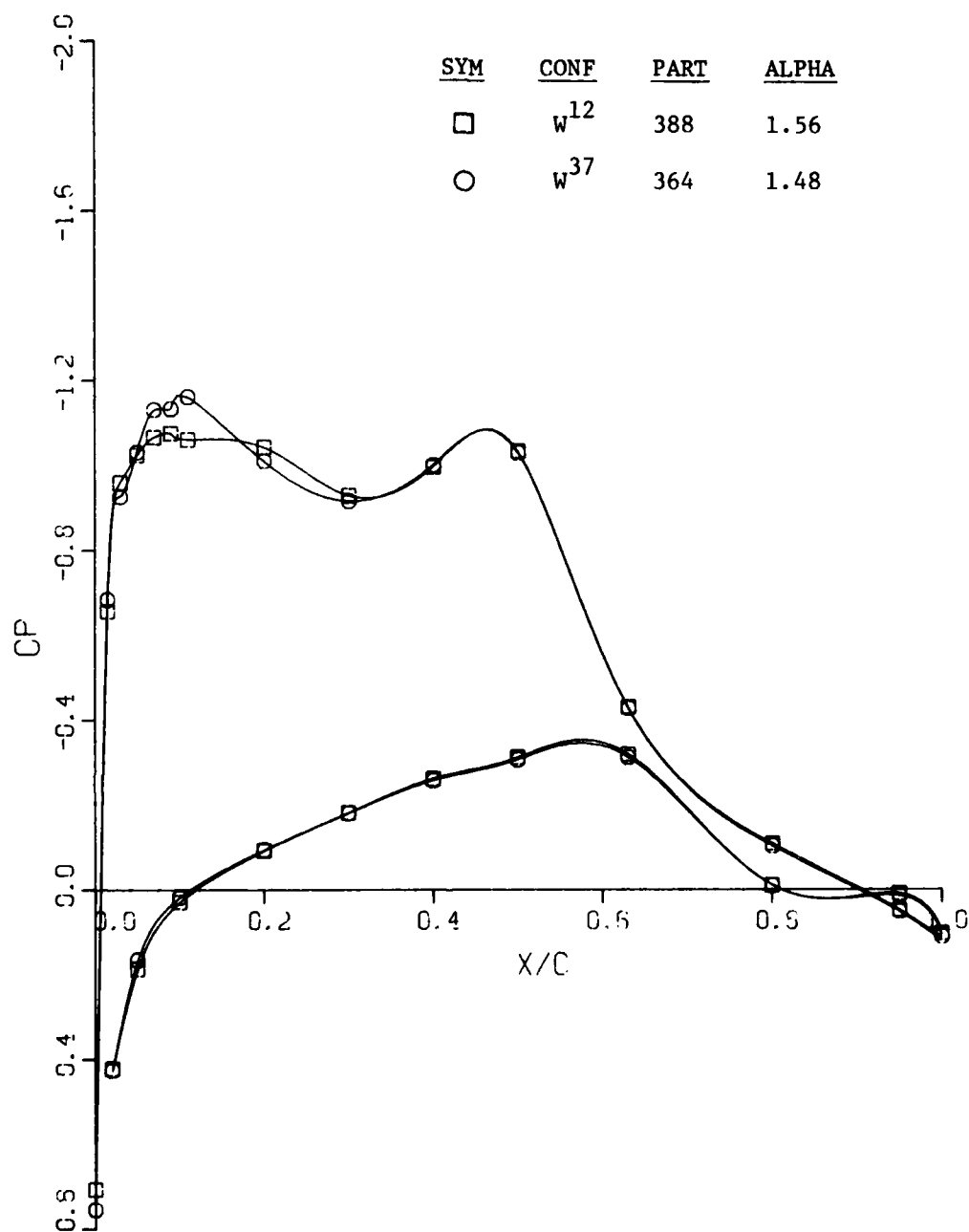


c.  $\eta = 0.636$

Figure 23. Continued

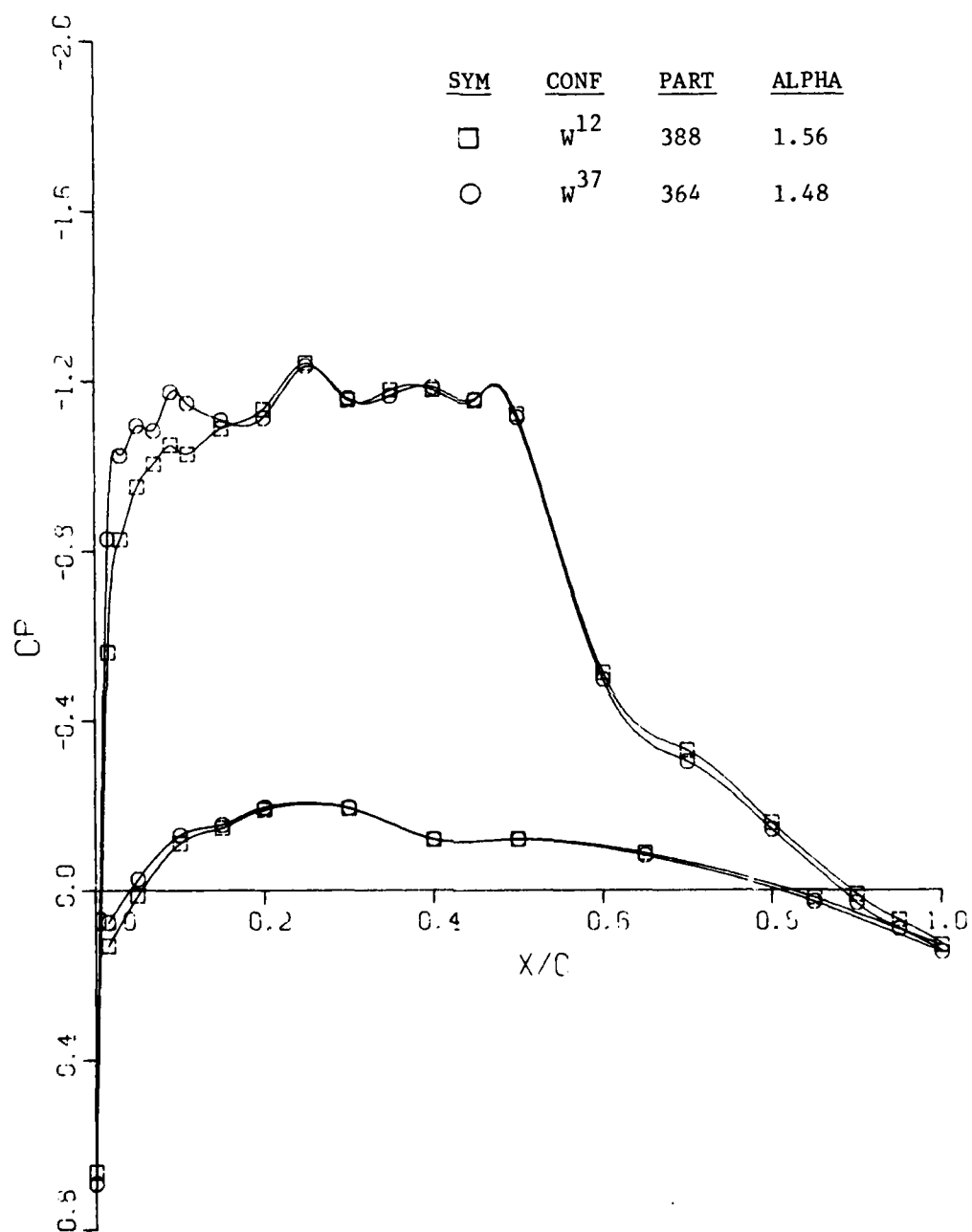


d.  $\eta = 0.793$   
 Figure 23. Concluded



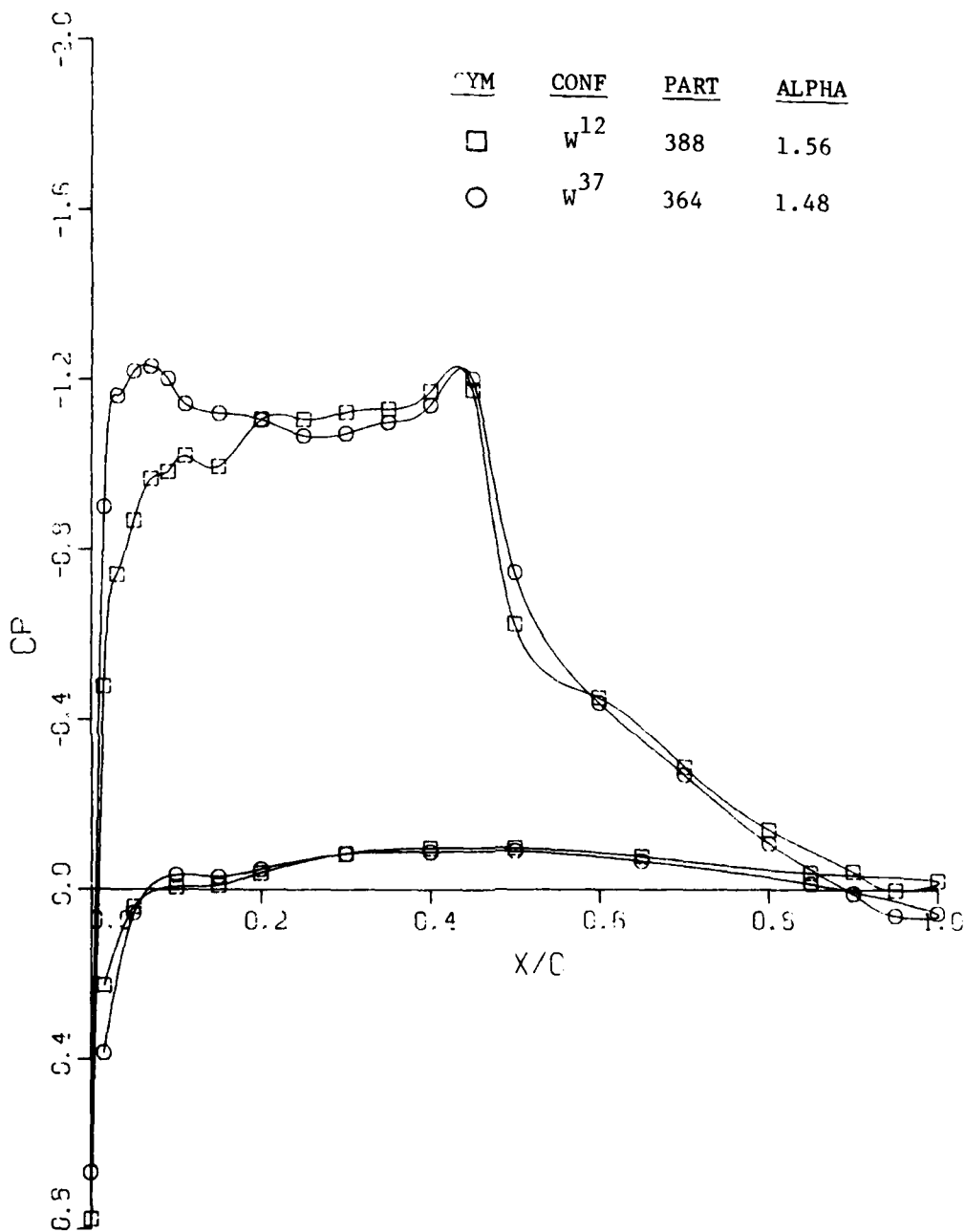
a.  $\eta = 0.193$

Figure 24. Effect of W<sup>37</sup> Leading Edge Modification on Chordwise Pressure Distributions at  $M = 0.79$



a.  $\eta = 0.418$

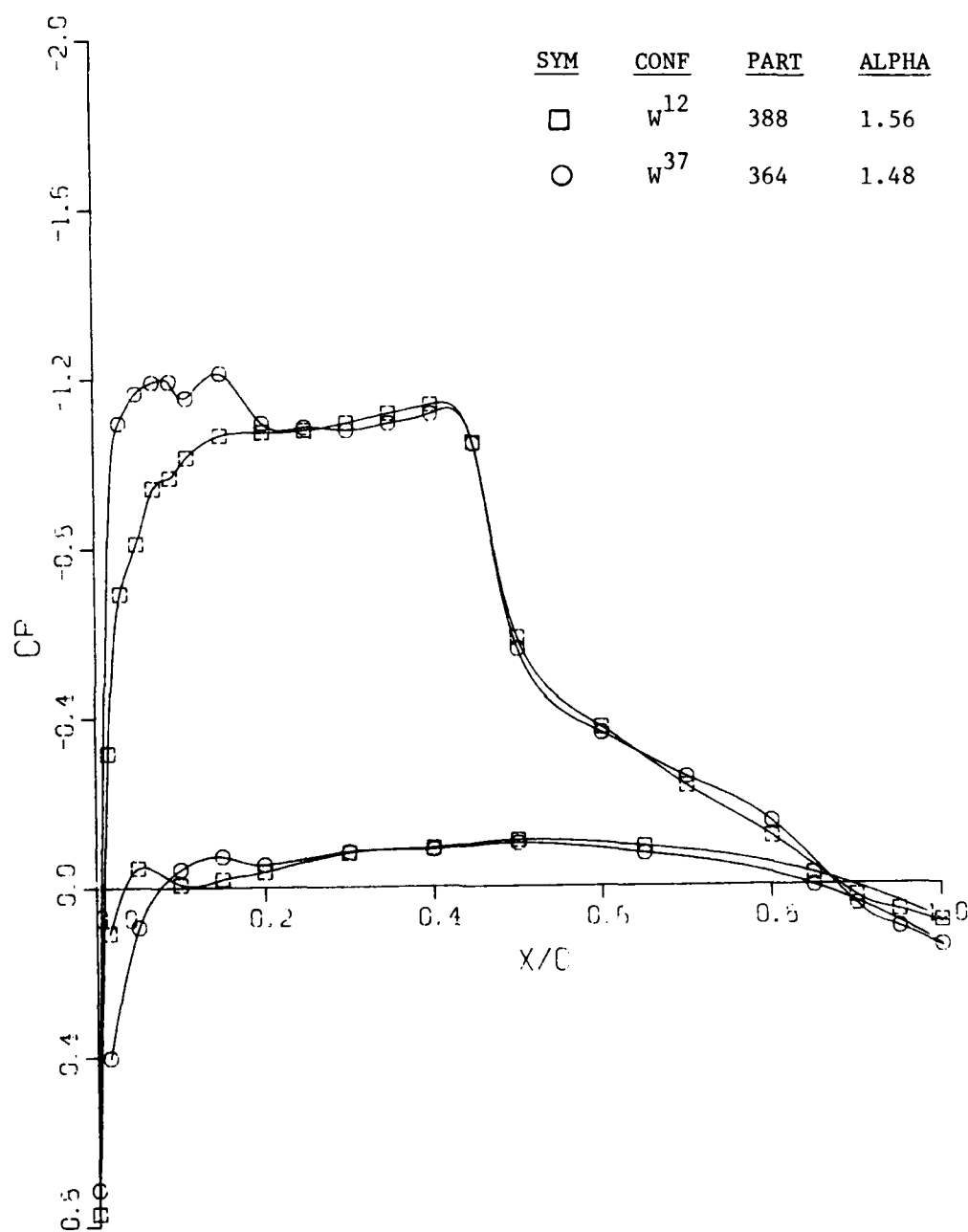
Figure 24. Continued



c.  $\eta = 0.636$

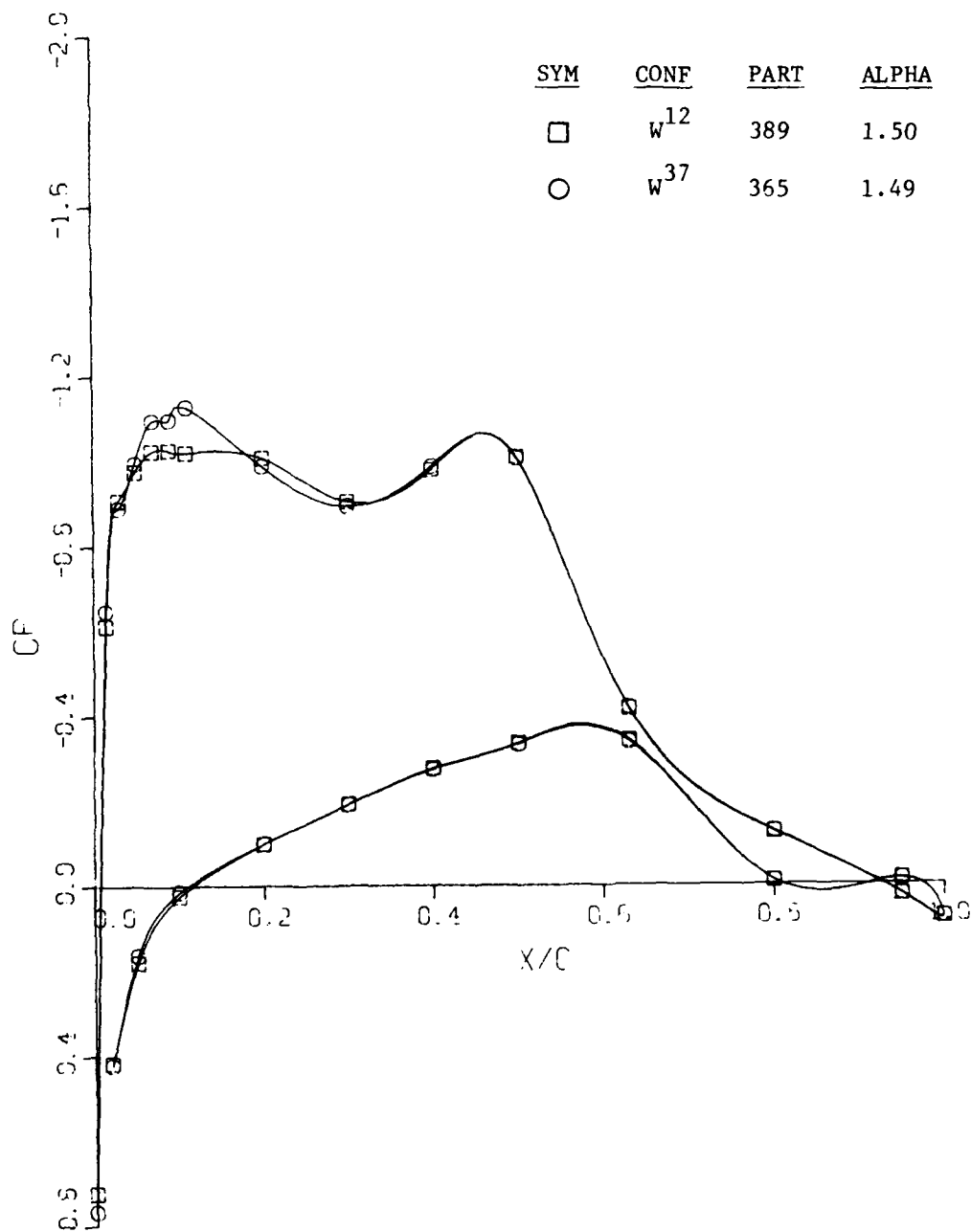
Figure 24. Continued





d.  $\eta = 0.793$

Figure 24. Concluded



a.  $\eta = 0.193$

Figure 25. Effect of W<sup>37</sup> Leading Edge Modification on Chordwise Pressure Distributions at  $M = 0.80$

AD-A099 662

LOCKHEED-GEORGIA CO MARIETTA

F/G 20/4

AERODYNAMIC INVESTIGATION OF C-141 LEADING EDGE MODIFICATIONS F--ETC(U)

APR 81 R A LARGE, W T BLACKERBY

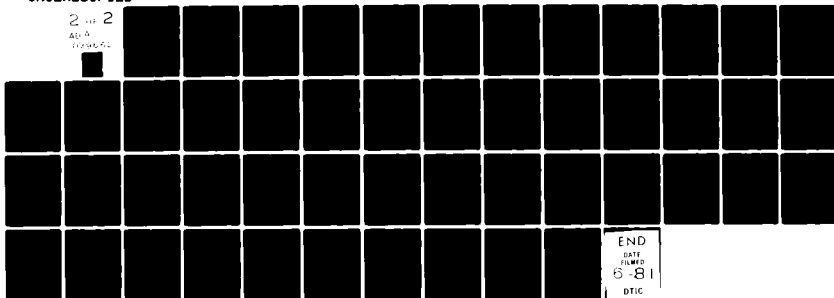
UNCLASSIFIED

AFWAL-TD-R1-1079

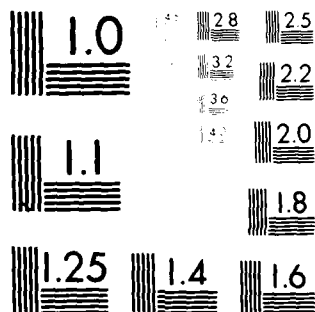
AR

2 of 2

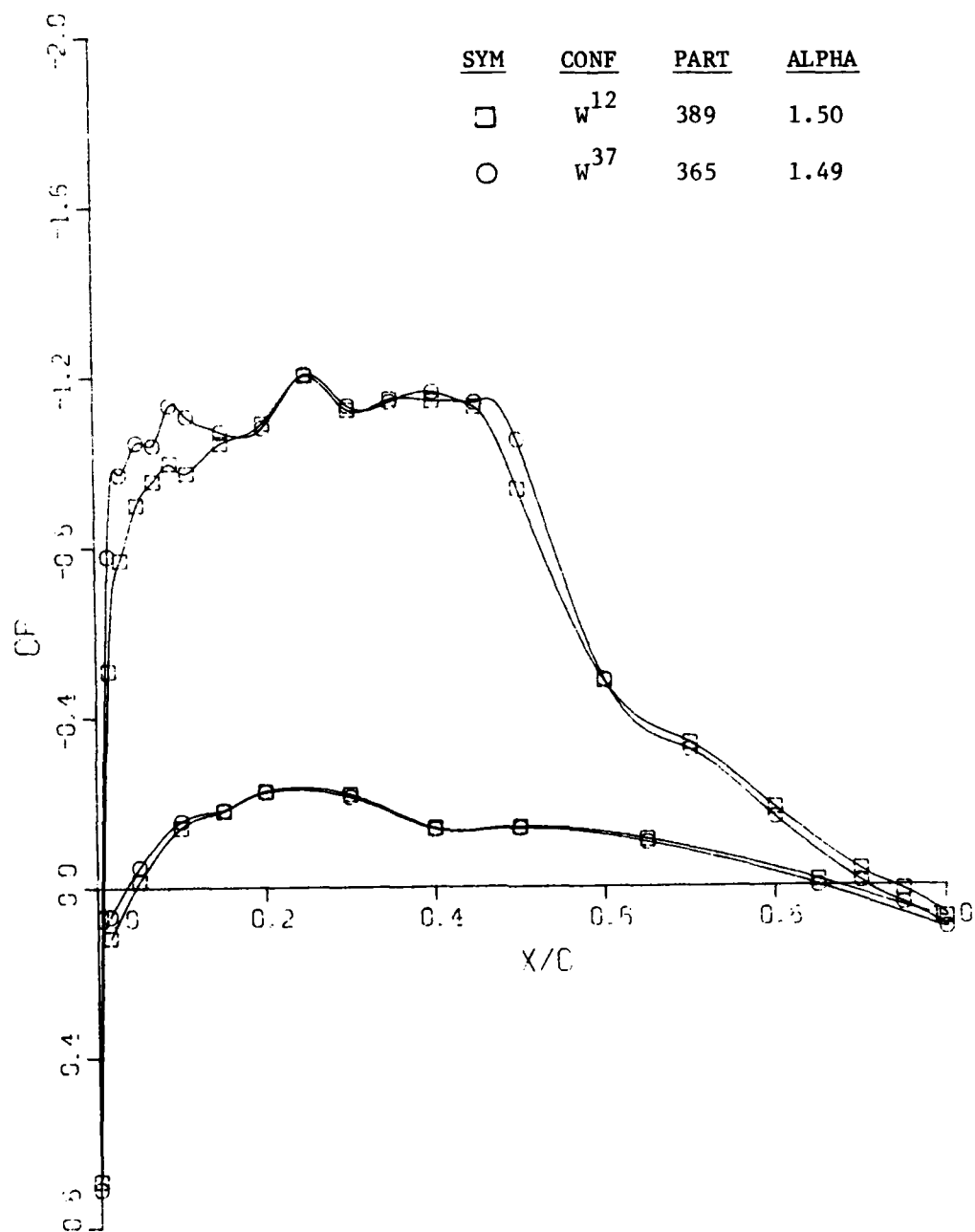
AD-A  
0999662



END  
DATE  
FILMED  
6-81  
DTIC

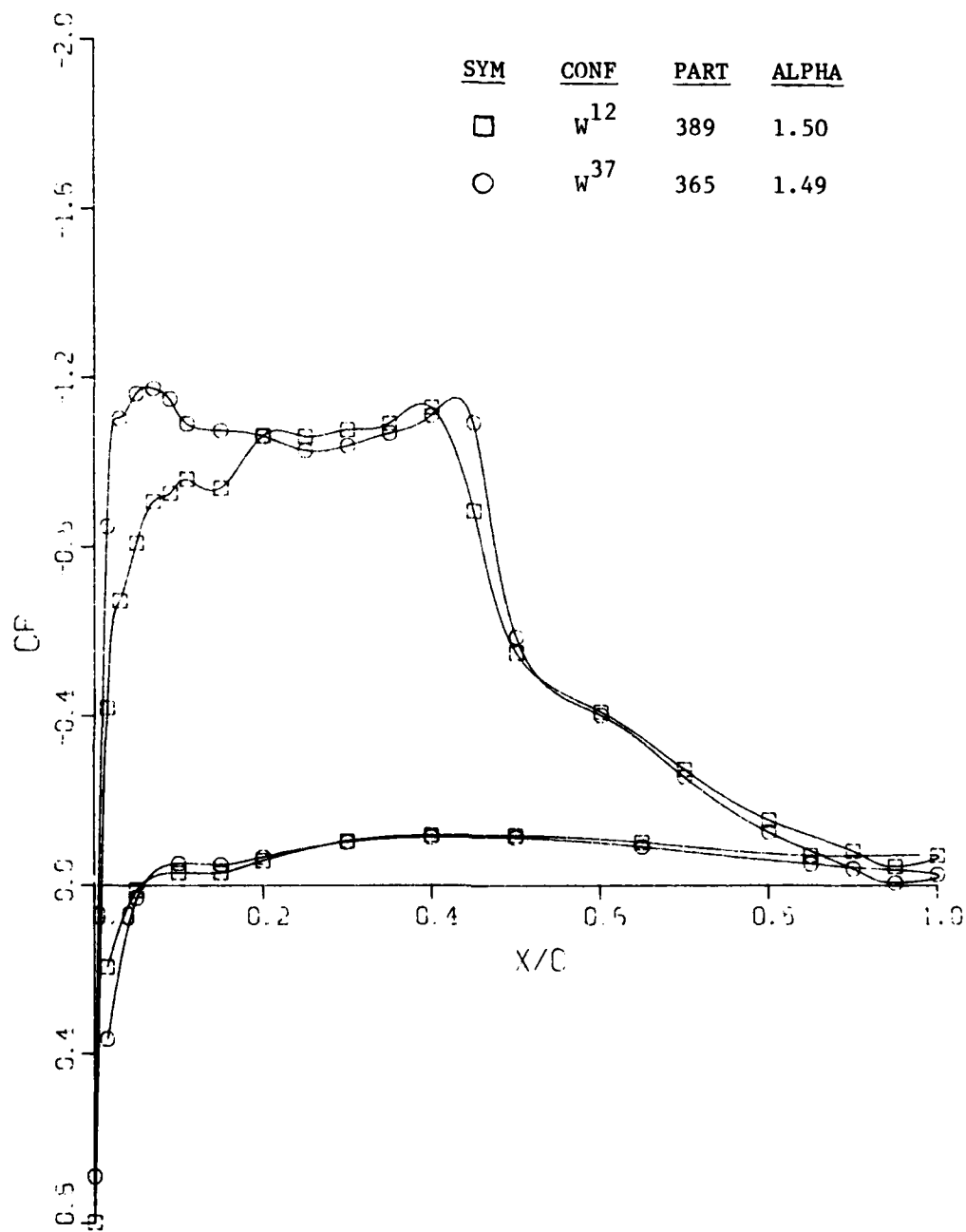


MICROCOPY RESOLUTION TEST CHART  
NATIONAL BUREAU OF STANDARDS-1963-A



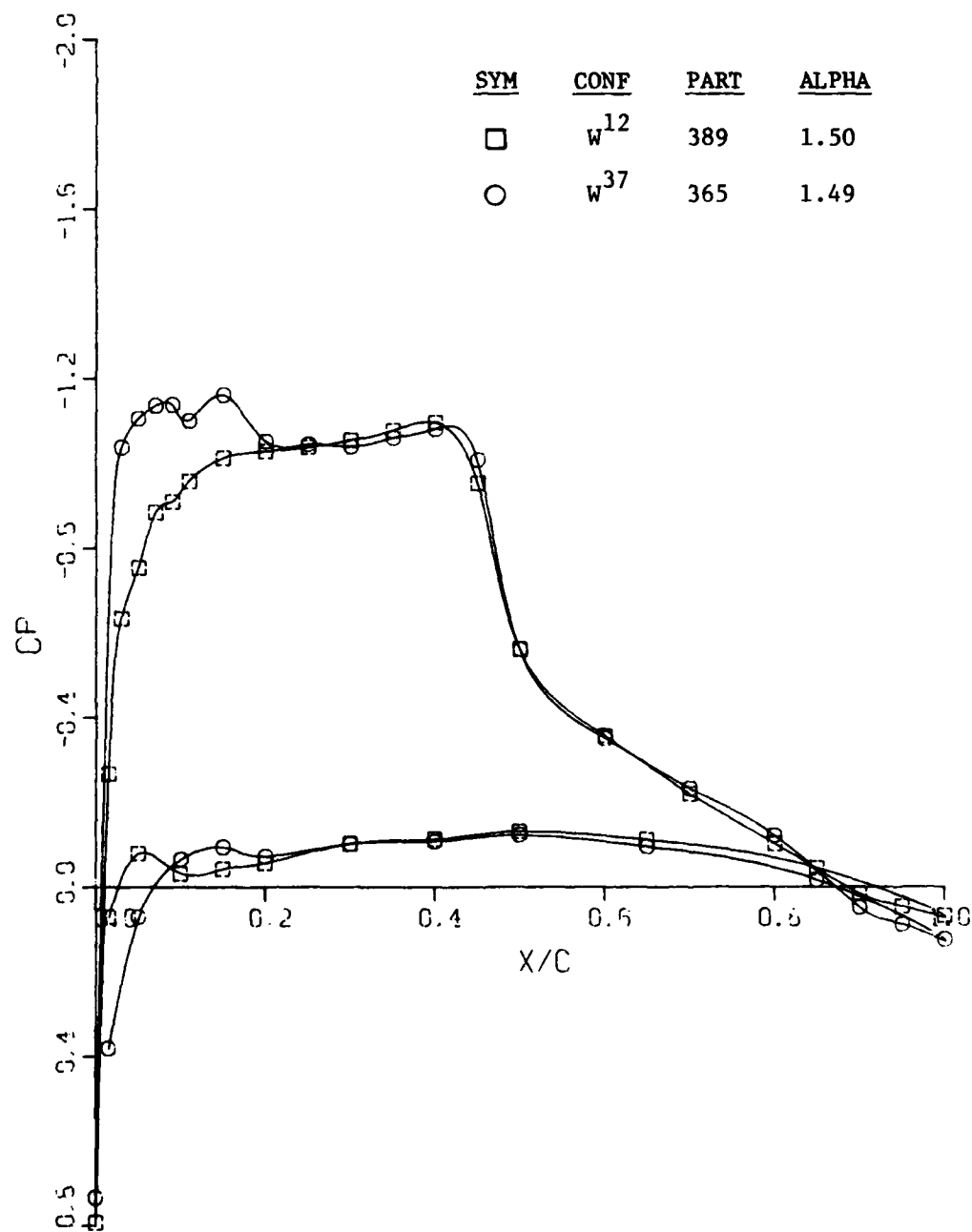
b.  $\eta = 0.418$

Figure 25. Continued



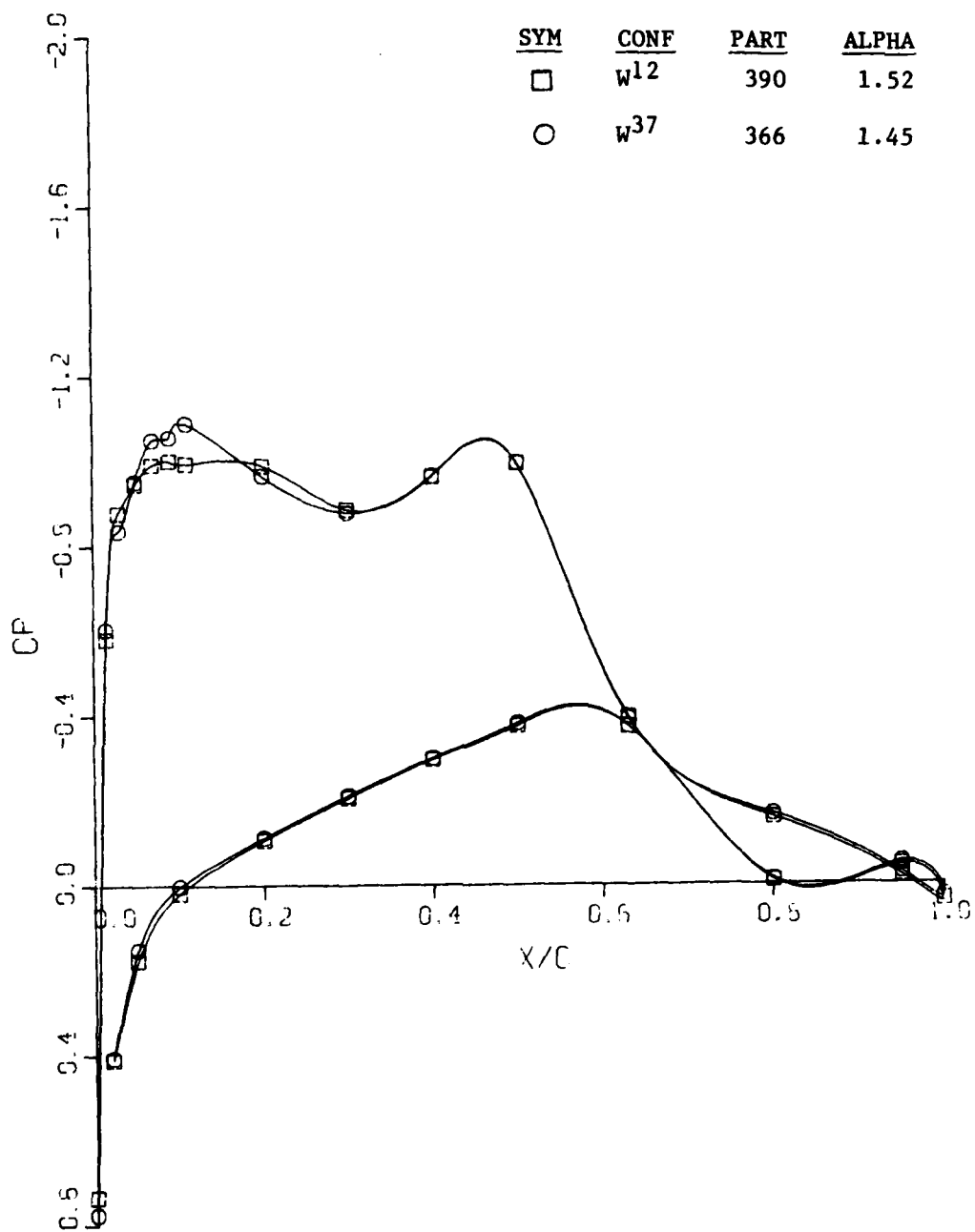
c.  $\eta = 0.636$

Figure 25. Continued



d.  $\eta = 0.793$

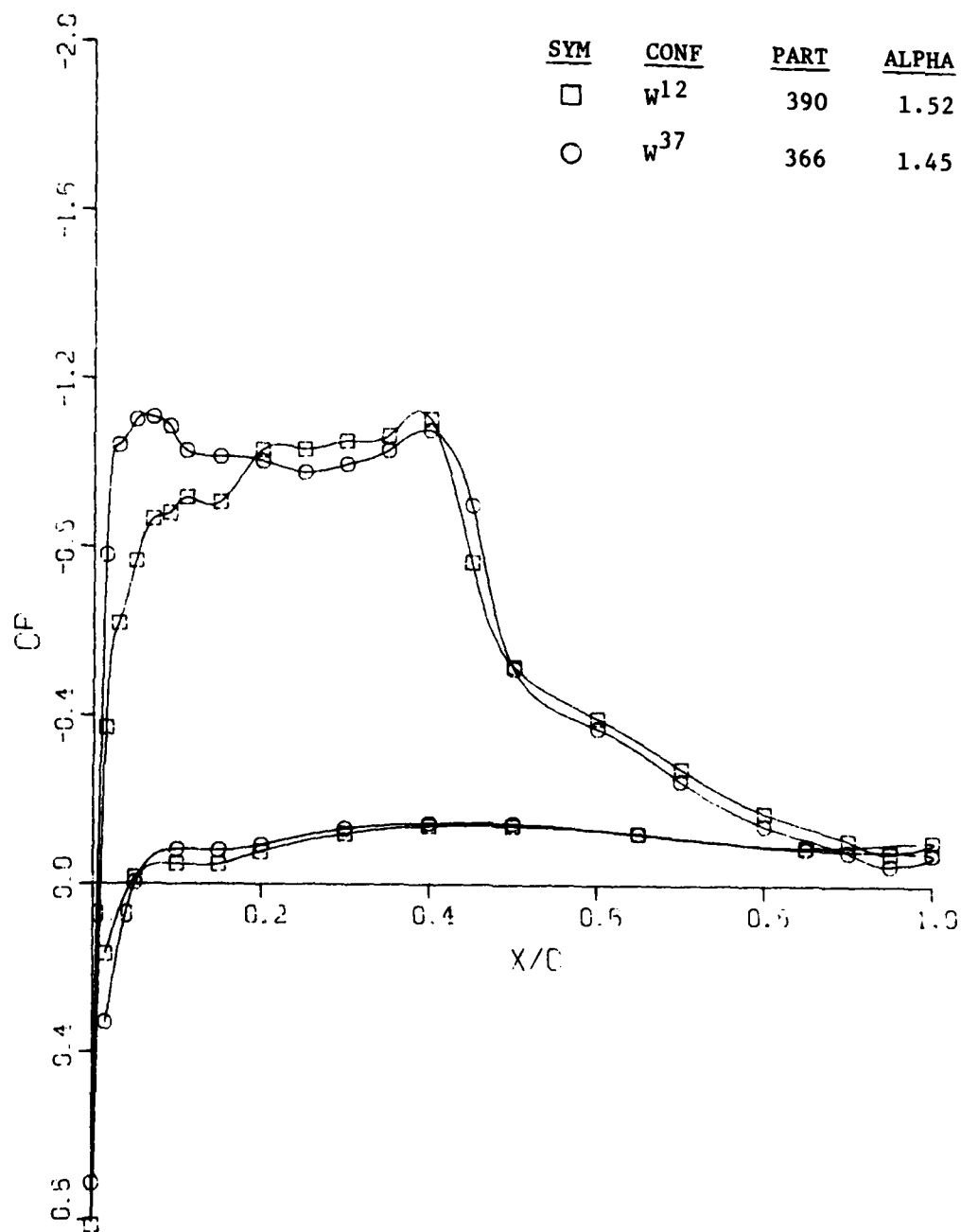
Figure 25. Concluded



a.  $\eta = 0.193$

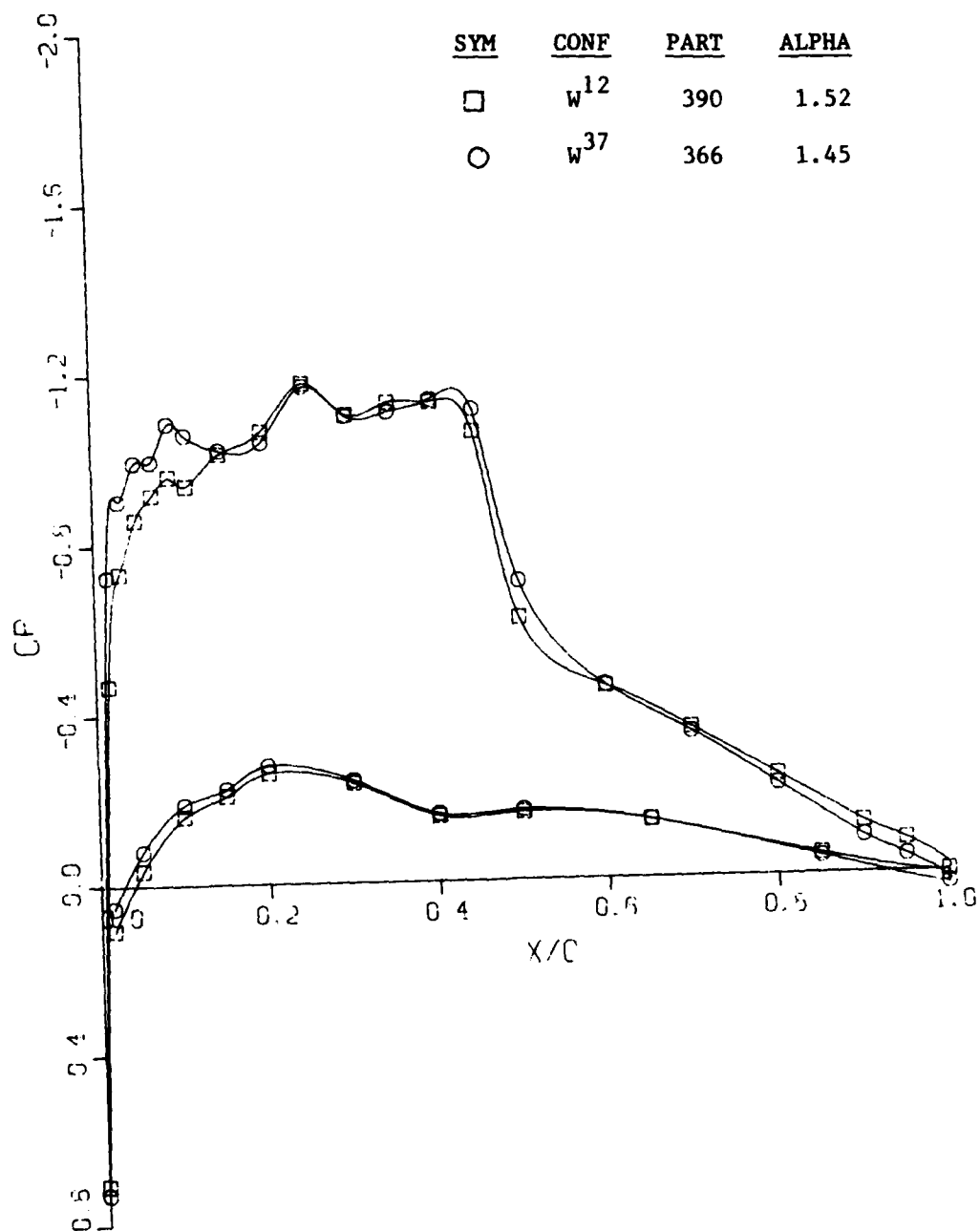
Figure 26. Effect of W<sup>37</sup> Leading Edge Modification on Chordwise Pressure Distributions at  $M = 0.81$





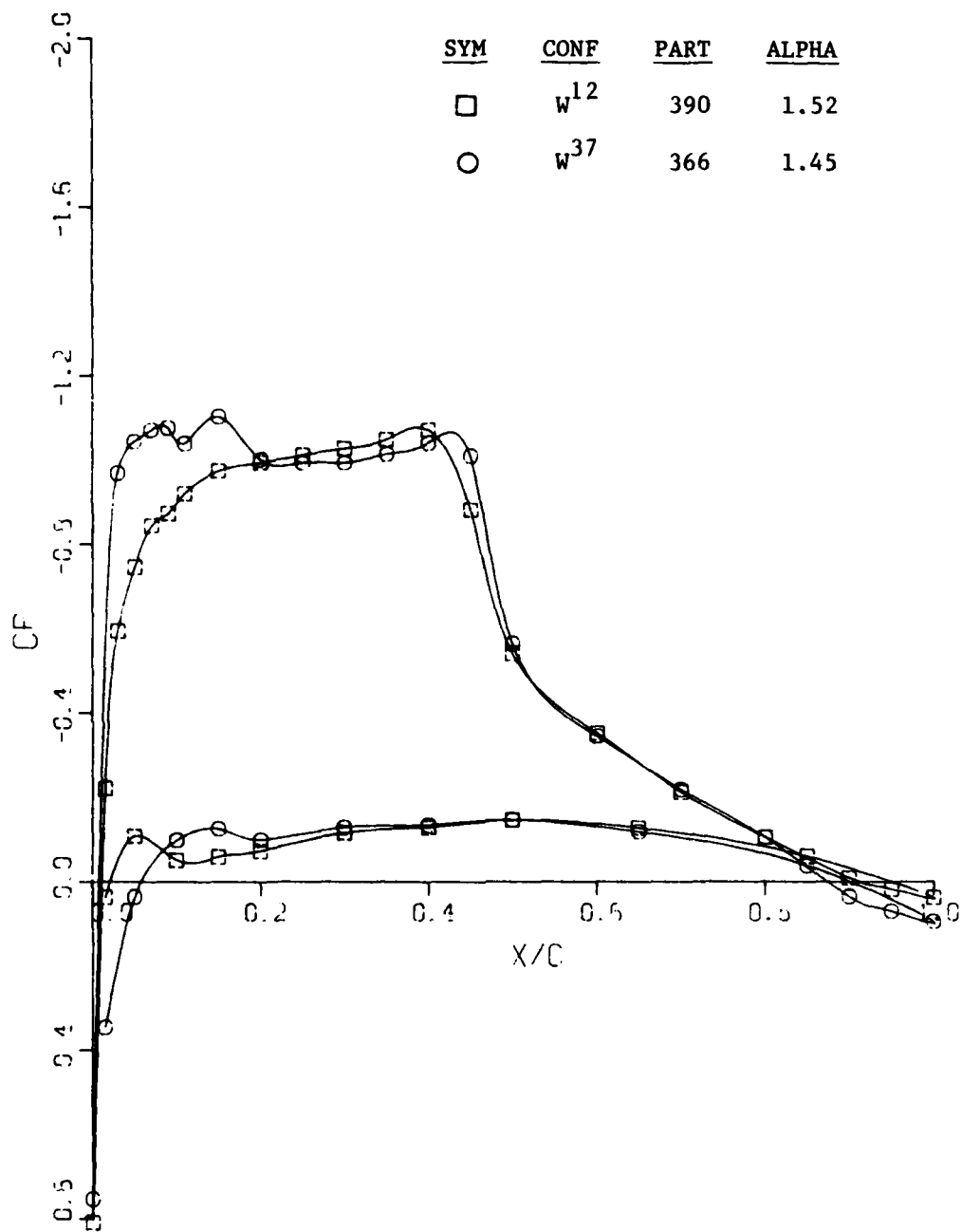
b.  $\eta = 0.418$

Figure 26. Continued



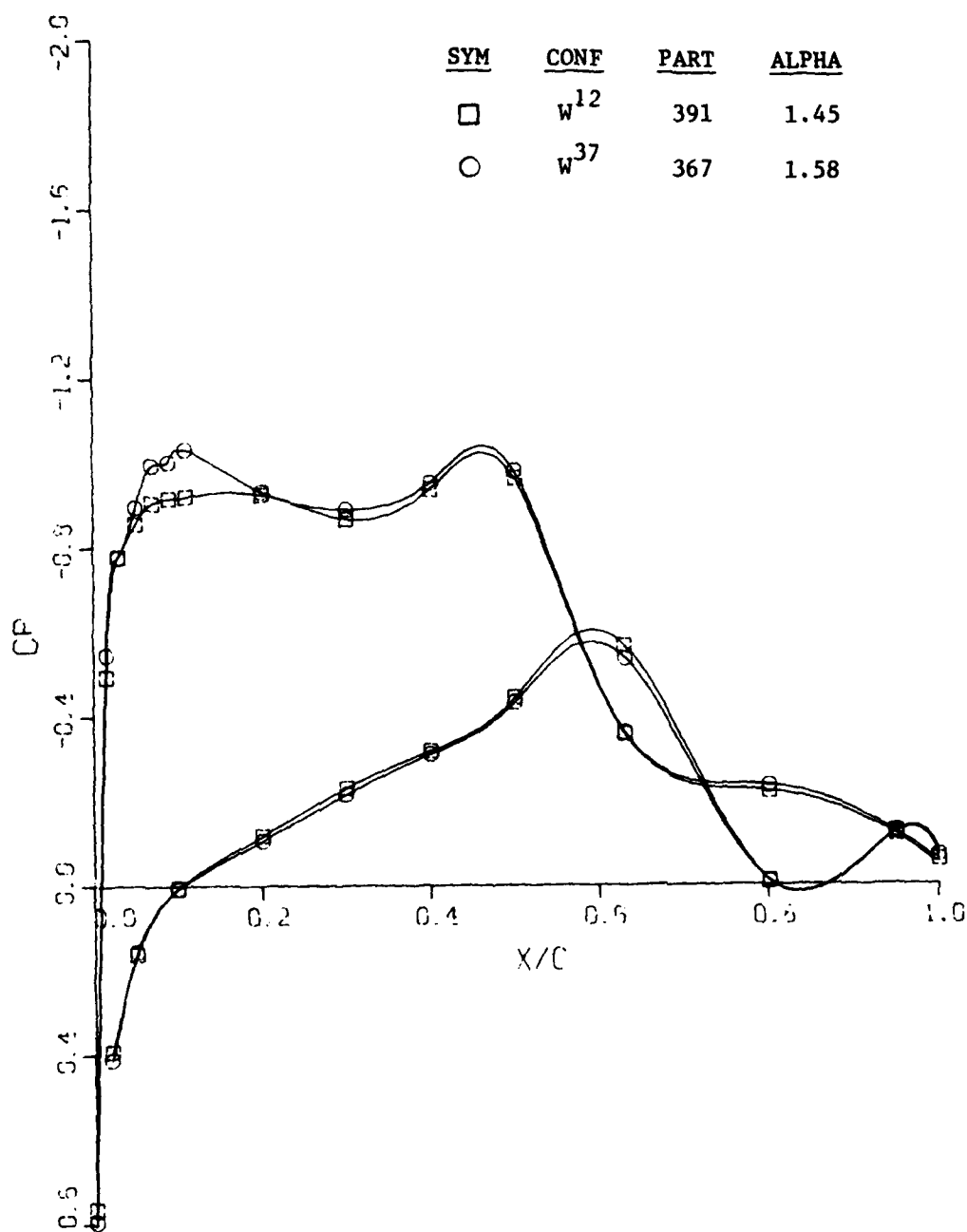
c.  $\eta = 0.636$

Figure 26. Continued



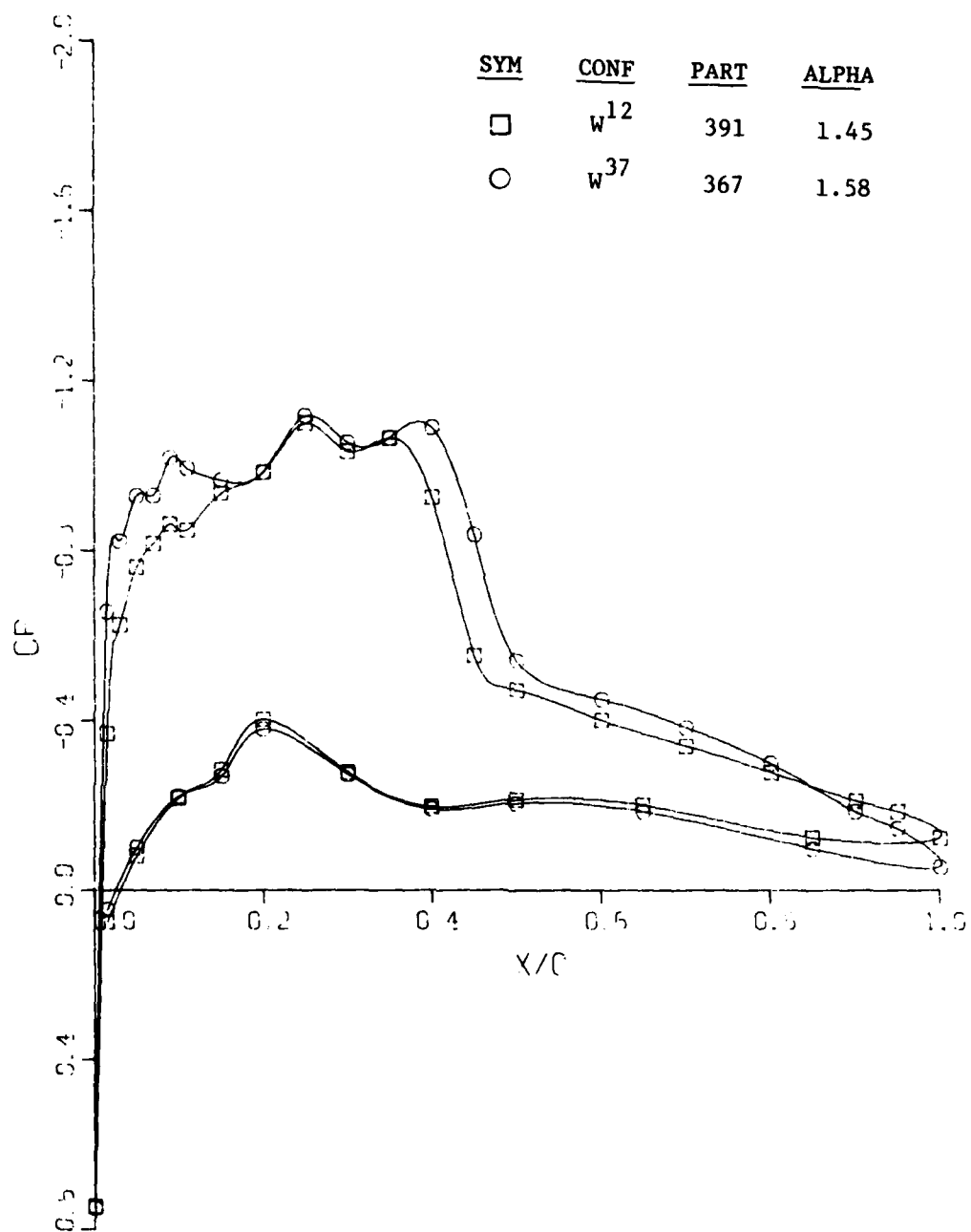
d.  $\eta = 0.793$

Figure 26. Concluded



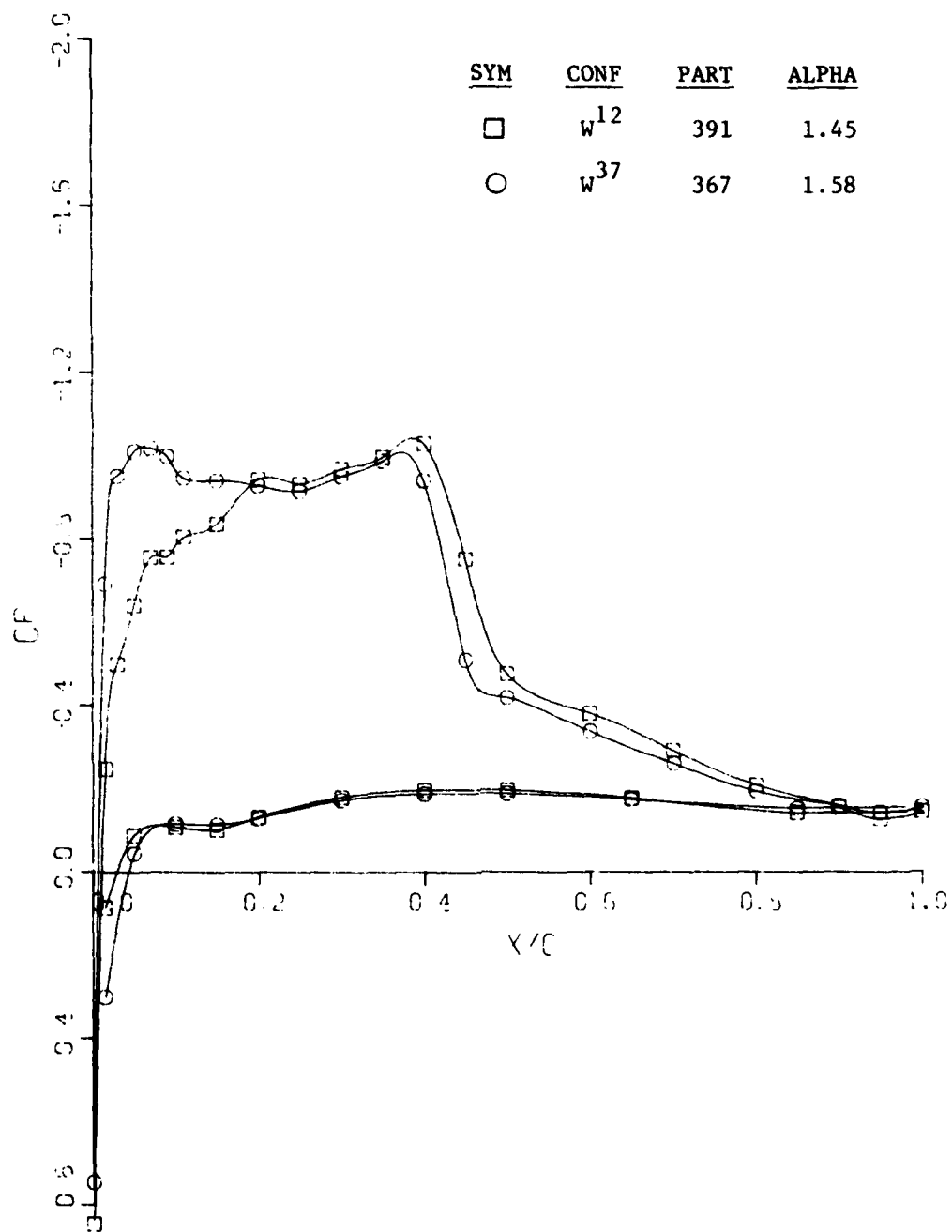
a.  $\eta = 0.193$

Figure 27. Effect of W<sup>37</sup> Leading Edge Modification on Chordwise Pressure Distributions at M = 0.83



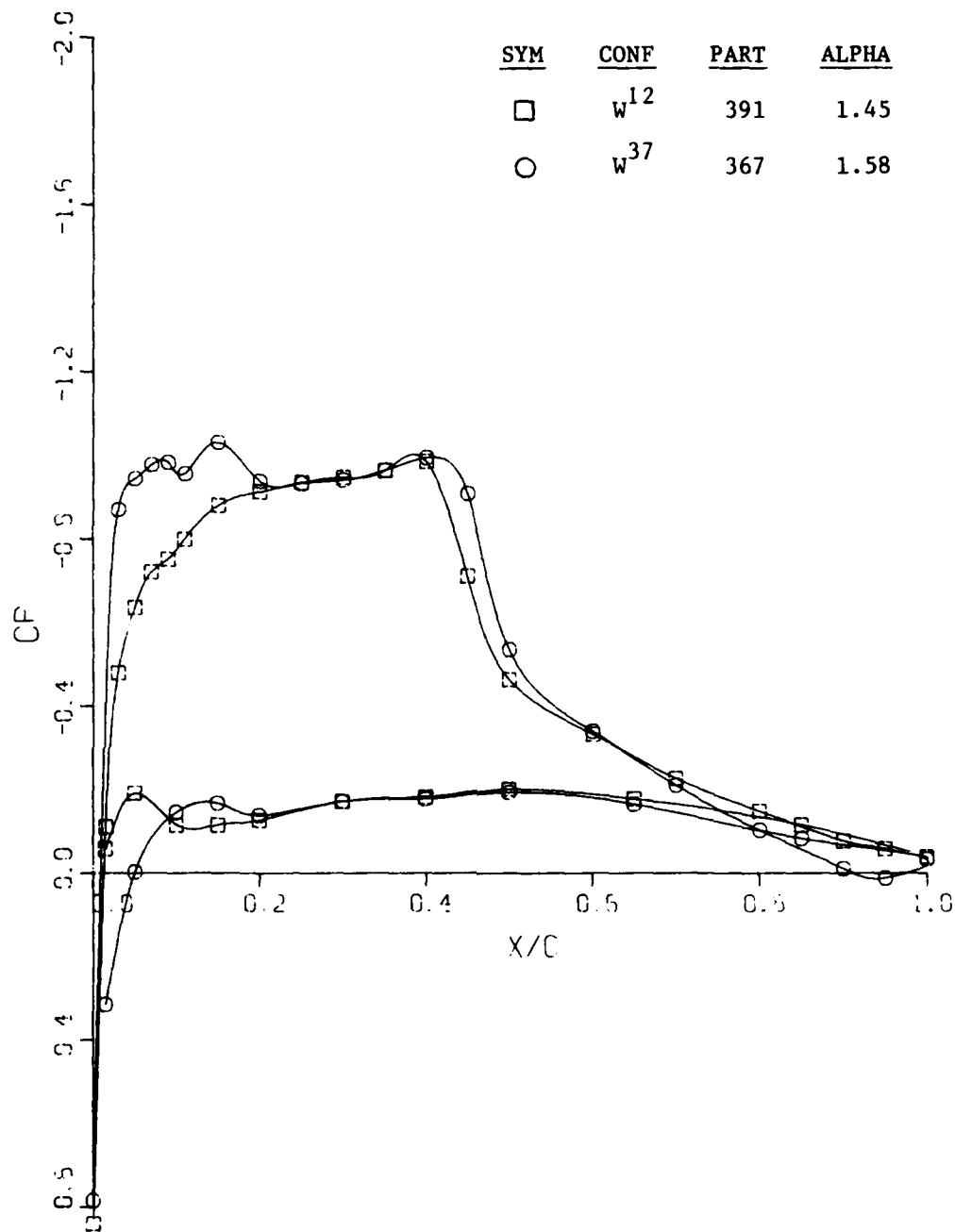
b.  $\eta = 0.418$

Figure 27. Continued



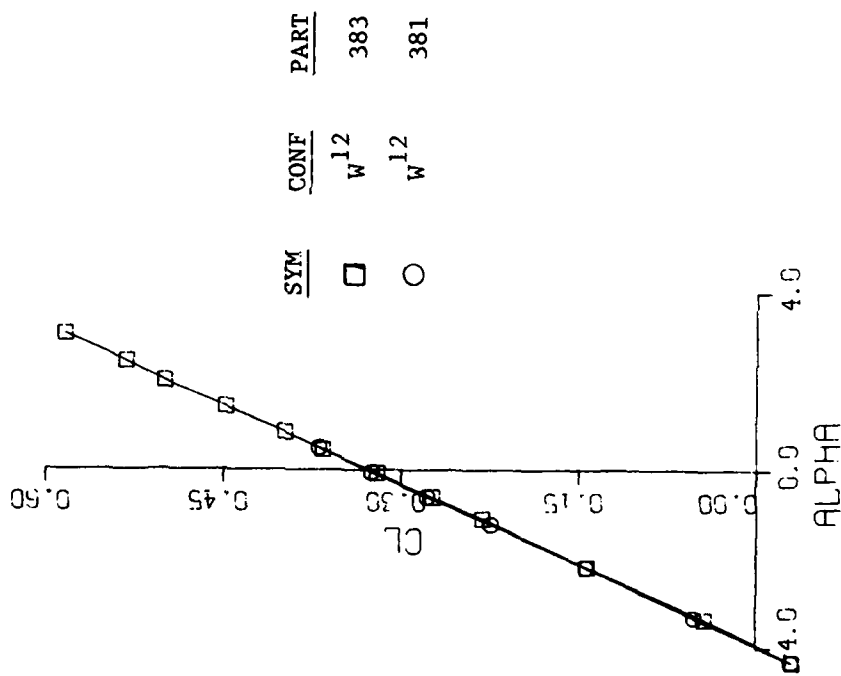
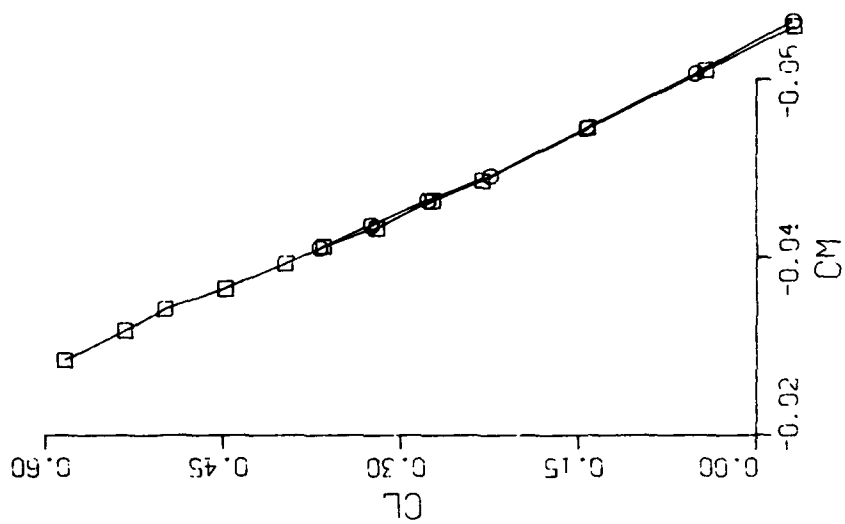
c.  $\eta = 0.636$

Figure 27. Continued



d.  $\eta = 0.793$

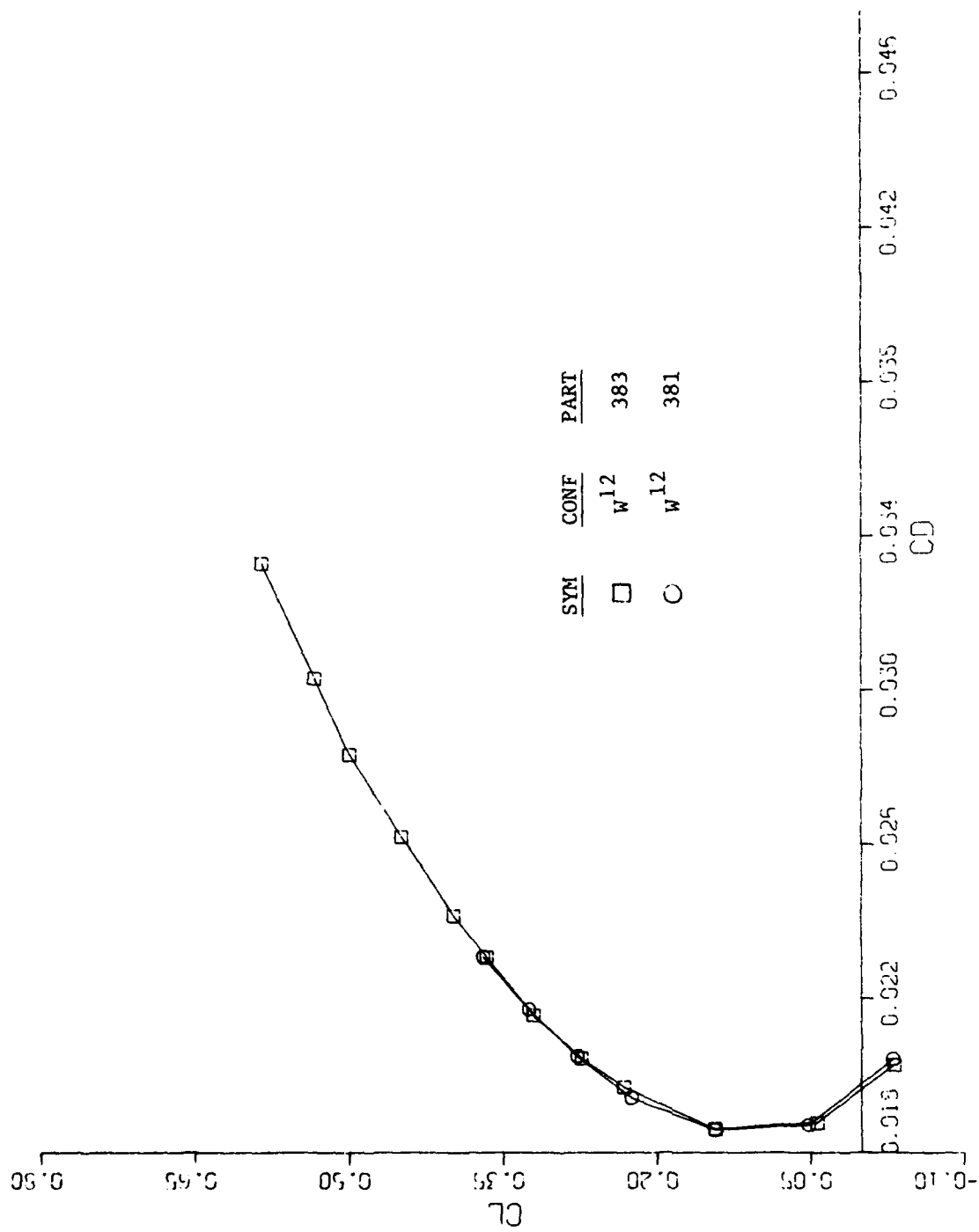
Figure 27. Concluded



SYM	CONF	PART
□	$W^{12}$	383
○	$W^{12}$	381

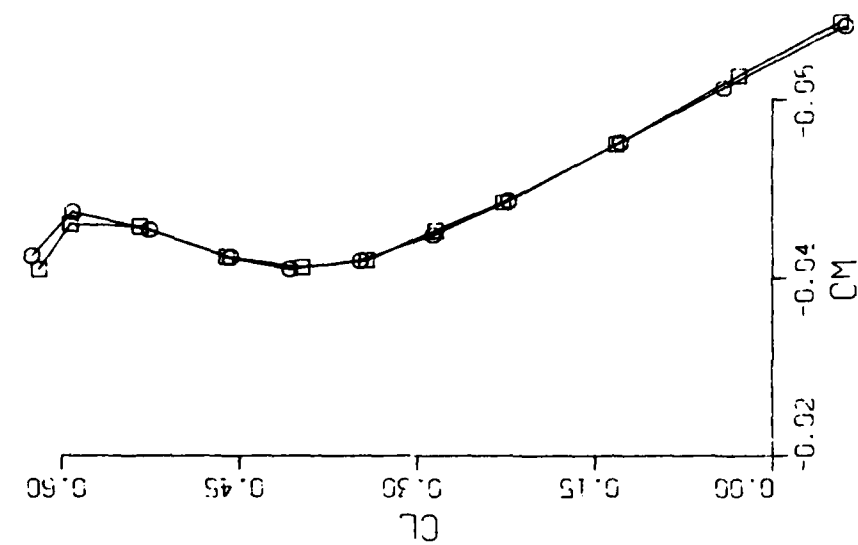
a. Lift and Pitching Moment  
Figure 28. Baseline Data Repeatability at  $M = 0.60$



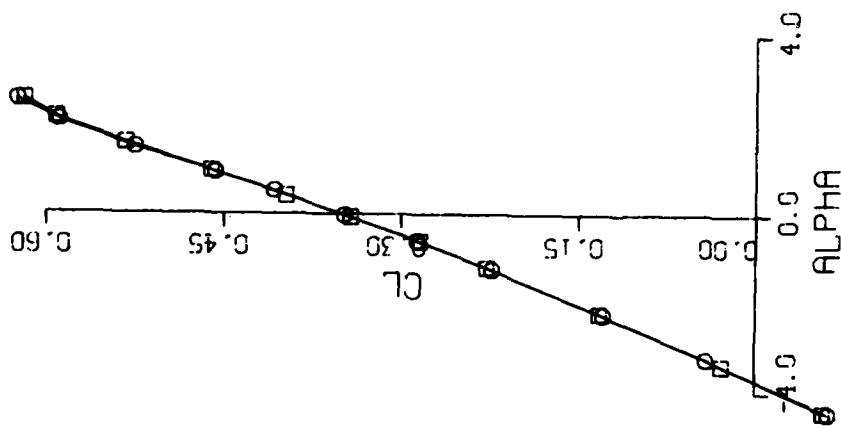


b. Drag Polar

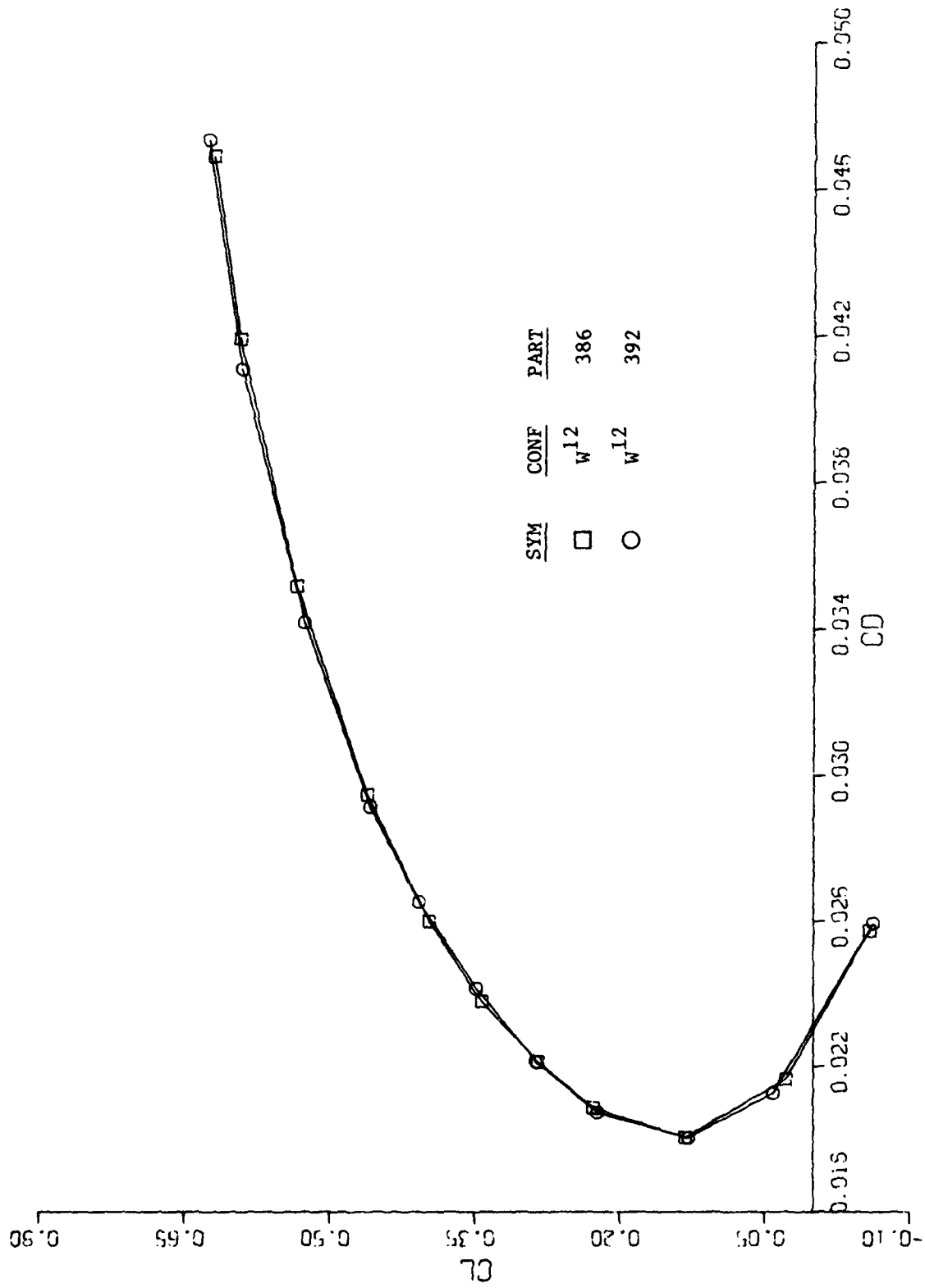
Figure 28. Concluded



SYM	CONF	PART
□	$w^{12}$	386
○	$w^{12}$	392

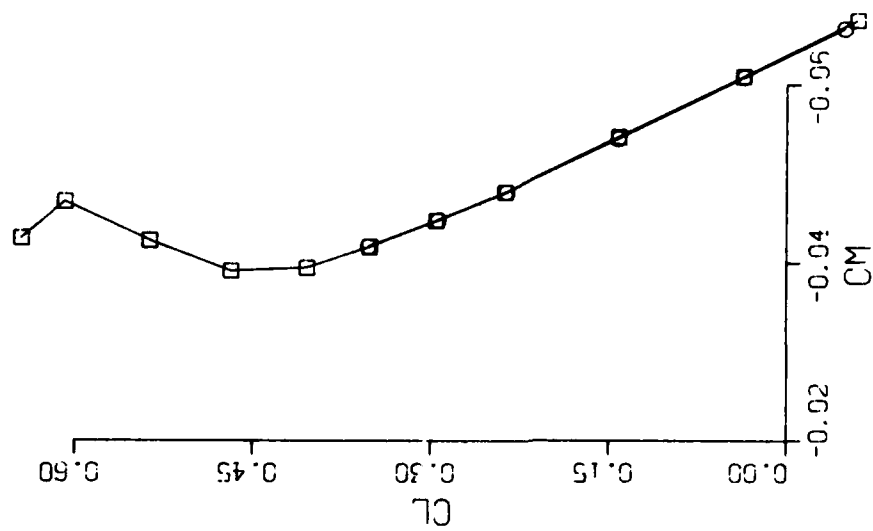


a. Lift and Pitching Moment  
Figure 29. Baseline Data Repeatability at  $M = 0.77$

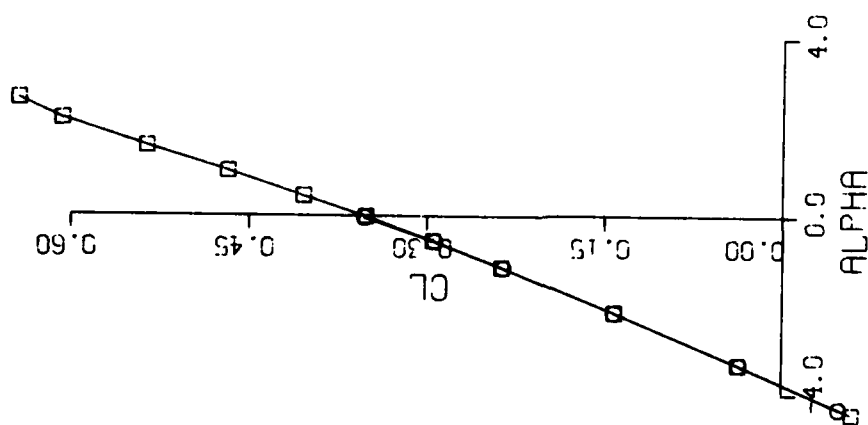


b. Drag Polar

Figure 29. Concluded

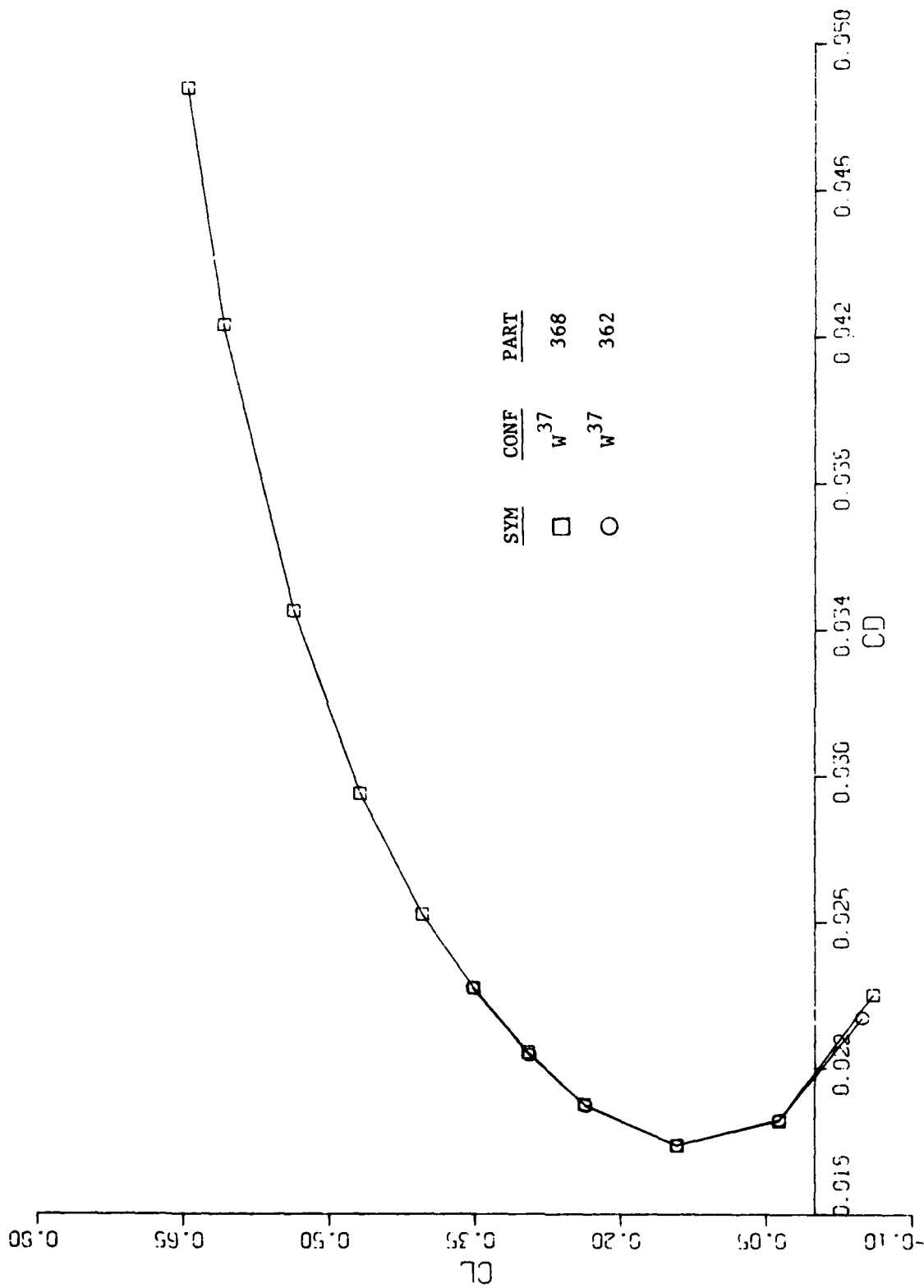


<u>SYM</u>	<u>CONF</u>	<u>PART</u>
□	$W^{37}$	368
○	$W^{37}$	362



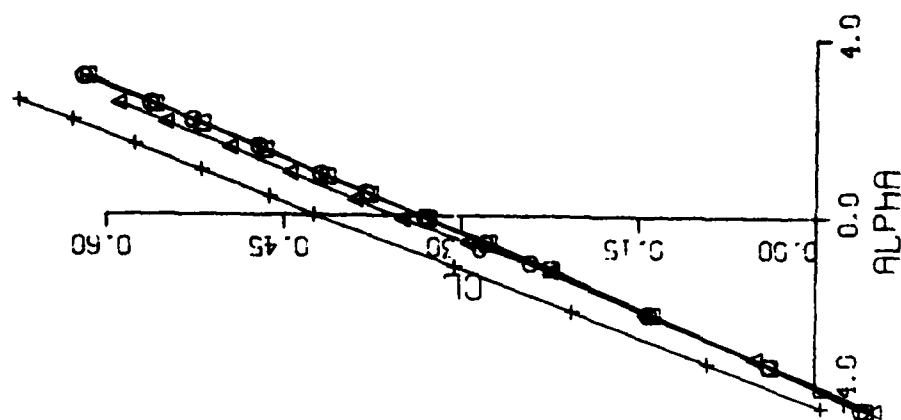
a. Lift and Pitching Moment

Figure 30. Modified Wing Data Repeatability at  $M = 0.77$

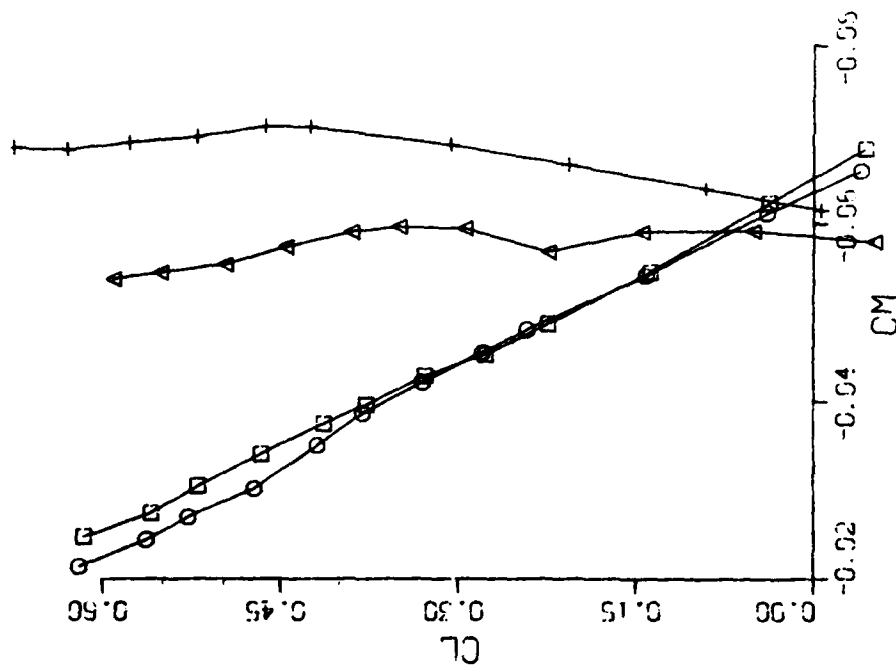


b. Drag Polar

Figure 30. Concluded

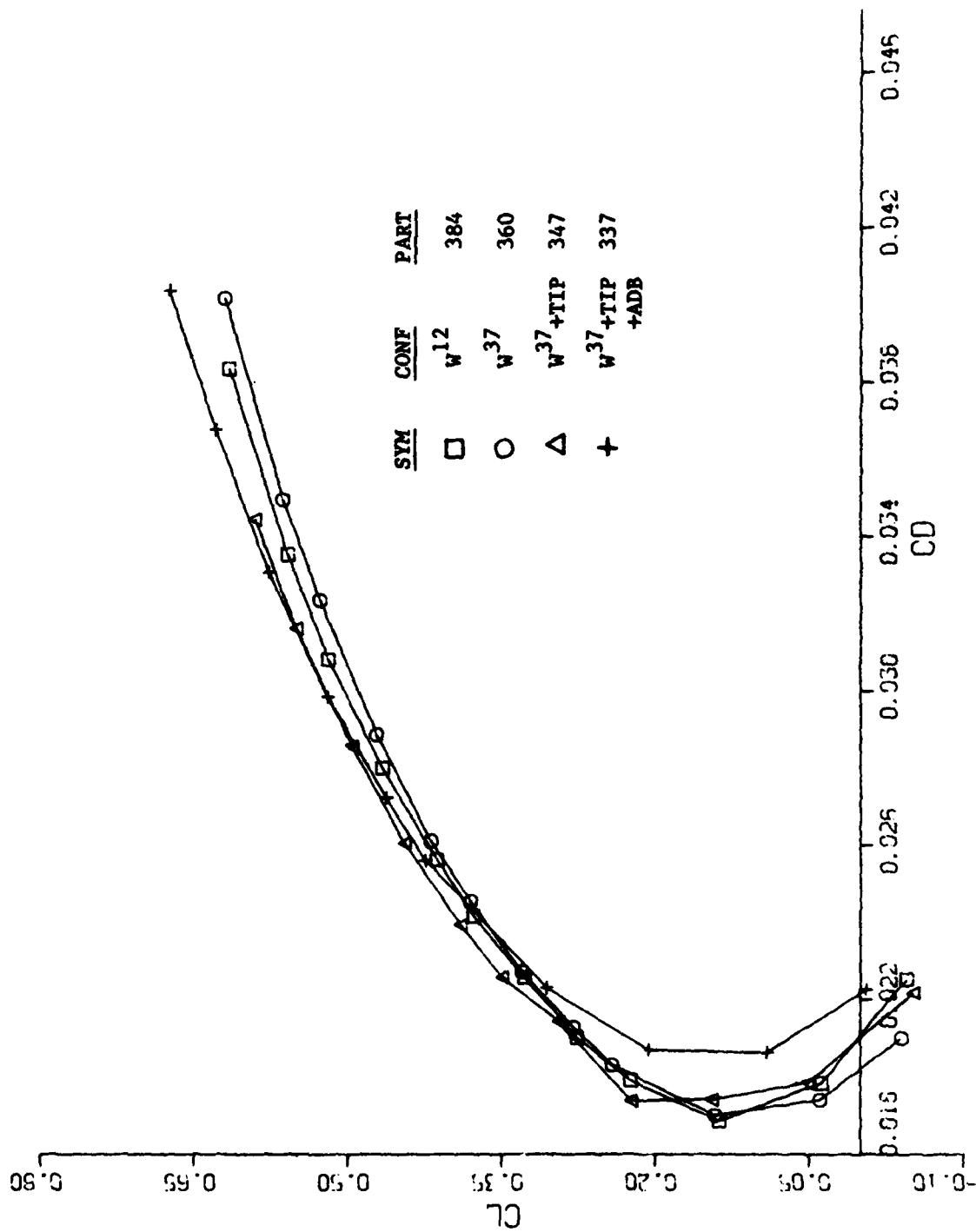


SYM	CONF	PART
□	W <sup>12</sup>	384
○	W <sup>37</sup>	360
△	W <sup>37</sup> +TIP	347
+	W <sup>37</sup> +TIP	337 +ADB



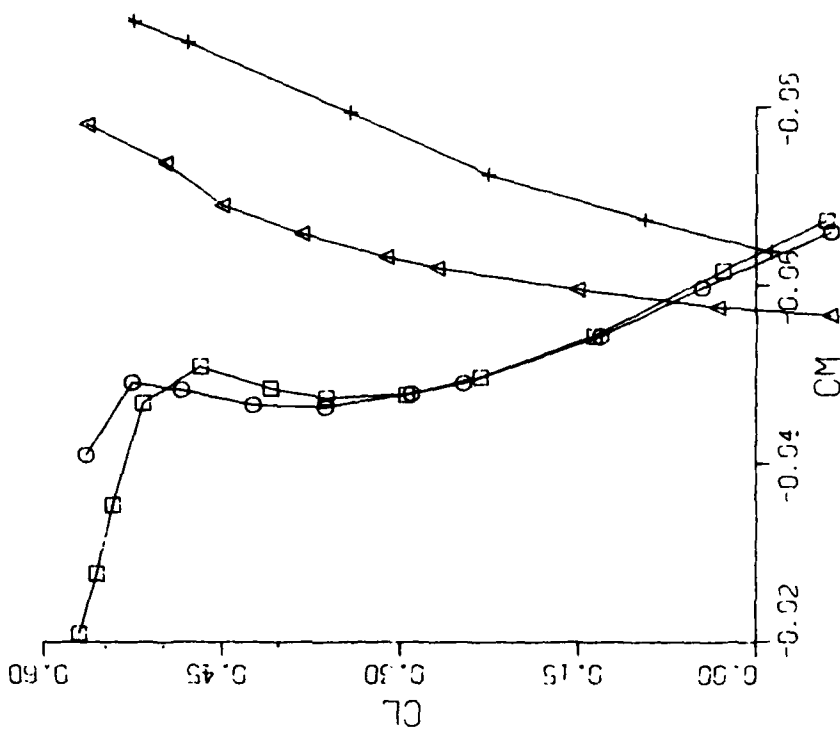
a. Lift and Pitching Moment

Figure 31. Lift, Drag and Pitching Moment Characteristics at  $M = 0.70$

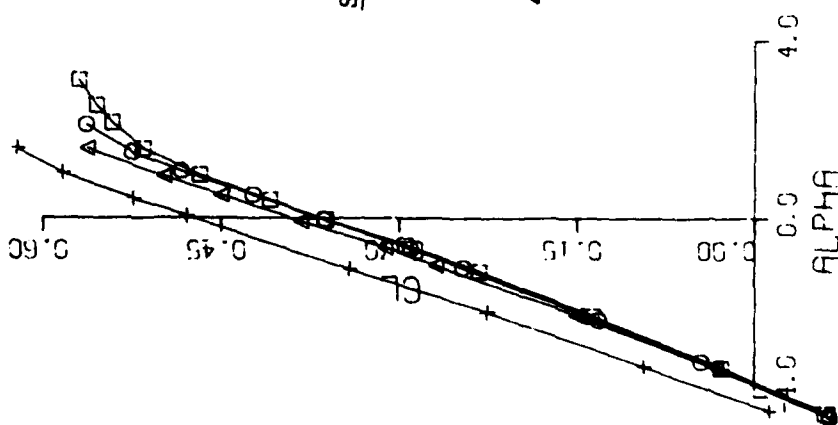


b. Drag Polar

Figure 31. Concluded



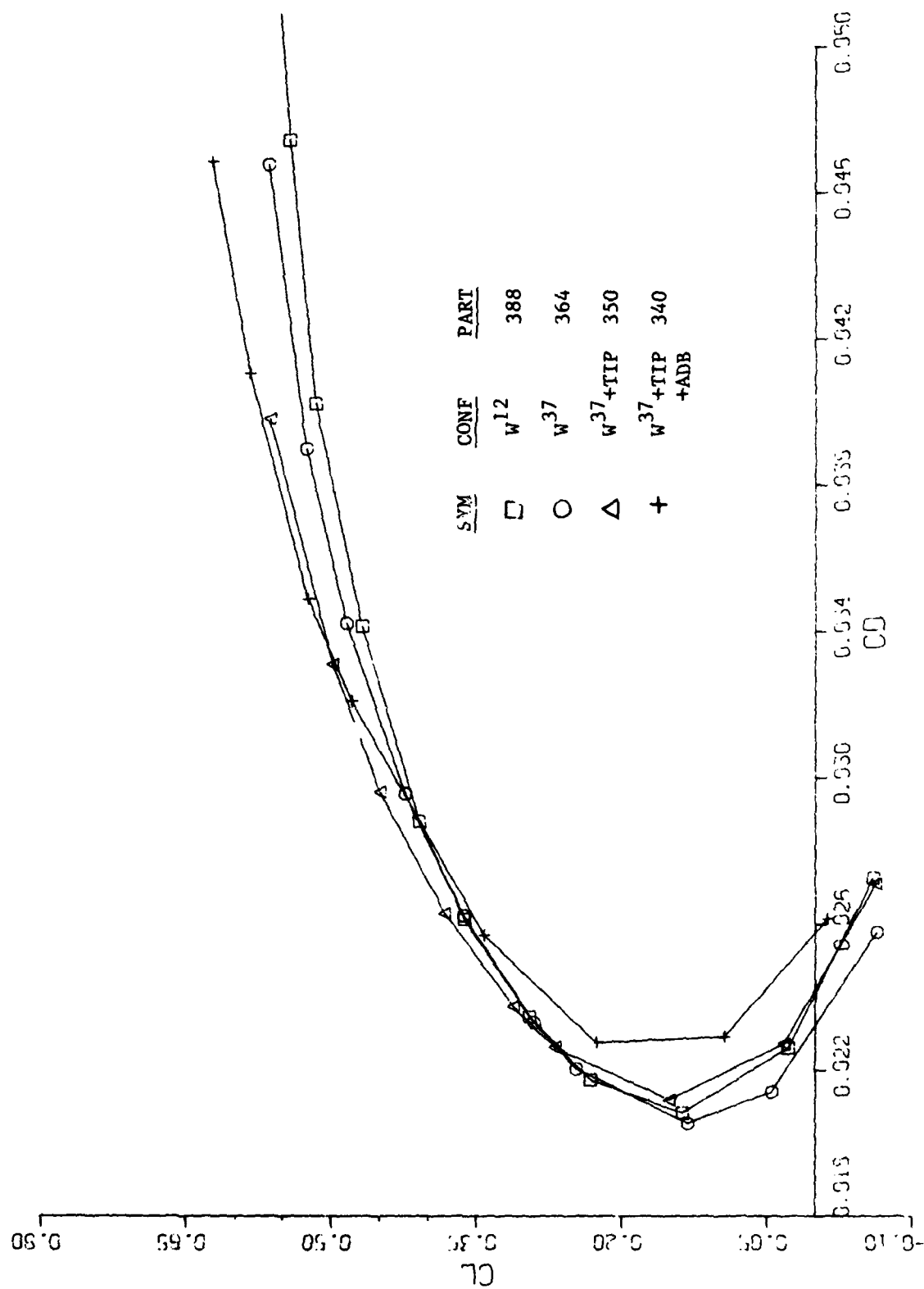
SYM	CONF	PART
□	W <sup>12</sup>	388
○	W <sup>37</sup>	364
△	W <sup>37</sup> +TIP	350
+	W <sup>37</sup> +TIP+ADB	340



a. Lift and Pitching Moment

Figure 32. Lift Drag and Pitching Moment Characteristics at  $M = 0.79$





b. Drag Polar

Figure 32. Concluded

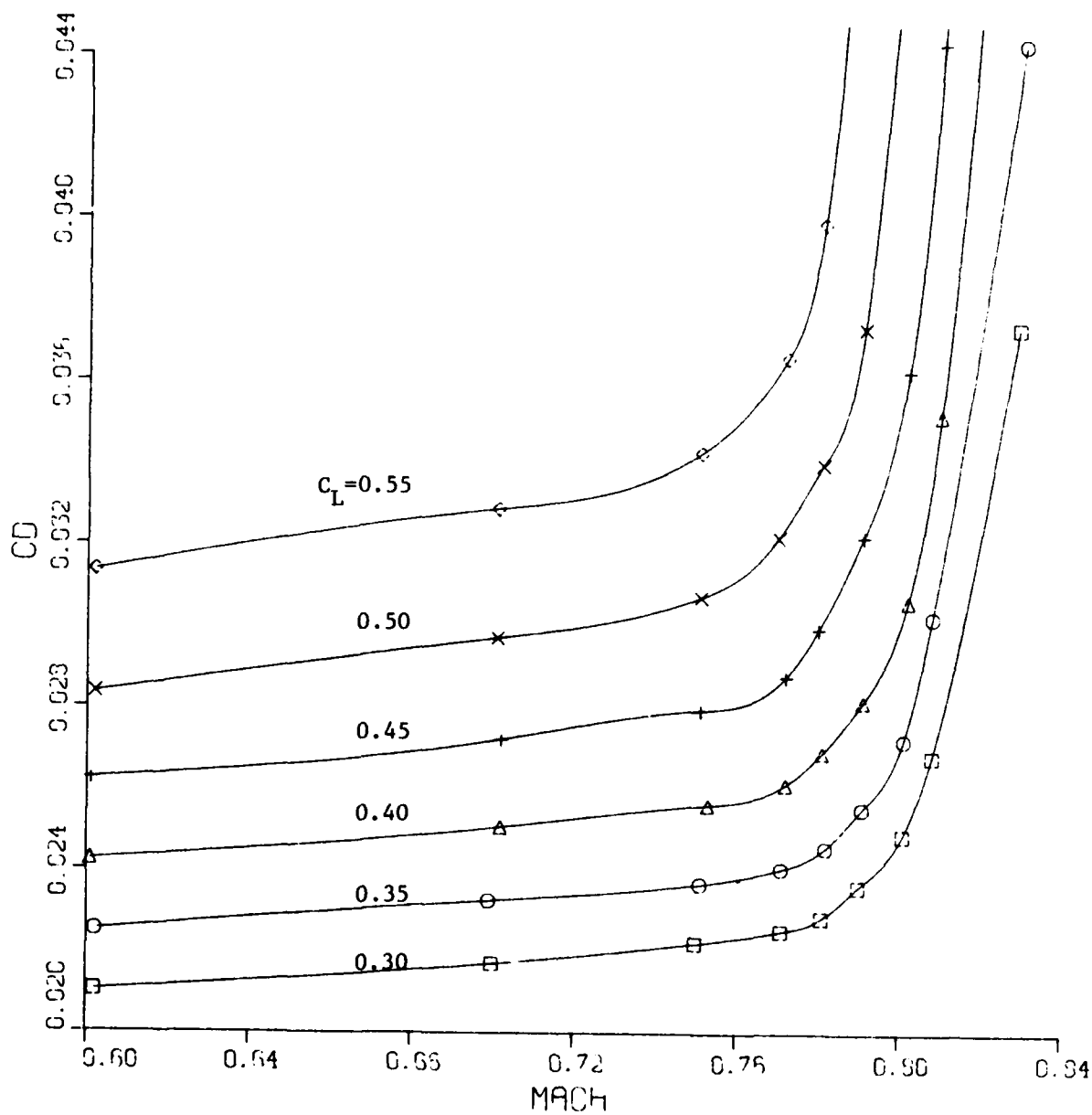


Figure 33. Drag Rise Characteristics of  $W^{12}$

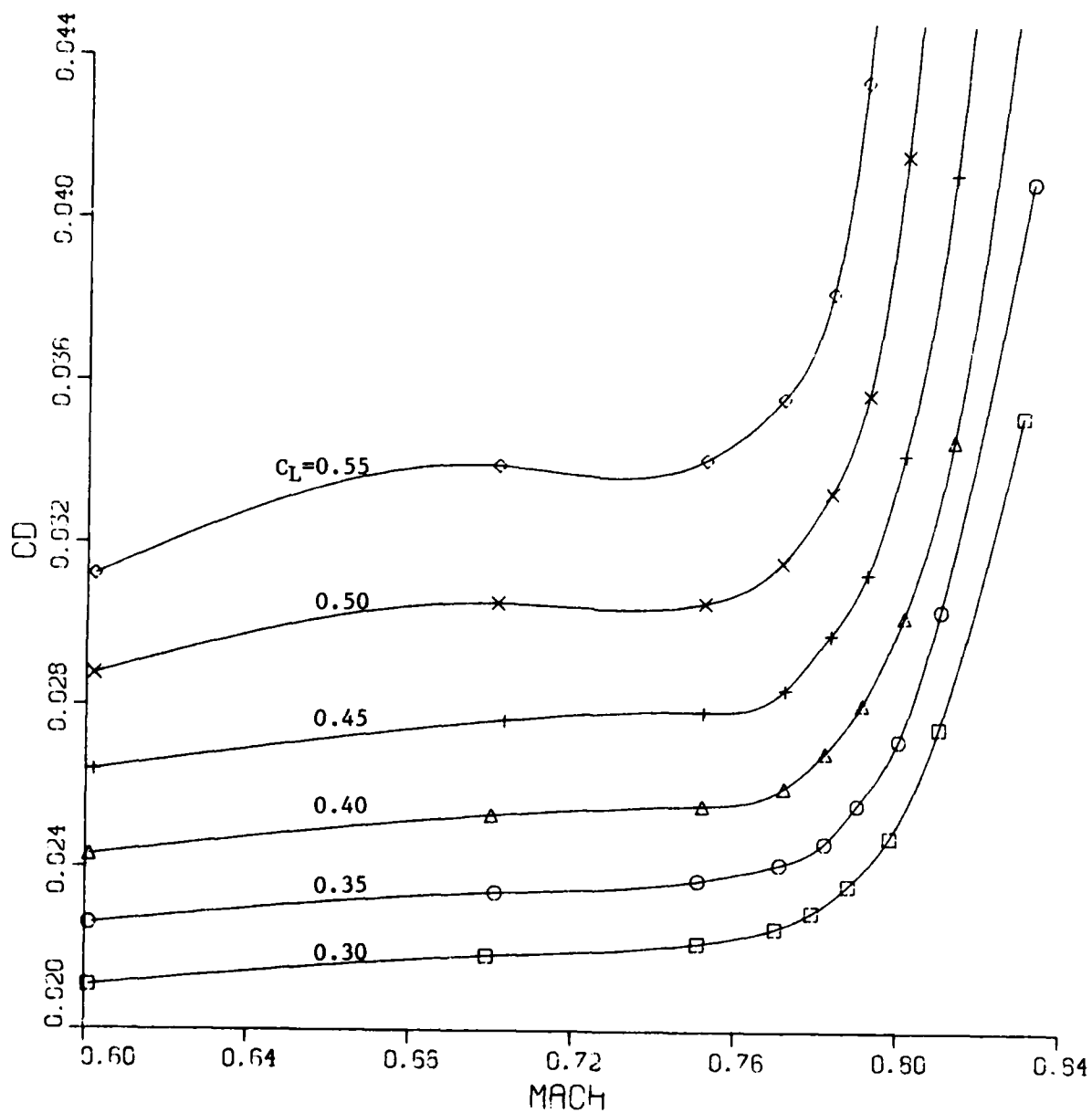


Figure 34. Drag Rise Characteristics of  $W^{37}$

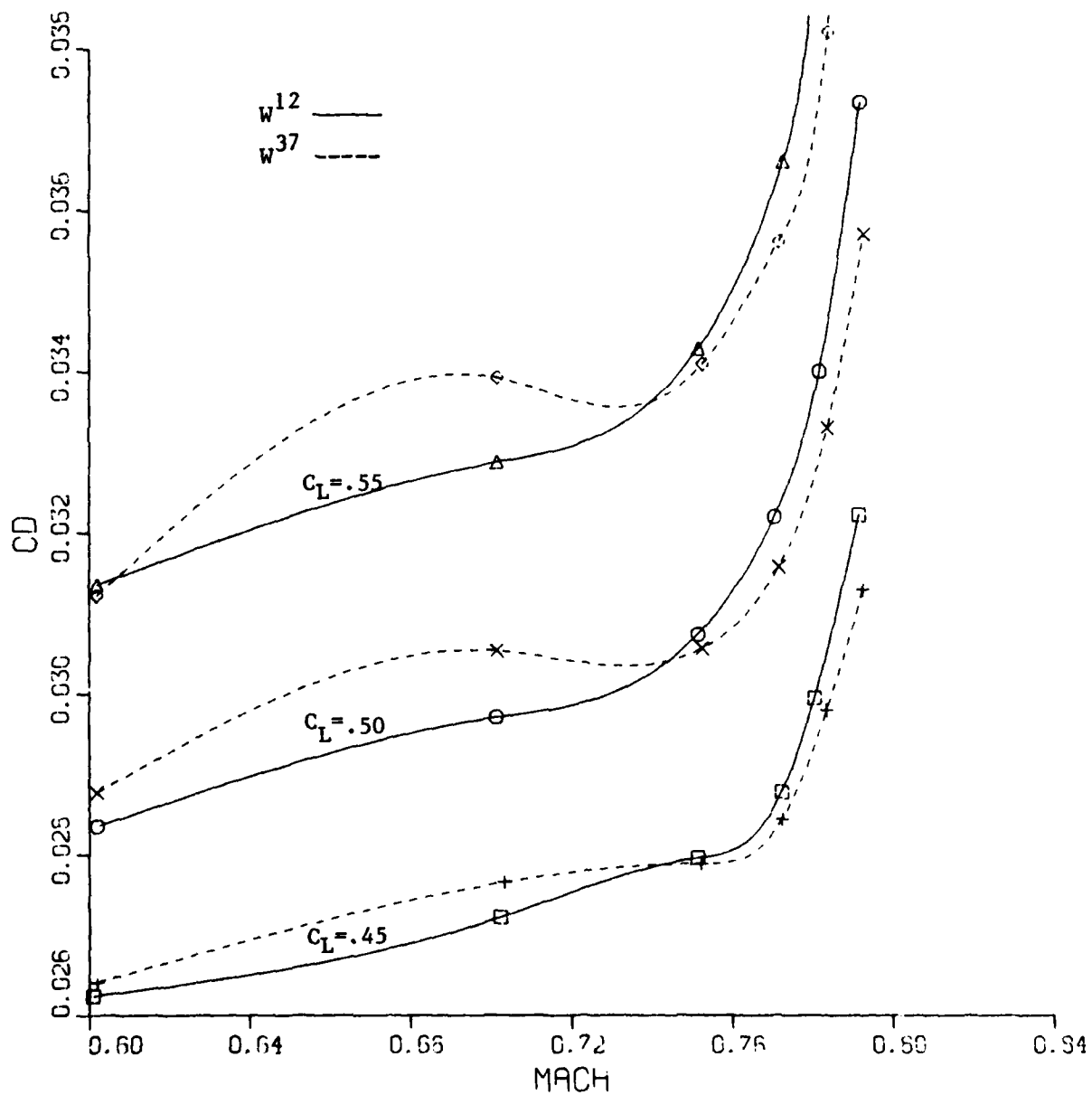
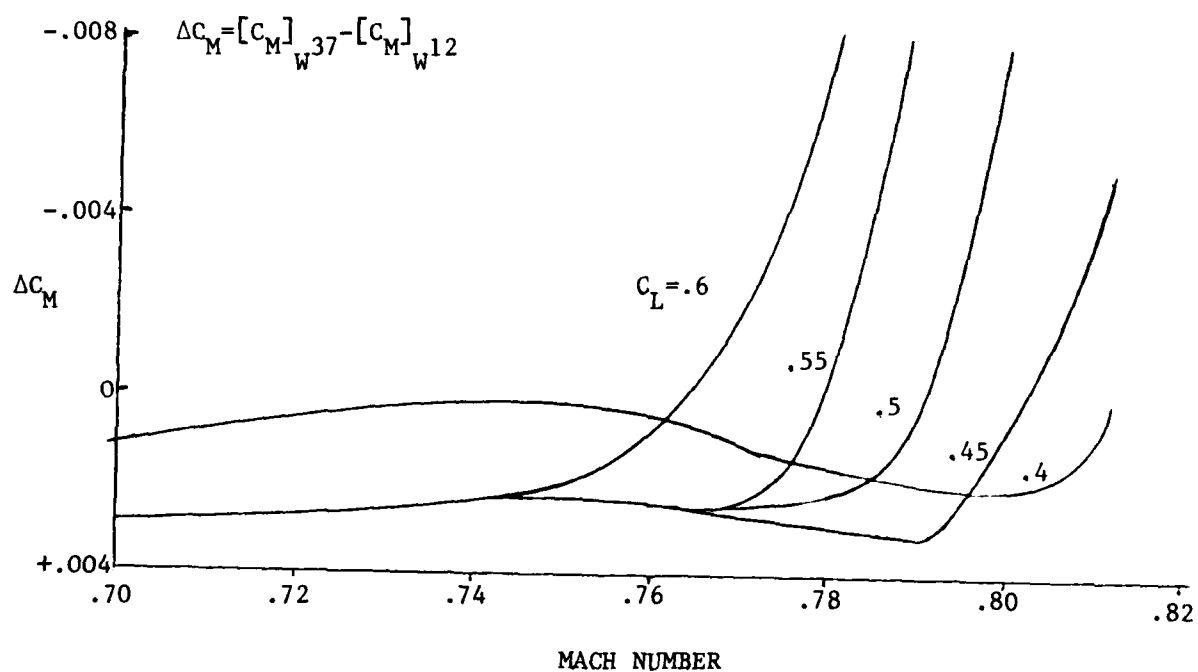
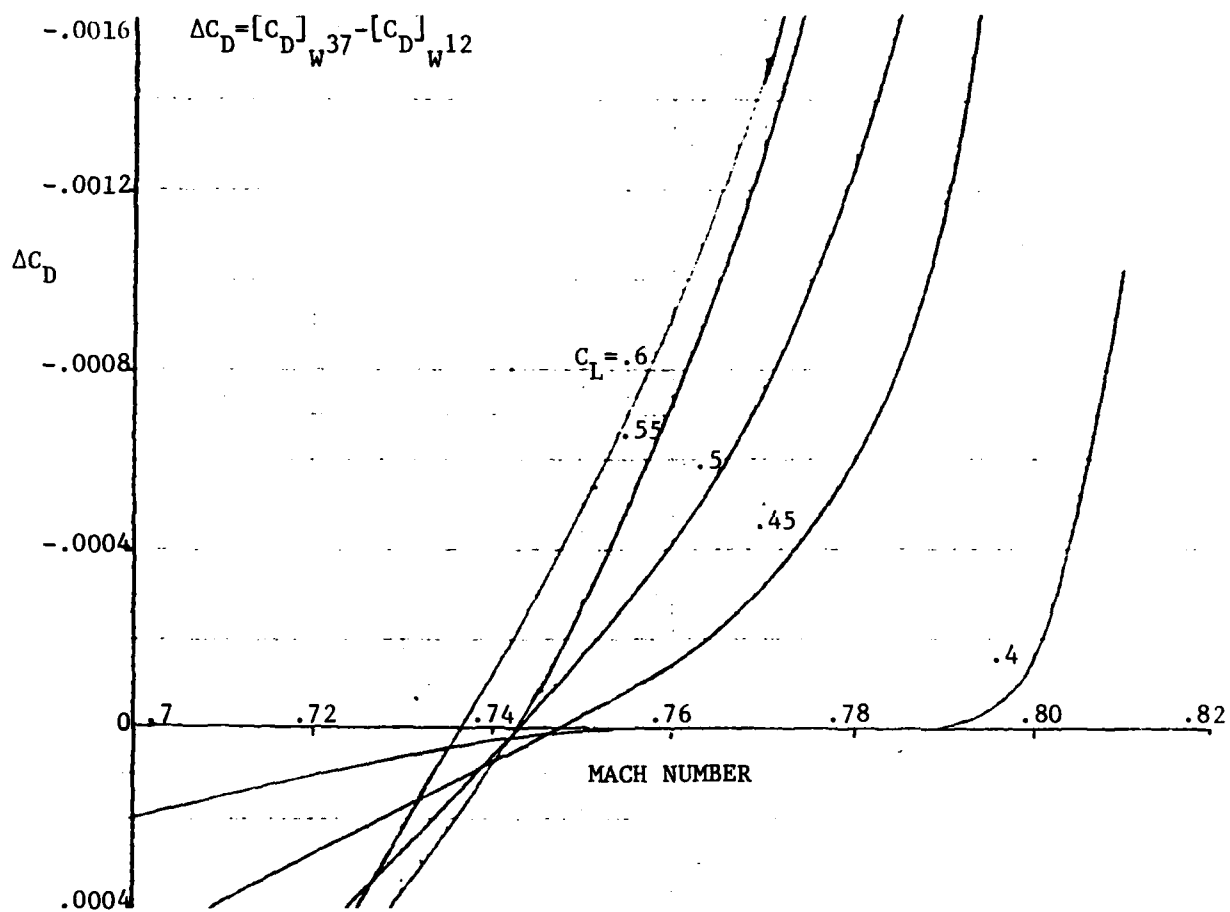


Figure 35. Effect of  $W^{37}$  on Drag Rise Characteristics



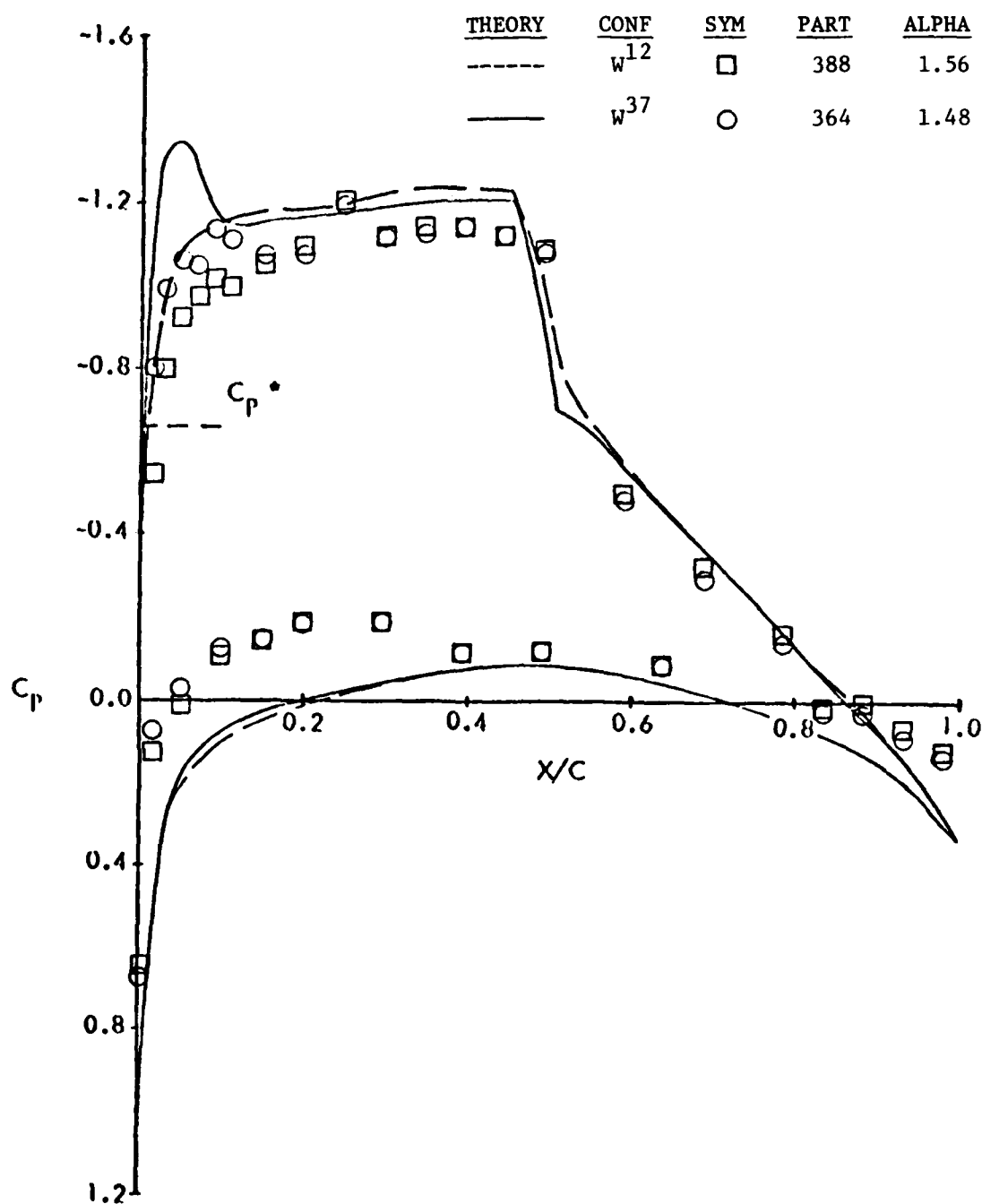
a. Pitching Moment Increments

Figure 36. Incremental Drag and Pitching Moment Coefficients for  $W^{37}$



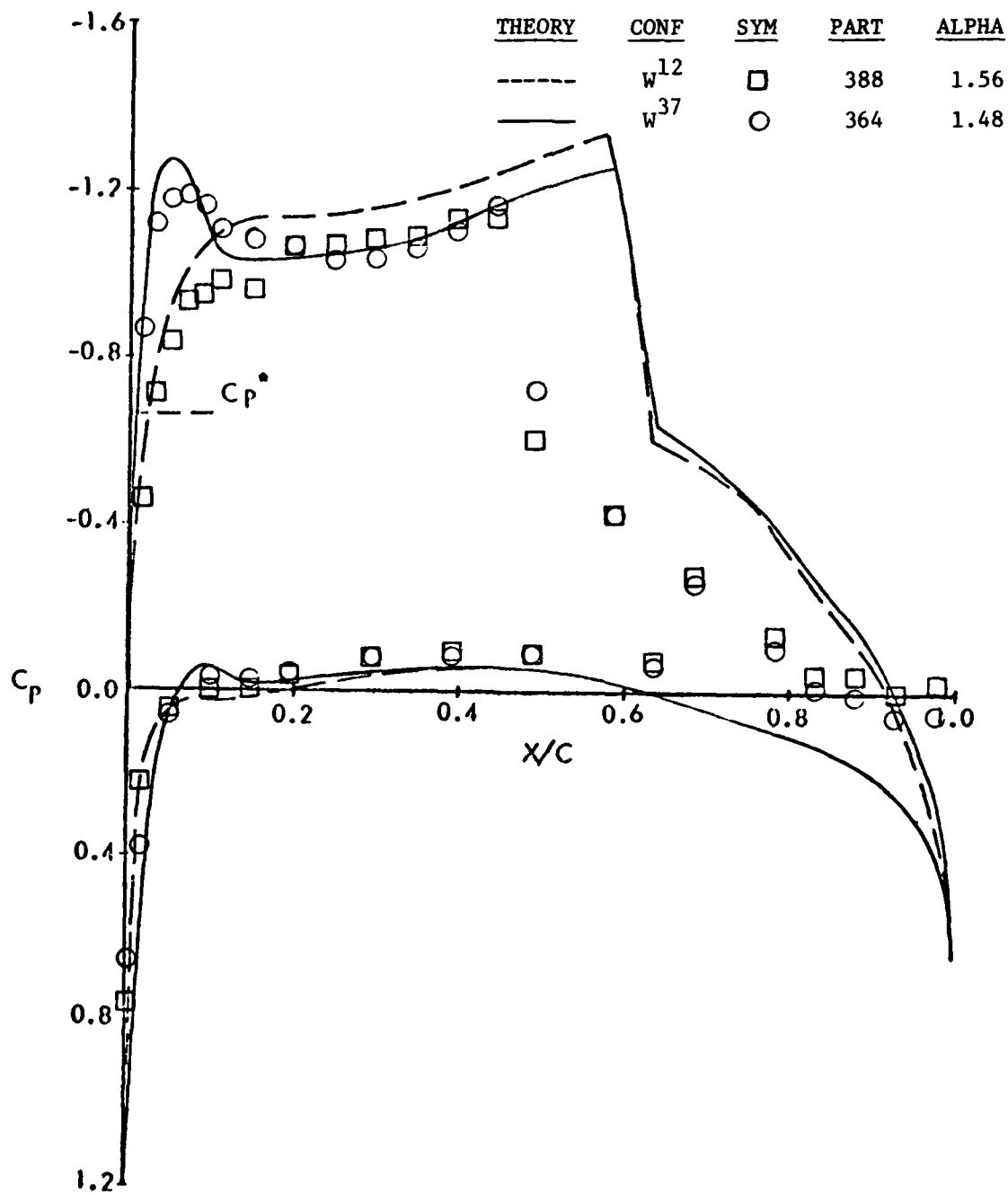
b. Drag Increments

Figure 36. Concluded



a.  $\eta = 0.418$

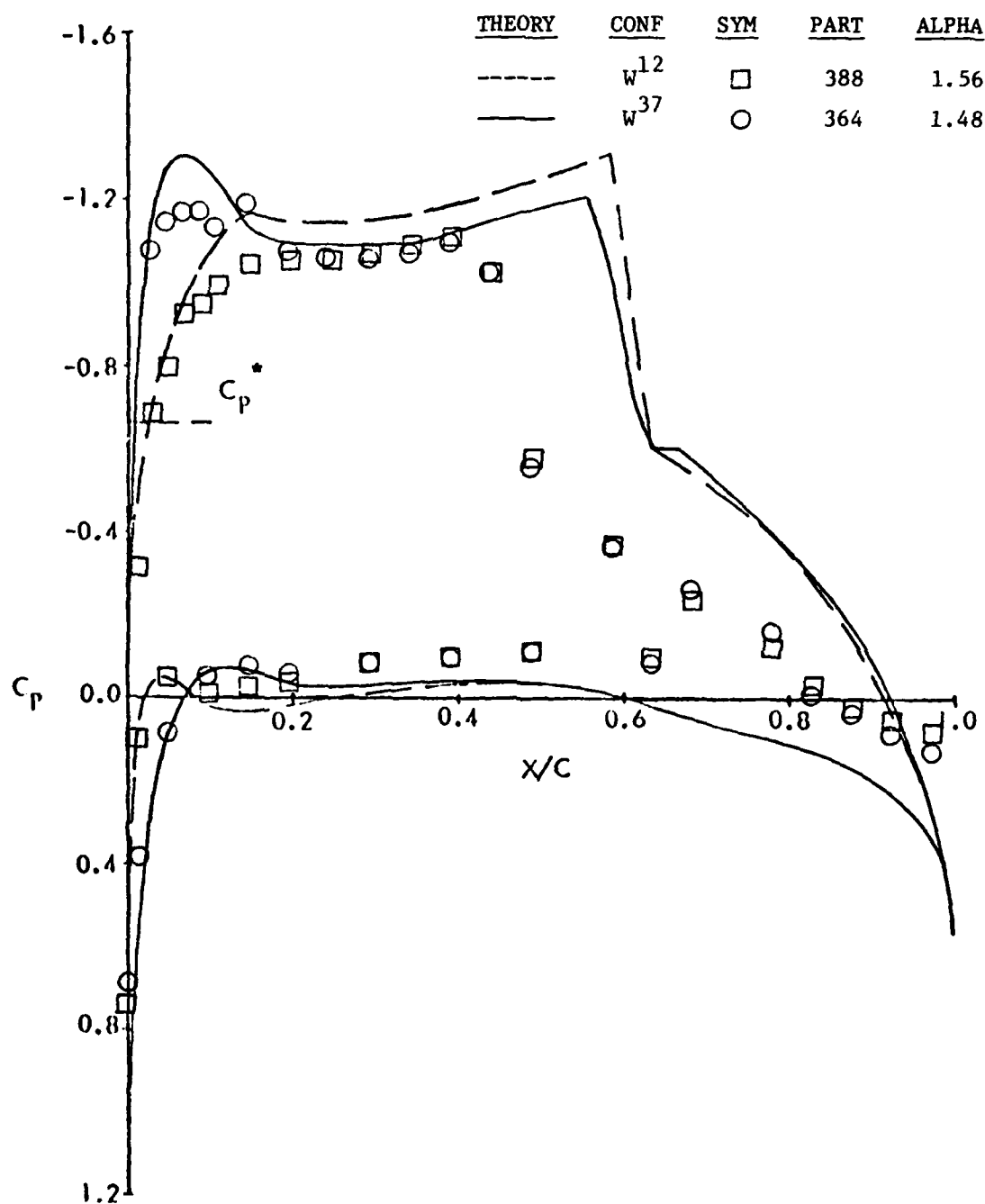
Figure 37. Comparison of 2-D Equivalent Theory to Experimental Pressure Distributions at  $M_{\text{Test}} = 0.79$



b.  $\eta = 0.636$

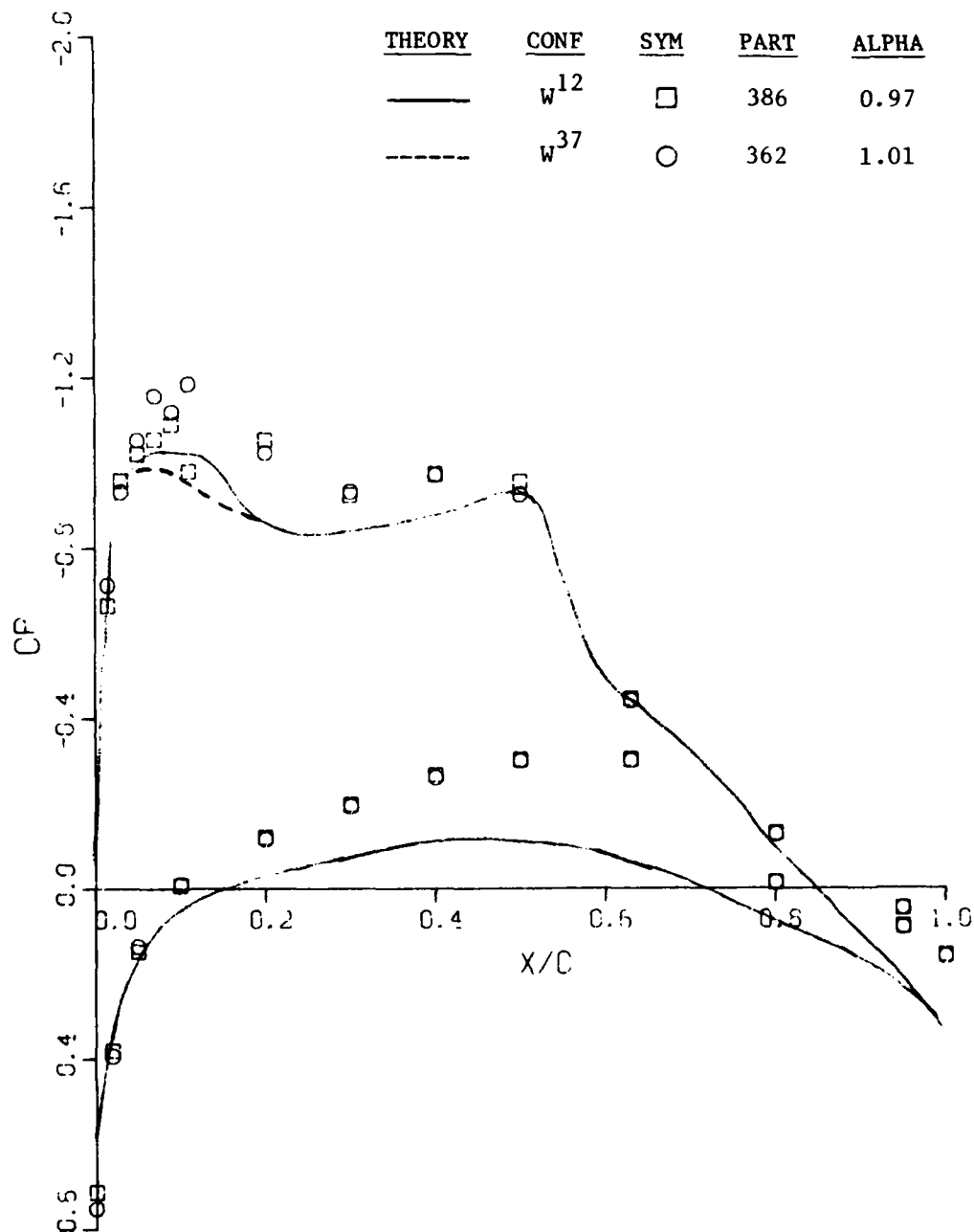
Figure 37. Continued





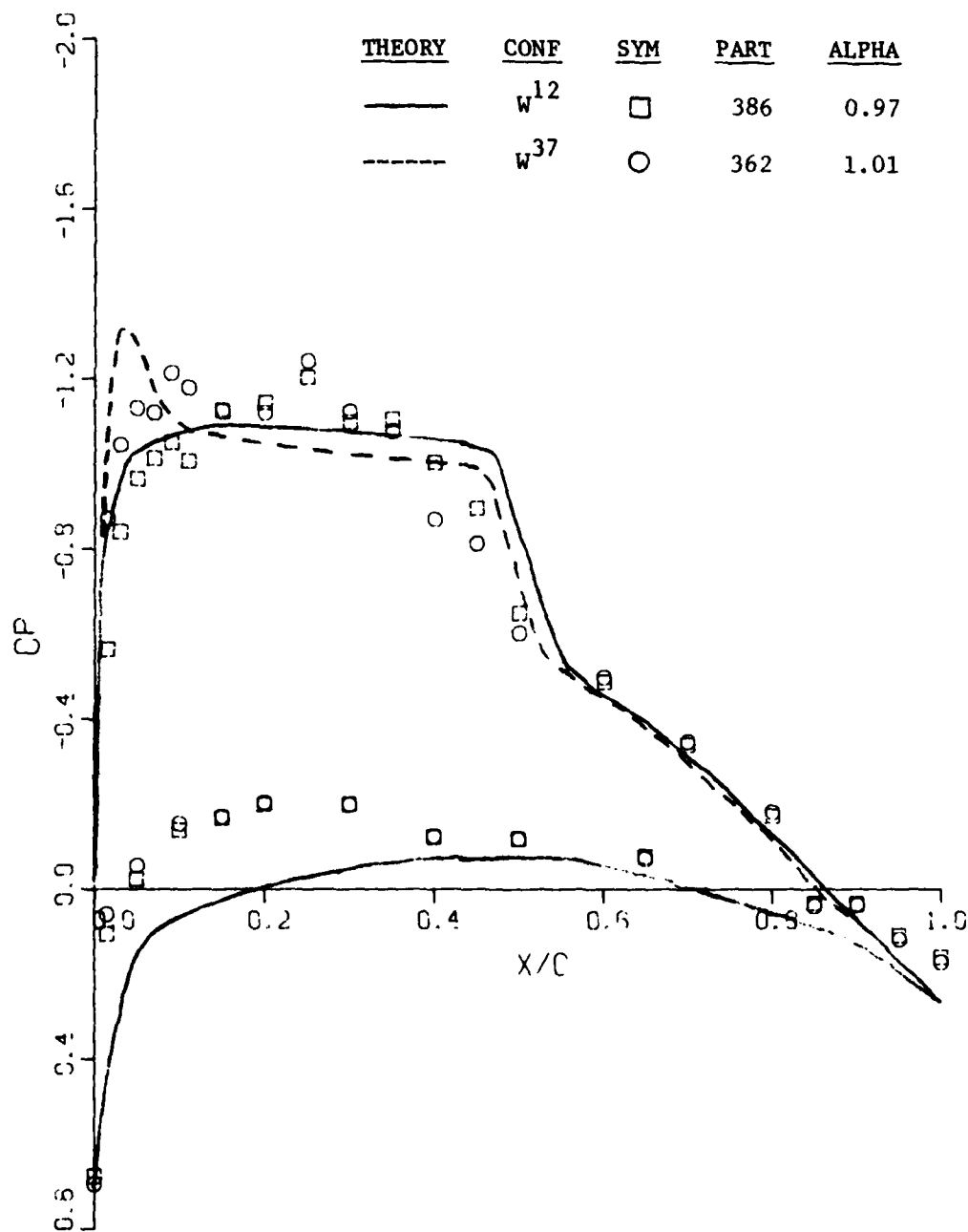
c.  $\eta = 0.793$

Figure 37. Concluded



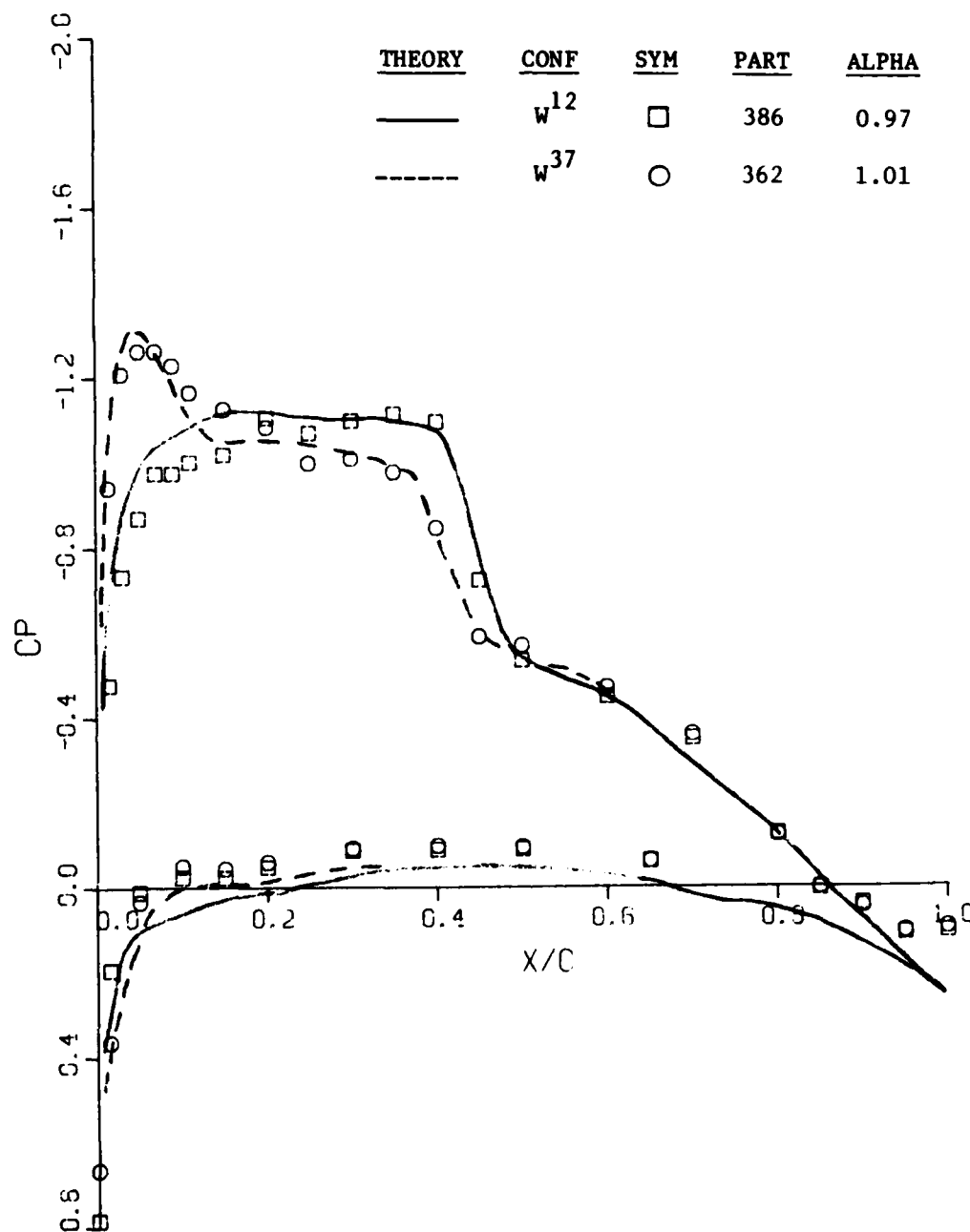
a.  $\eta = 0.193$

Figure 38. Comparison of FLO-22 Predictions to Experimental Pressure Distributions at  $M = 0.77$



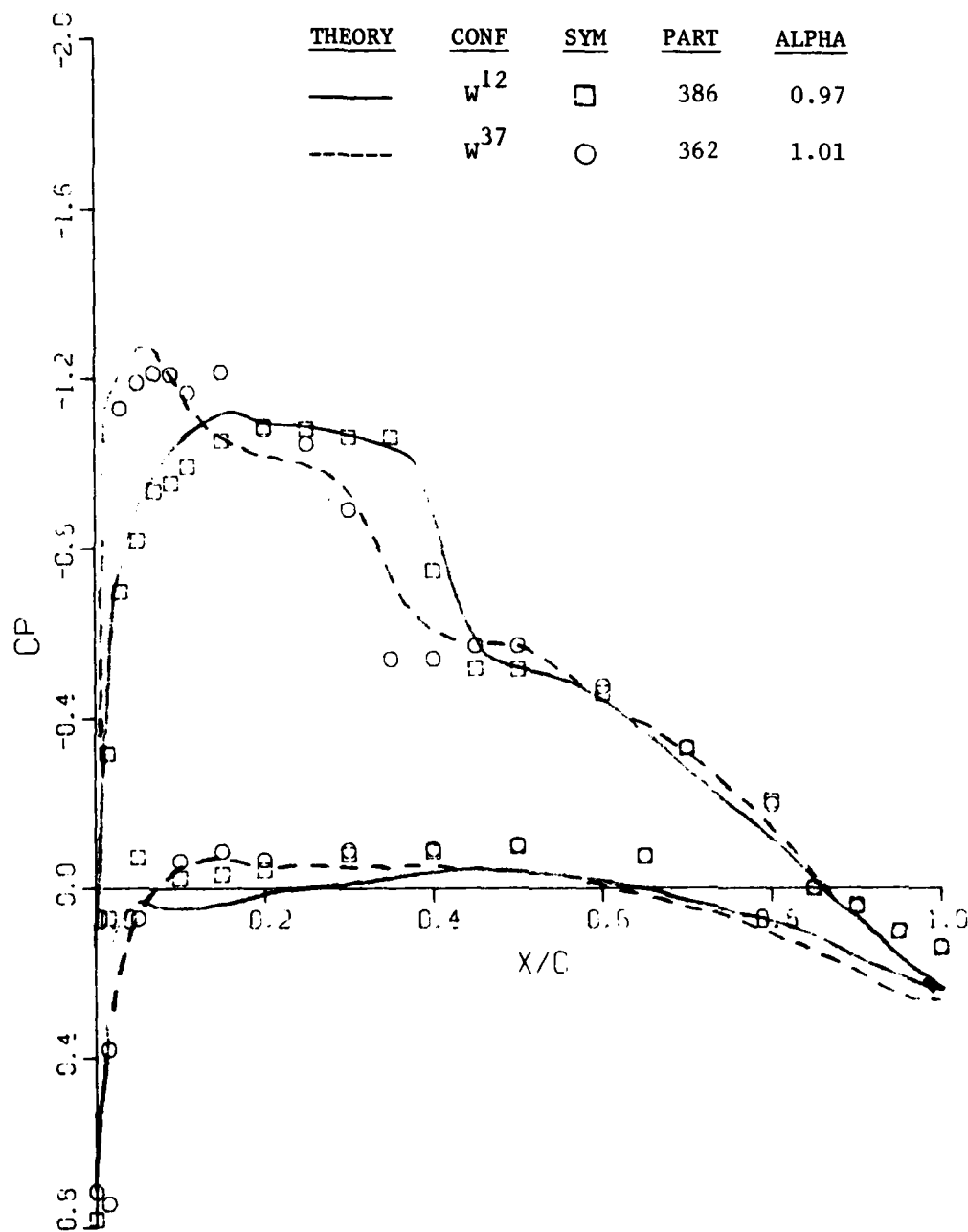
b.  $\eta = 0.418$

Figure 38. Continued



c.  $\eta = 0.636$

Figure 38. Continued



d.  $\eta = 0.793$

Figure 38. Concluded

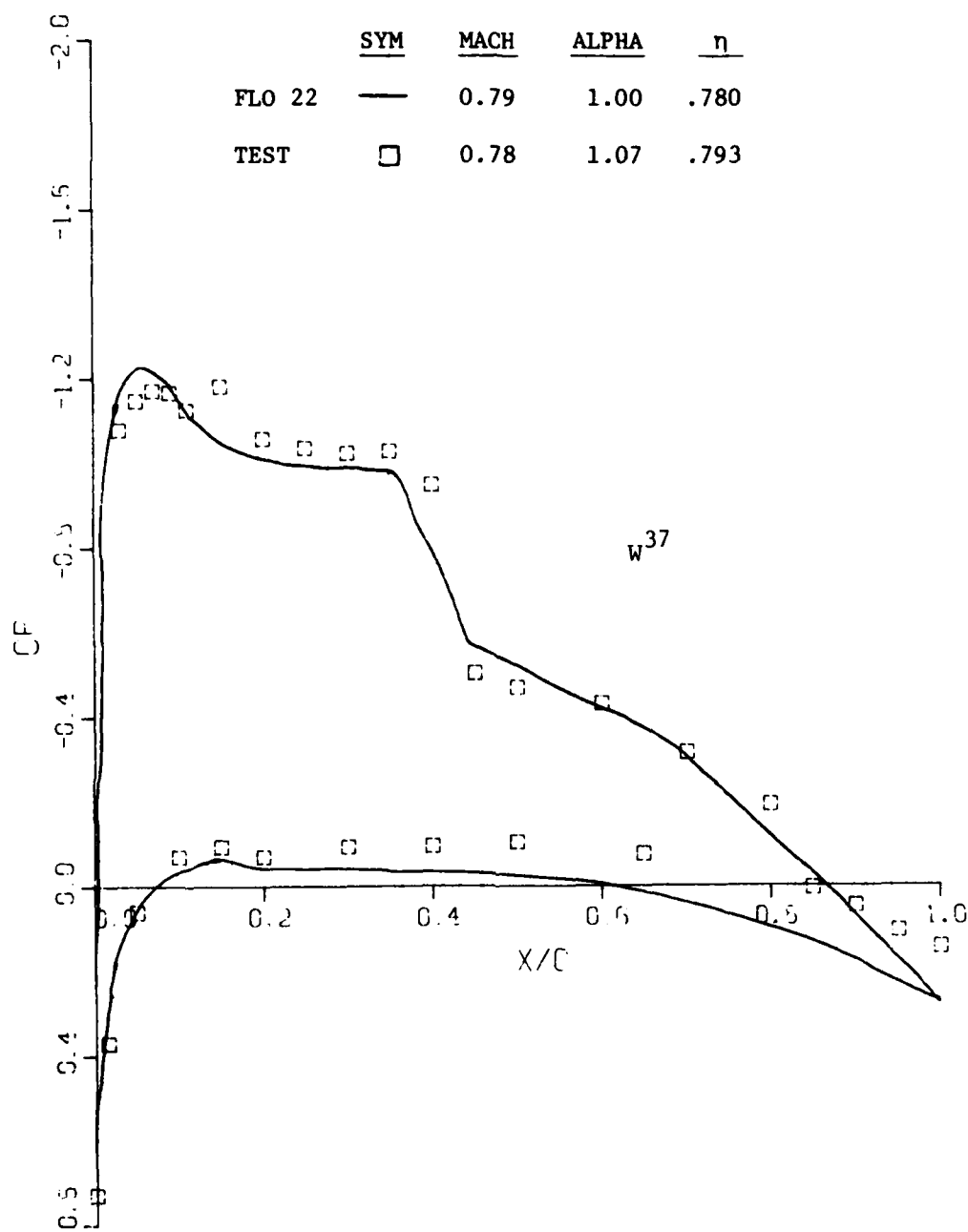


Figure 39. Comparison of FLO-22 Predictions to Experimental Pressure Distributions

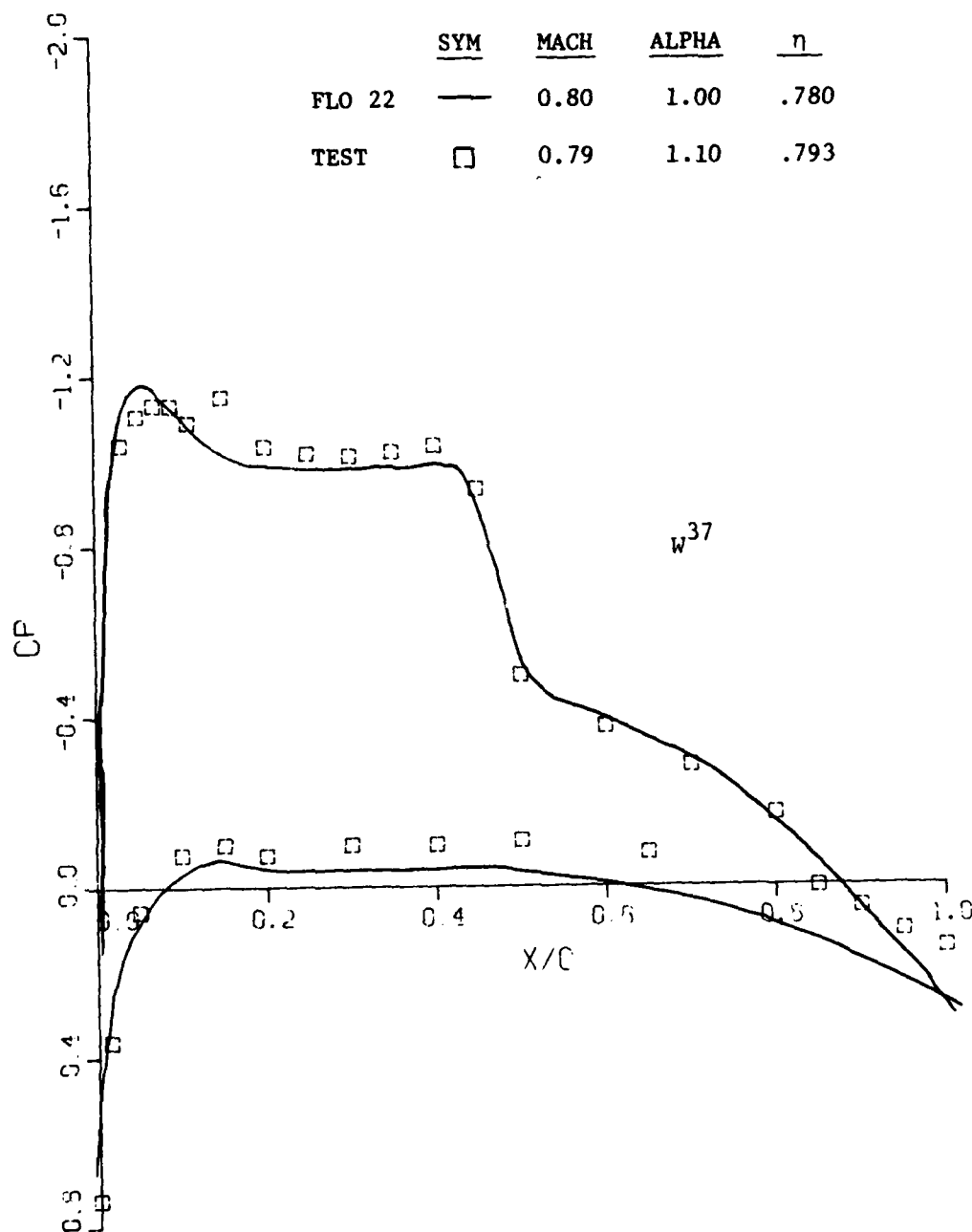


Figure 40. Comparison of FLO-22 Predictions to Experimental Pressure Distributions at  $M = 0.79$

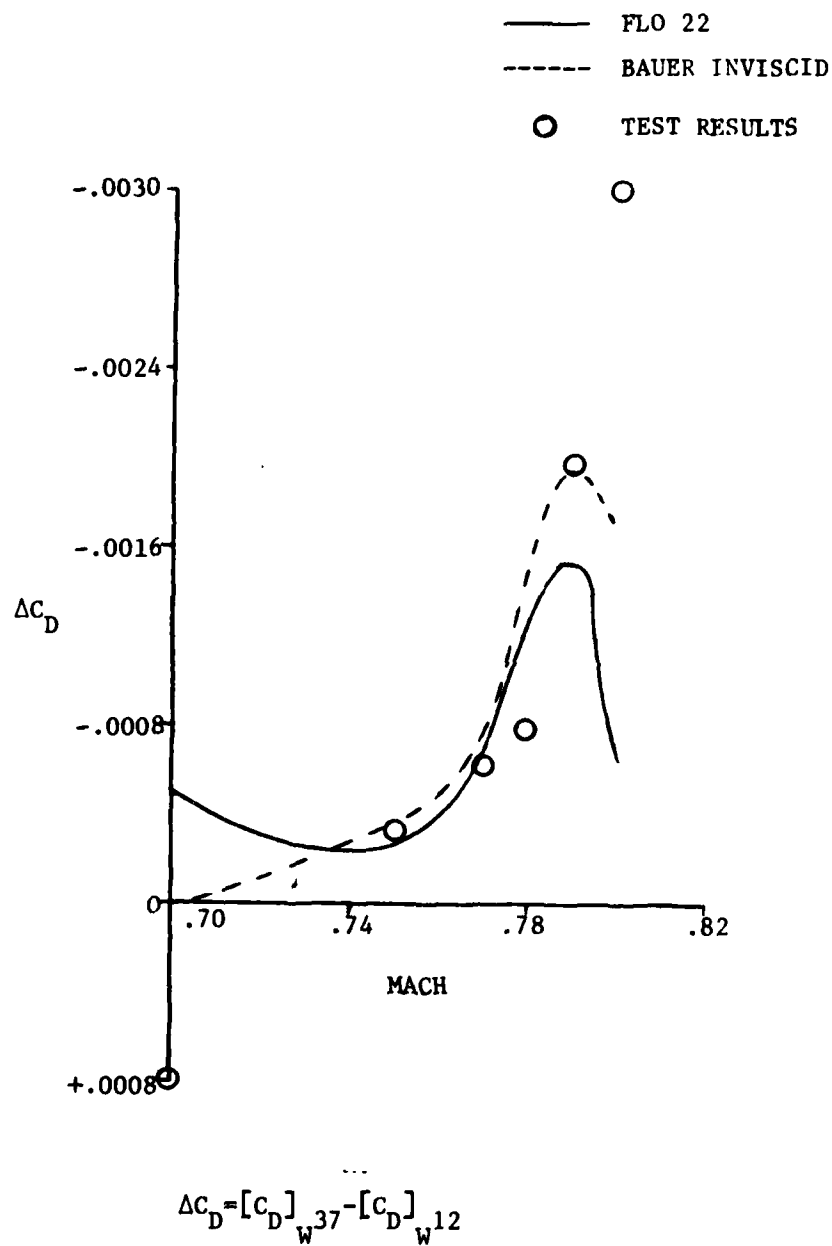
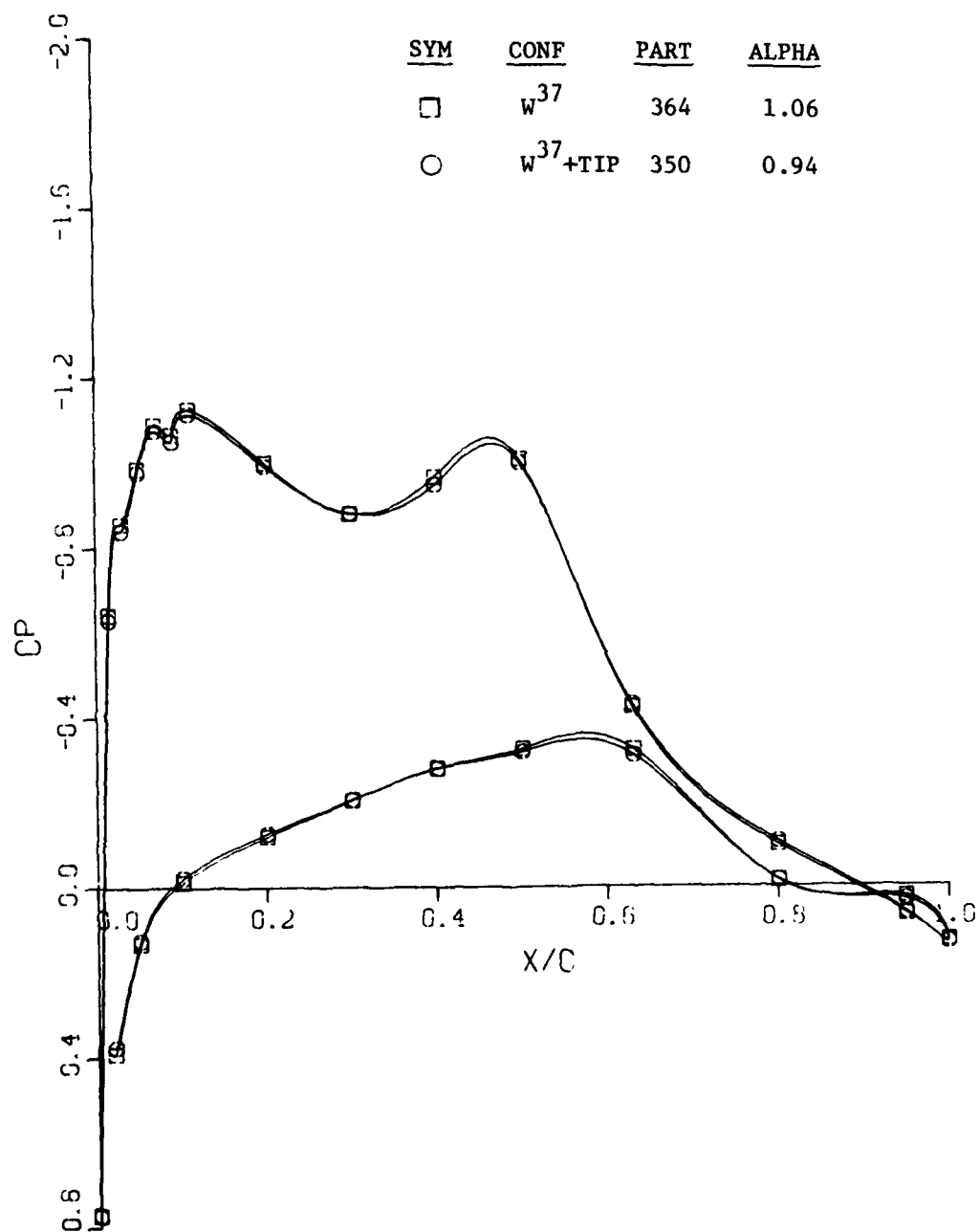


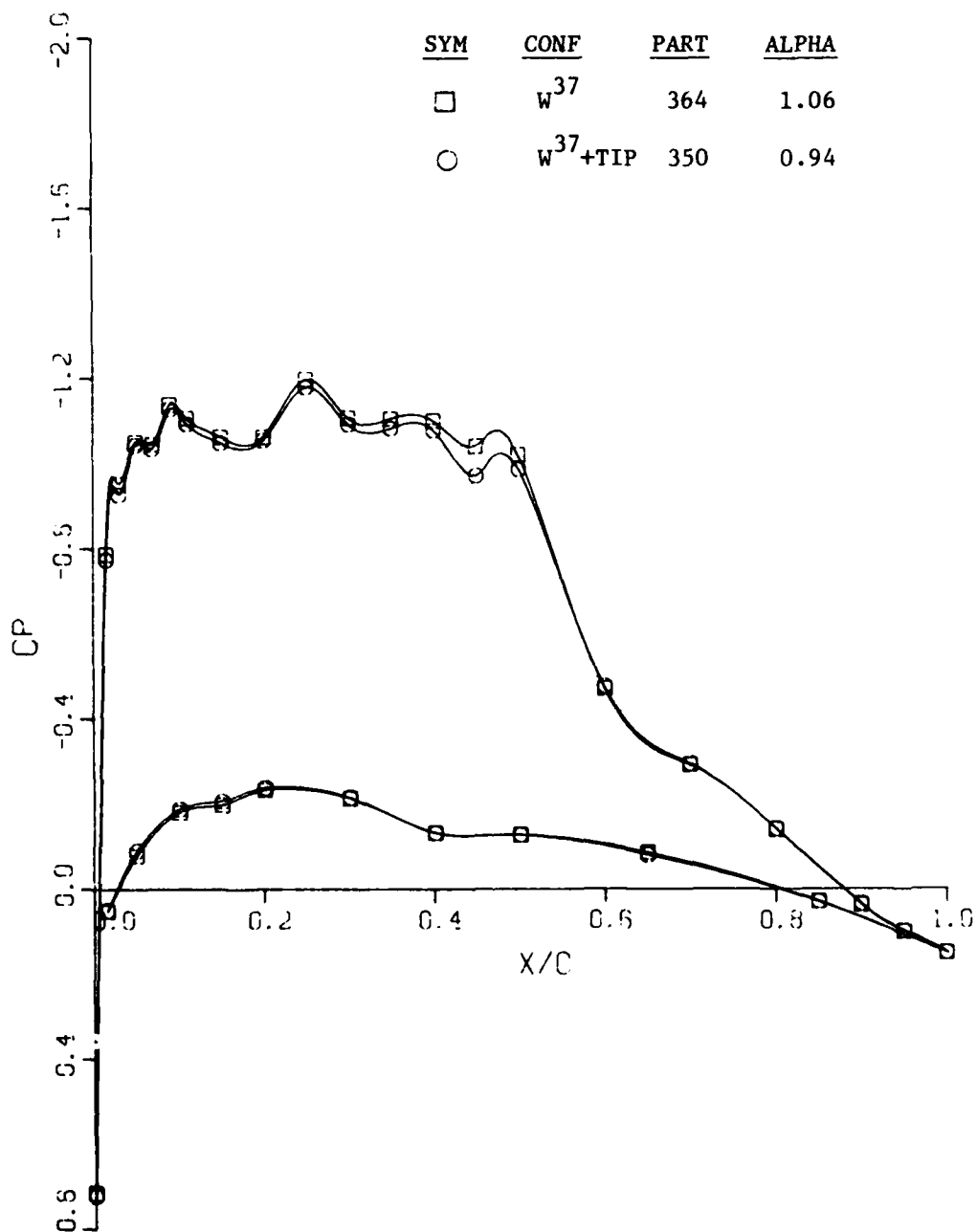
Figure 41. Comparison of Predicted and Measured Drag Increments for  $W^{37}$





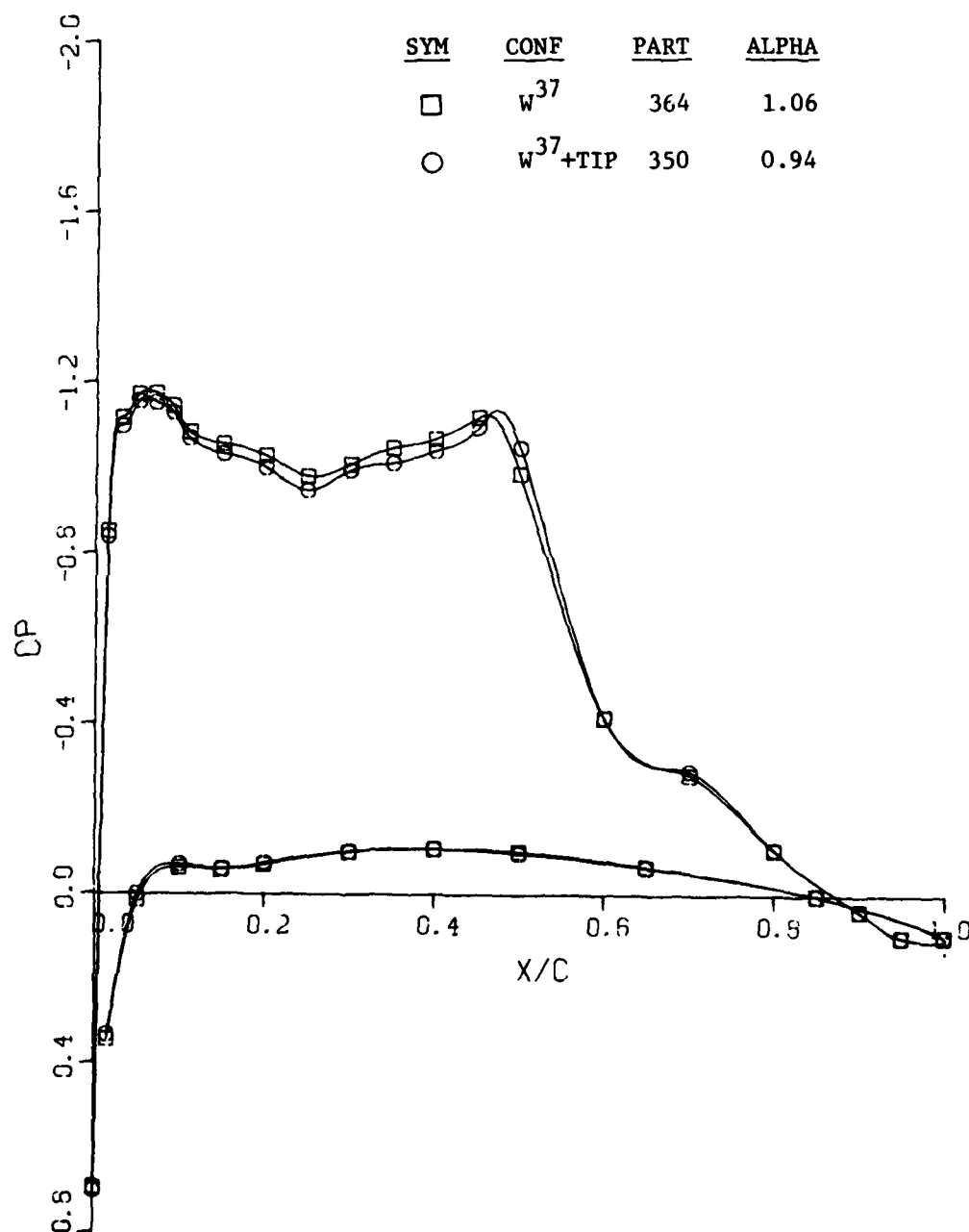
a.  $\eta = 0.193$

Figure 42. Effect of Swept Tip on Chordwise Pressure Distributions of W<sup>37</sup> at M = 0.79



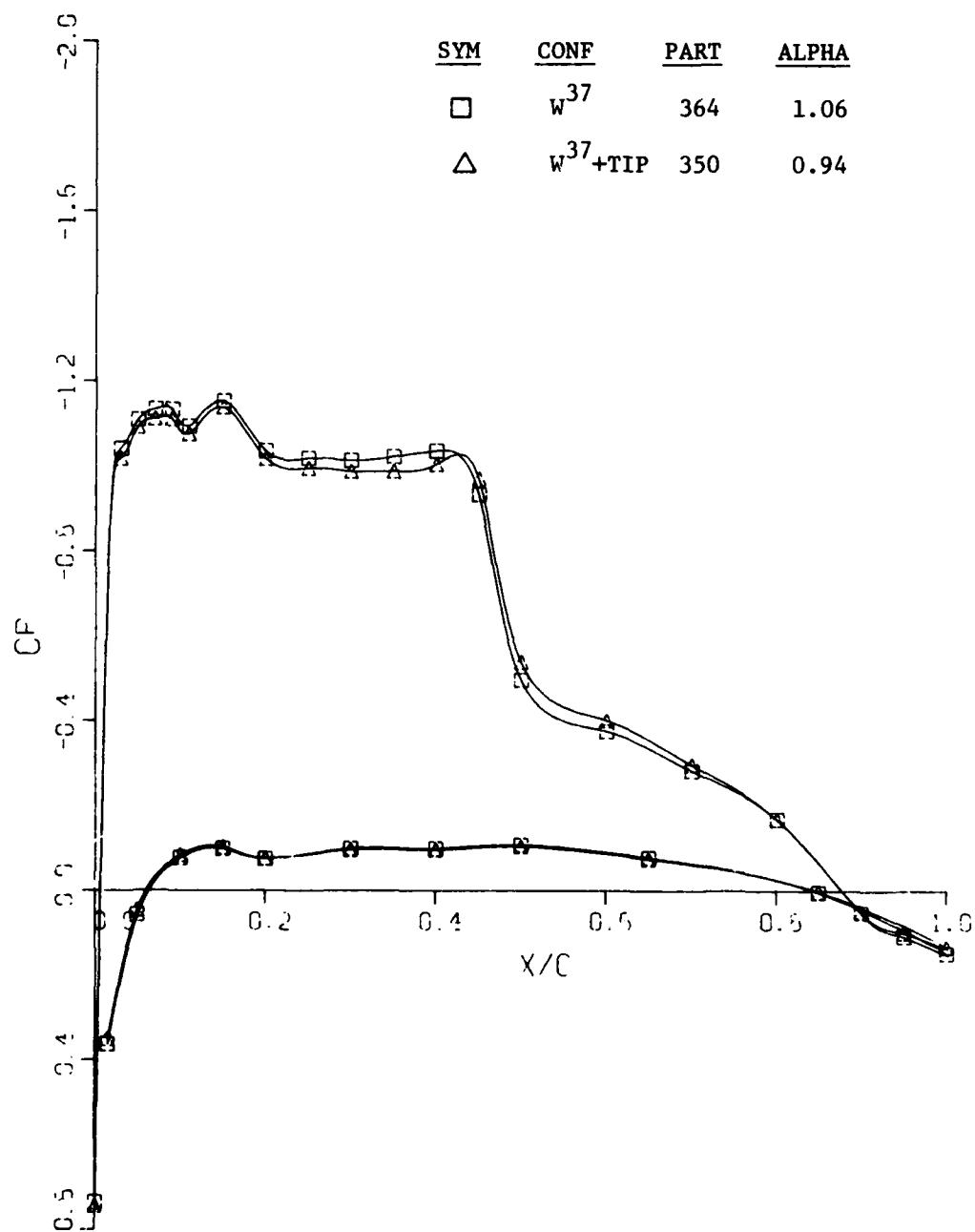
b.  $\eta = 0.418$

Figure 42. Continued



c.  $\eta = 0.636$

Figure 42. Continued



d.  $\eta = 0.793$

Figure 42. Concluded

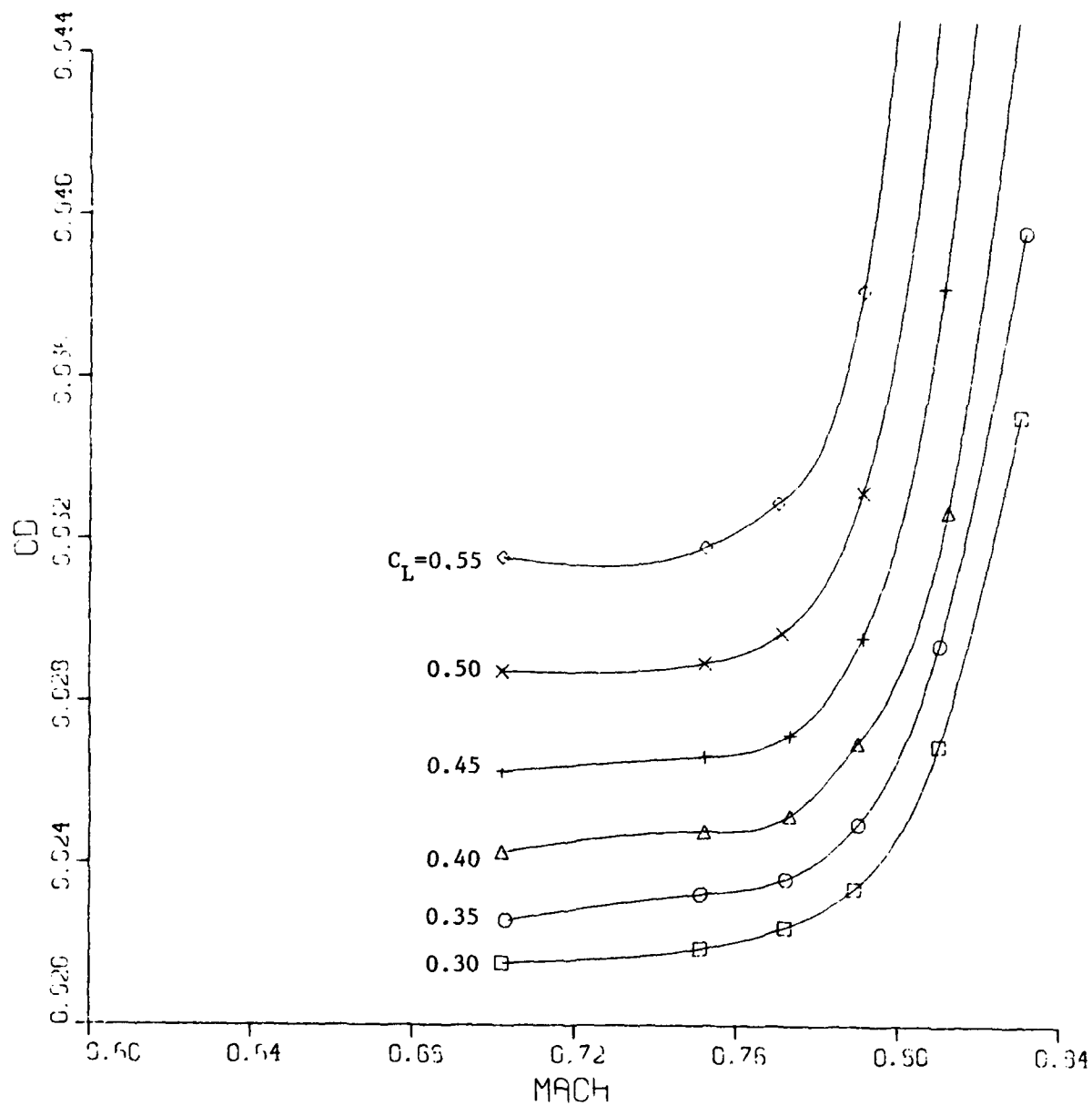


Figure 43. Drag Rise Characteristics of  $W^{37}$  Plus Swept Tip

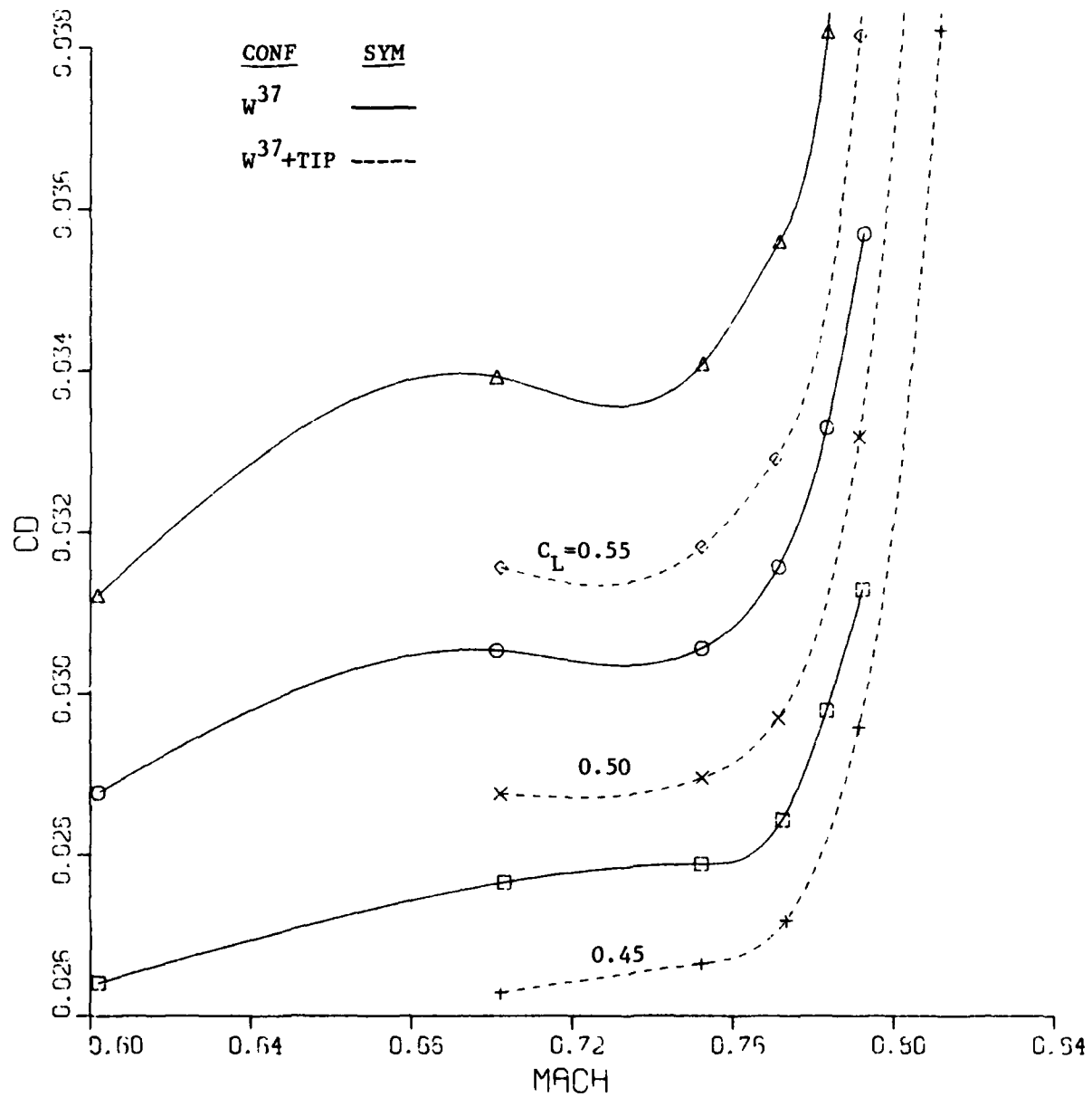
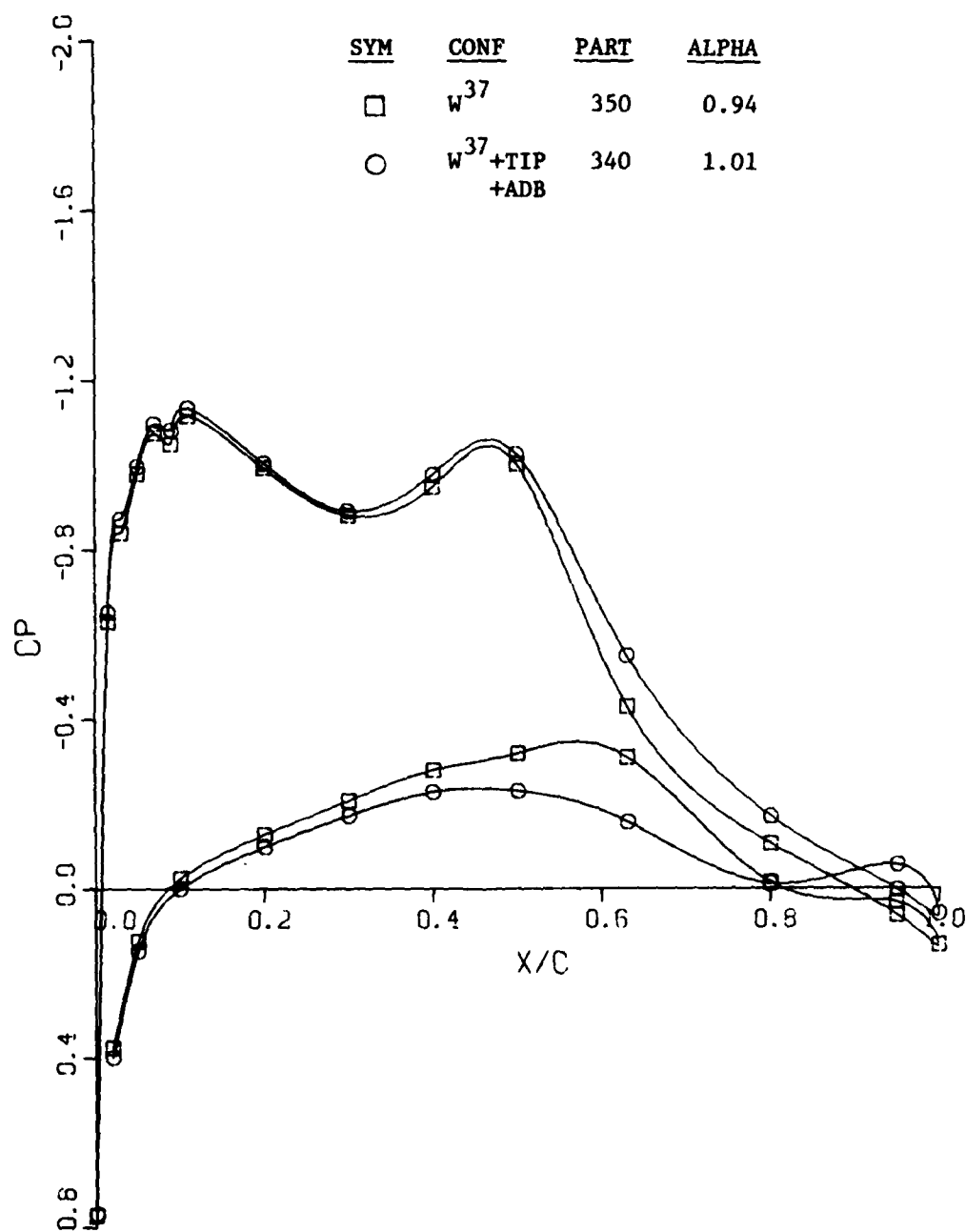
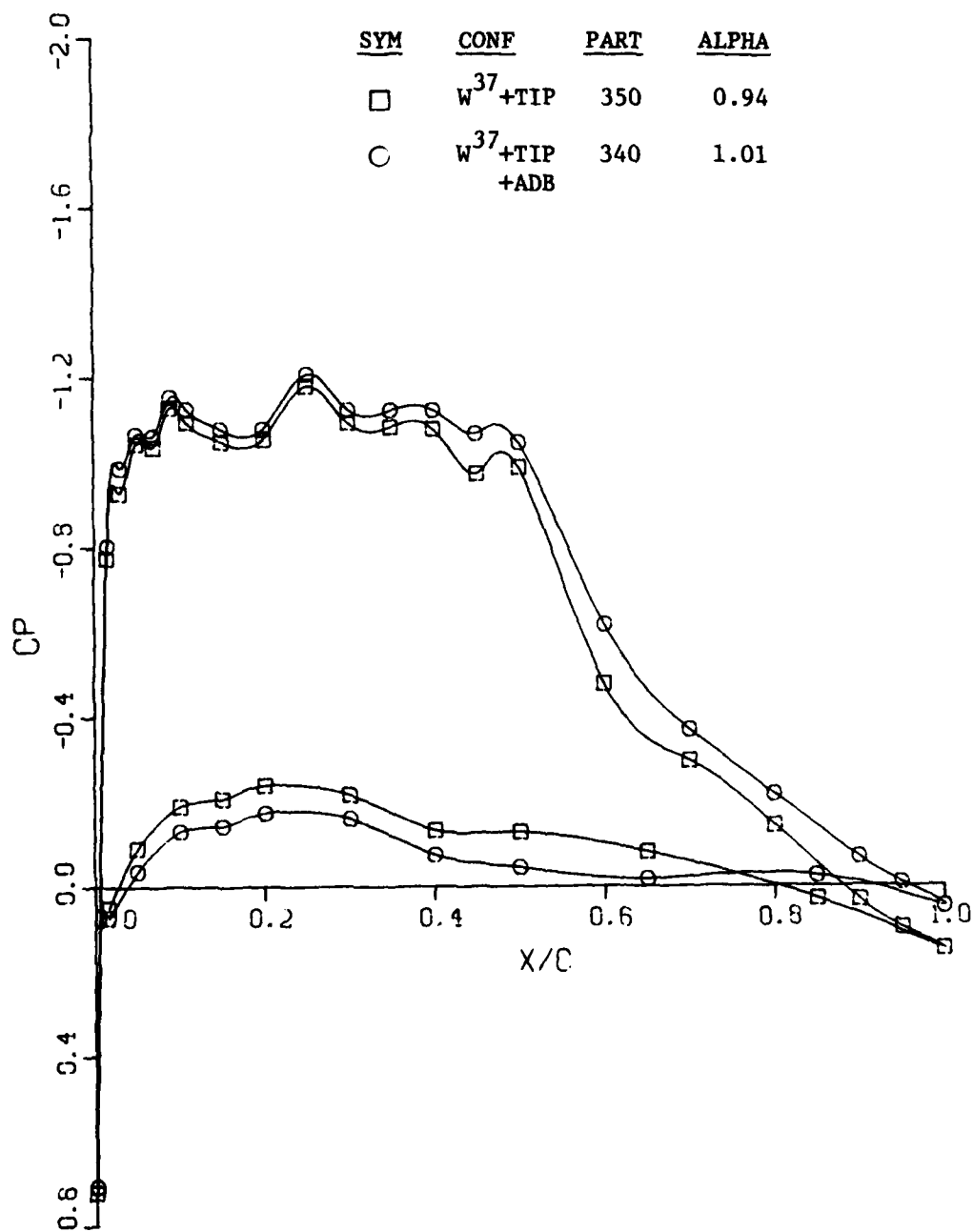


Figure 44. Effect of Swept Tip on Drag Rise Characteristics



a.  $\eta = 0.193$

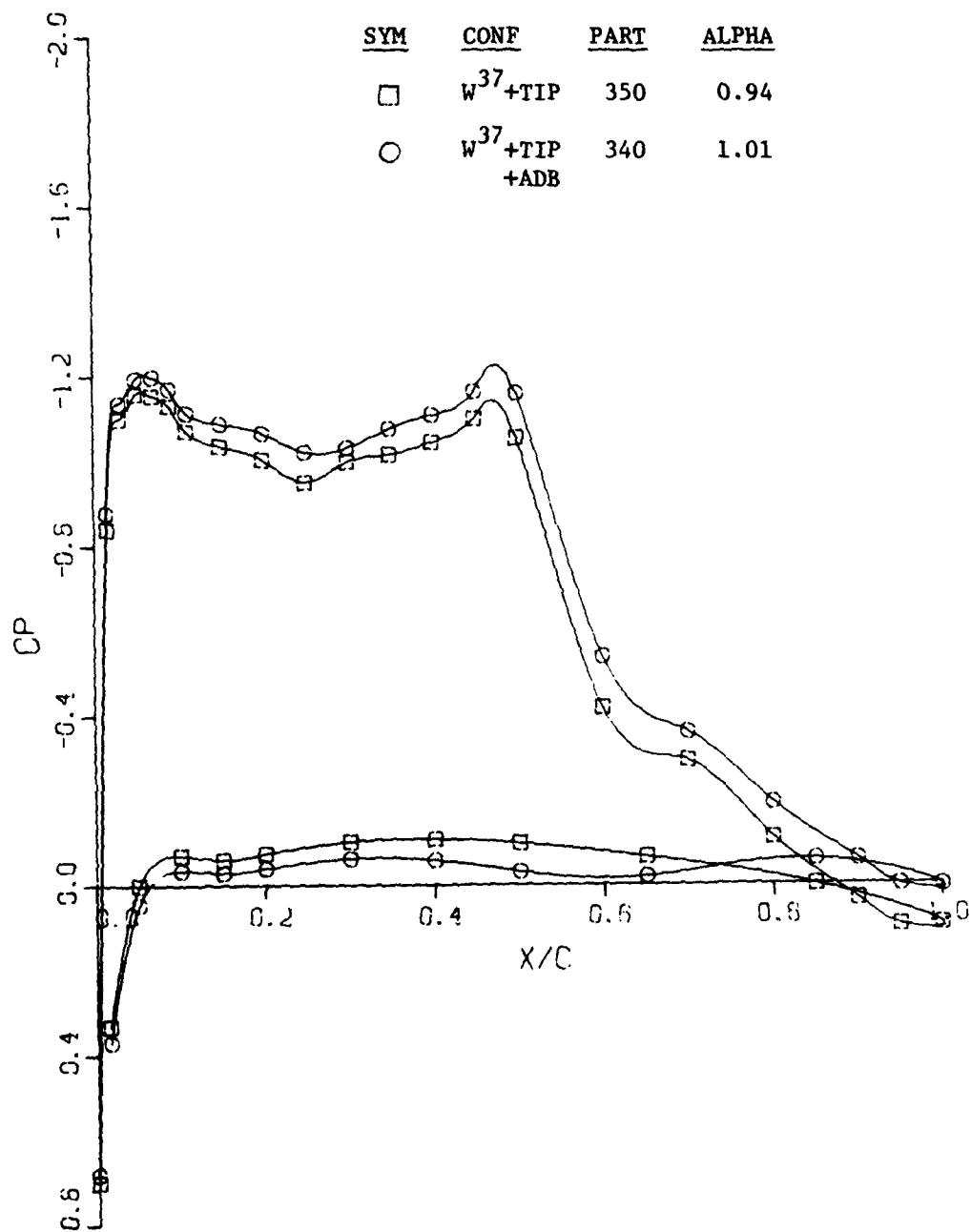
Figure 45. Effect of Anti-Drag Bodies on Chordwise Pressure Distributions at  $M = 0.79$



b.  $\eta=0.418$

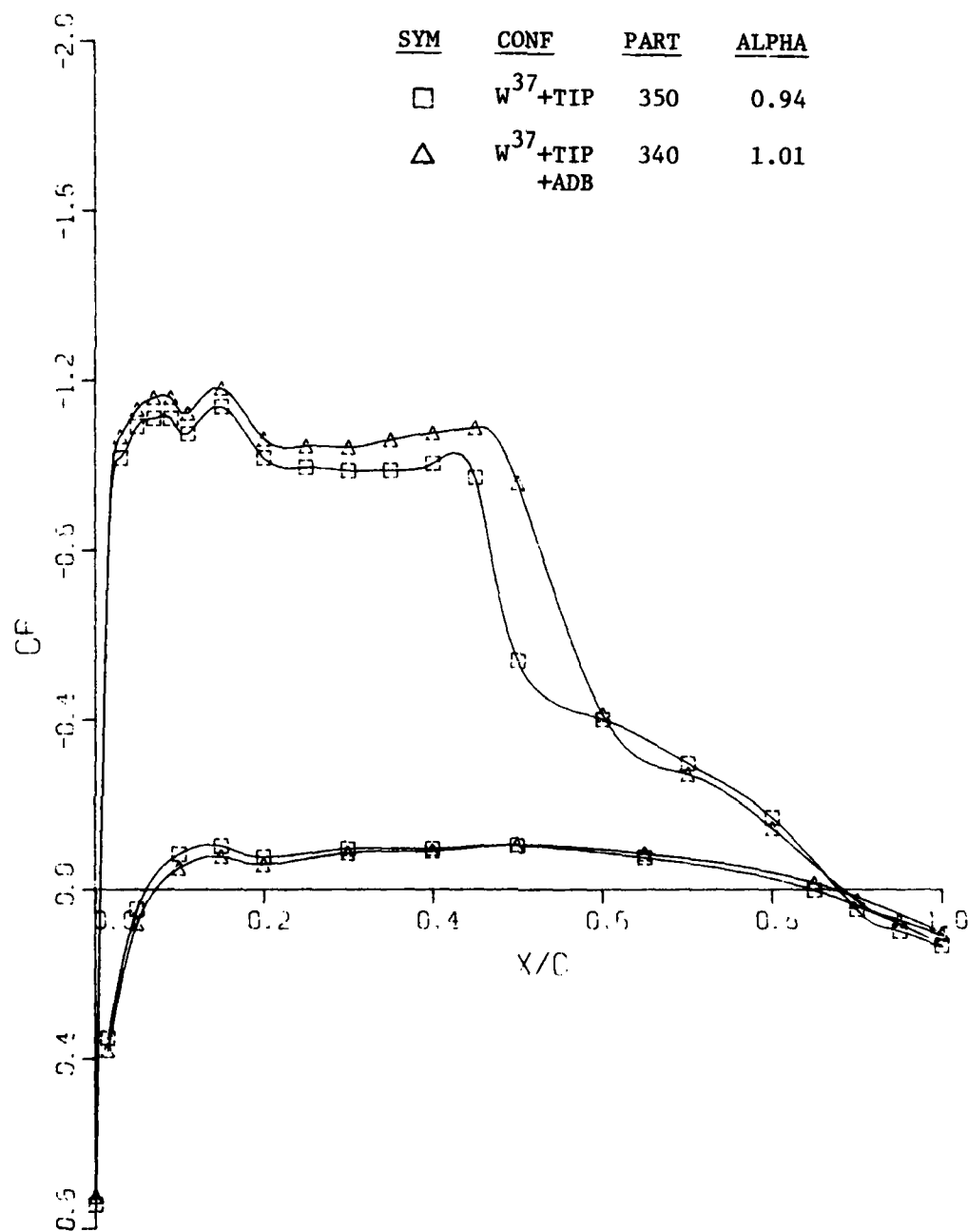
Figure 45. Continued





c.  $\eta = 0.636$

Figure 45. Continued



d.  $\eta = 0.793$

Figure 45. Concluded

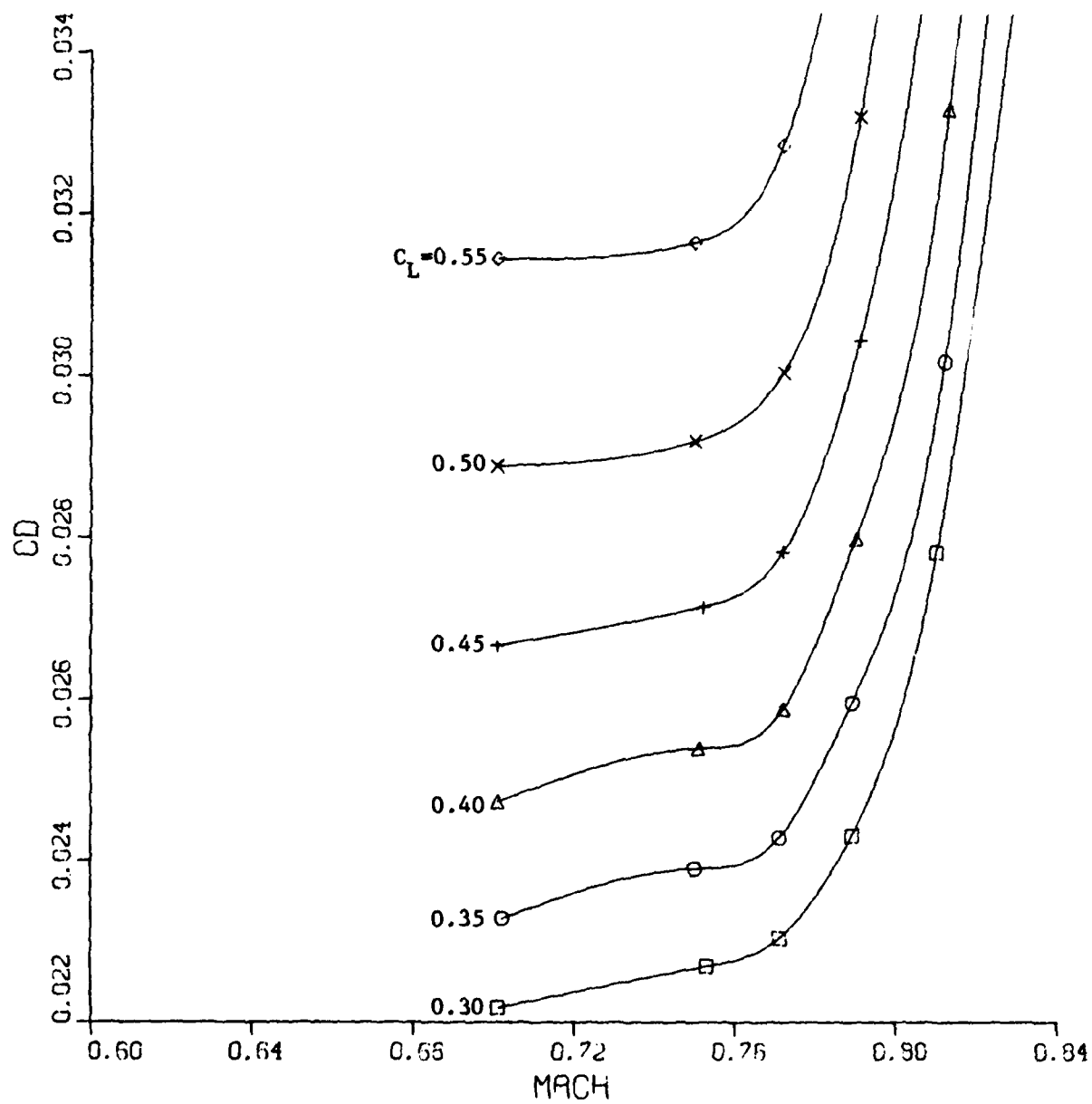


Figure 46. Drag Rise Characteristics of  $W^{37}$  and Swept Tip Plus Anti-Drag Bodies

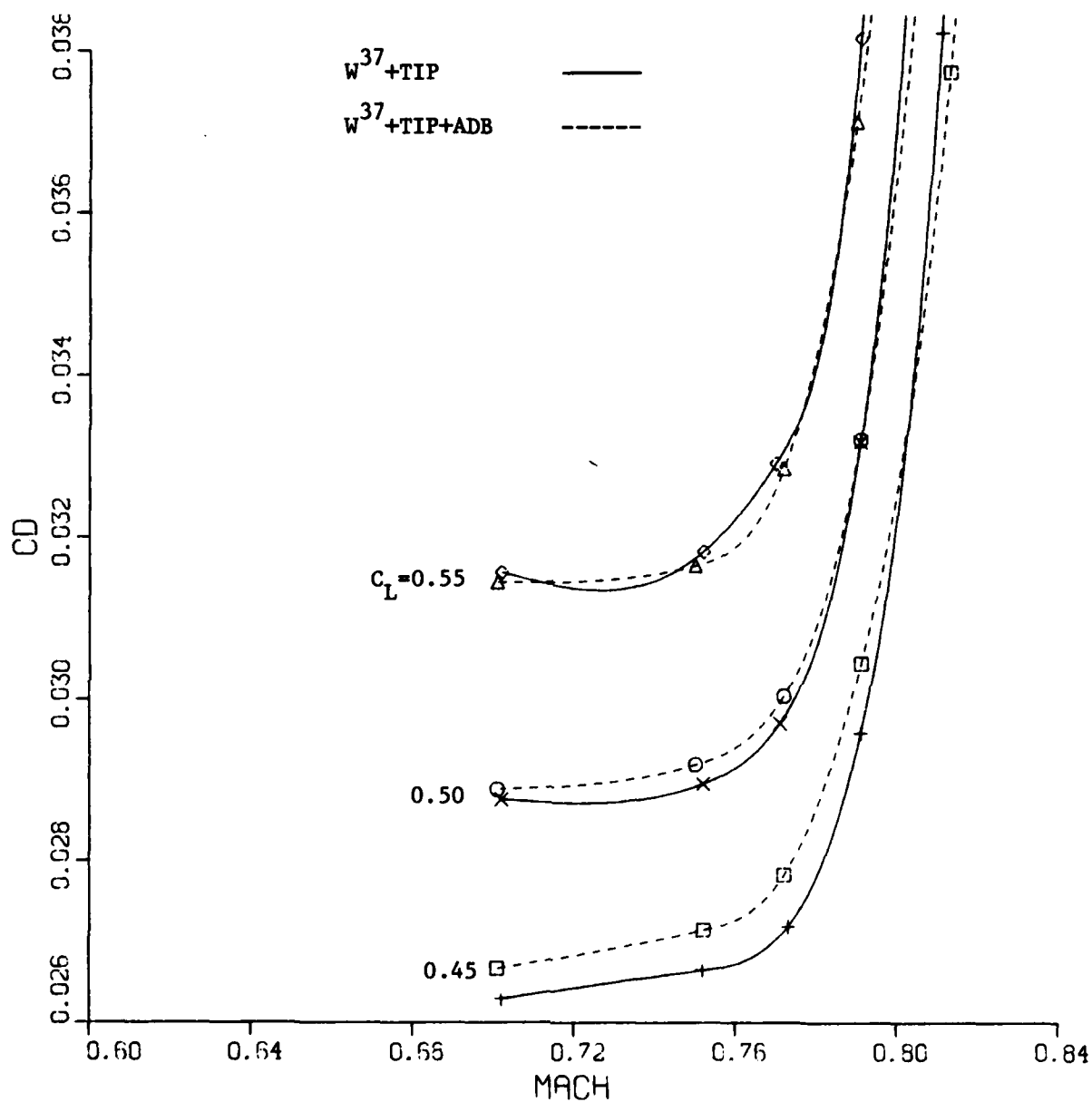


Figure 47. Effect of Anti-Drag Bodies on Drag Rise Characteristics

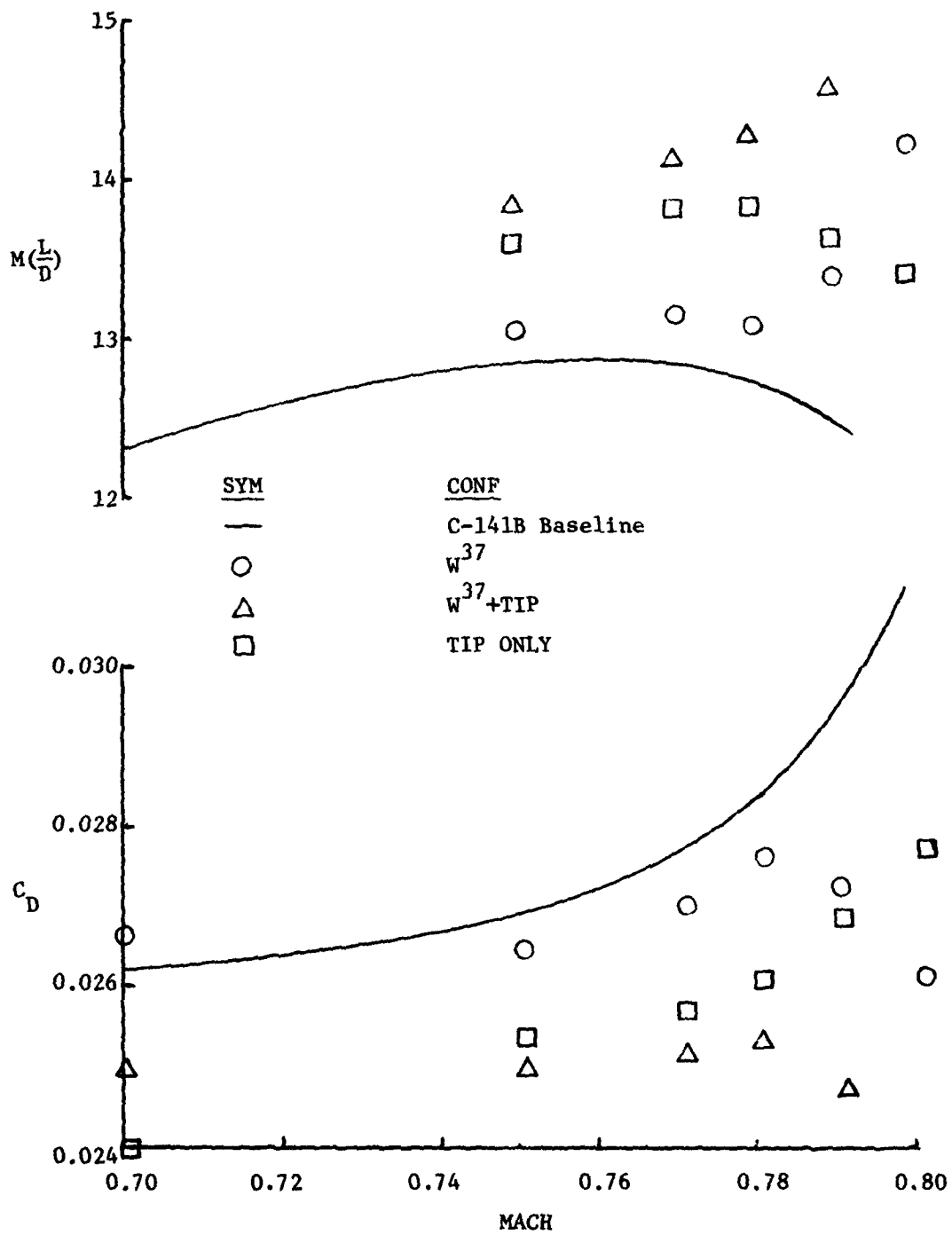


Figure 48. Performance Summary for Leading Edge and Swept Tip Modifications

#### REFERENCES

1. F. Bauer, P. Garabedian, D. Korn, and A. Jameson, Supercritical Wing Sections II. Lecture Notes in Economics and Mathematical Systems, Vol. 108, Springer-Verlag, New York, 1975.
2. R. M. Hicks and G. N. Vanderplaats, Design of Low-Speed Airfoils by Numerical Optimization, SAE Business Aircraft Meeting, Wichita, April 1975.
3. R. M. Hicks, J. P. Mendoza, and A. Bandettini, "Effects of Forward Contour Modification on the Aerodynamic Characteristics of the NACA 64-212 Airfoil Section", NASA TM X-3243, September 1975.
4. R. M. Hicks and P. A. Henne, "Wing Design by Numerical Optimization", AIAA Paper 77-1247, August 1977.
5. W. T. Blackerby and P. R. Smith, "Aerodynamic Investigation of C-141 Leading Edge Modification for Cruise Drag Reduction", AFFDL-TR-79-3059, Vol. I and II, June 1979.
6. M. E. Lores, P. R. Smith, and R. M. Hicks, "Supercritical Wing Design Using Numerical Optimization and Comparisons with Experiment", AIAA Paper 79-0065, January 1979.
7. W. T. Blackerby and J. K. Johnson, "Application of Advanced Technologies to Improve C-141 Cruise Performance", AIAA Paper 79-0066, January 1979.
8. G. N. Vanderplaats, "CONMIN - A Fortran Program for Constrained Function Minimization - User's Manual", NASA TMX-62282, August 1973.
9. A. Jameson, "Iterative Solution of Transonic Flows Over Airfoils and Wings", Communications Pure Applied Math, Vol 27, pp. 283-309, 1974.
10. S. W. Brown, "Results of a Cruise Drag Performance Test for the C-141B Transport", AEDC-TSR-80-P20, March 1980.

DATE  
FILME